Kohlschütter-Tönz protein ROGDI is the homolog of yeast Rav2 and a novel Rabconnectin-3 subunit

Samuel Winkley

A Dissertation/Thesis in

the Department of Biochemistry and Molecular Biology

Submitted in partial fulfillment of the requirements for the degree of Doctor of Philosophy in the College of Graduate Studies of State University of New York, Upstate Medical University.

Approved Patricia M. Kane

Date October 10, 2024

Table of Contents

Acknowledgments V
Abstract VI
Abbreviations VI
1 Introduction 1
1.1 V-ATPase structure and function 2
1.1.1 V_1 4
1.1.2 V_o 8
1.2 V-ATPase function in normal physiology 15
1.2.1 V-ATPases in the synaptic vesicle cycle 15
1.2.2 V-ATPase function in the kidney 19
1.2.3 V-ATPases as part of immunity 20
1.2.4 V-ATPases in cancer 22
1.3 V-ATPase regulation 24
1.3.1 Subunit composition 25
1.3.2 Reversible Disassembly 27
1.3.3 Phosphoinositide lipids 33
1.3.4 RAVE Complex - **R**egulator of H+-**A**TPases of **V**acuolar and **E**ndosomal membranes 34
1.3.5 RAVE and Reversible Disassembly 40
1.3.6 RAVE as part of V-ATPase biosynthetic assembly 44
1.3.7 Rabconnectin-3 50
1.3.8 Rabconnectin-3 as a regulator of V-ATPase assembly 56
1.4 Rabconnectin-3 related function and pathology 56
1.4.1 Developmental signaling 59
1.4.2 DMXL1 mutations and pathology 60
1.4.3 DMXL2 mutations and pathology 61
1.4.4 WDR72 mutations and pathology 63
1.4.5 Kohschutter-Tonz sydrome 65
1.5 Dissertation objectives 67
1.6 References 68
2 The ROGDI protein mutated in Kohlschutter-Tonz syndrome is a novel subunit of the Rabconnectin-3 complex implicated in V-ATPase assembly. 85
2.1 ABSTRACT 86

2.2 INTRODUCTION 87
2.3 RESULTS 89
2.3.1 Mammalian ROGDI shares structural and functional homology with yeast Rav2 89
2.3.2 ROGDI interacts with structurally conserved N-terminal β-propeller in yeast two-hybrid assay 94
2.3.3 ROGDI is modeled to interact with both Rabconnectin-3 subunits 98
2.3.4 DMXL1 co-immunoprecipitates WDR7, ROGDI and V_1 subuit A 101
2.3.5 Cellular localization of ROGDI and DMXL1 104
2.4 DISCUSSION 113
2.5 EXPERIMENTAL PROCEDURES 117
2.5.1 Materials and Media 117
2.5.2 Yeast strains 118
2.5.3 Rav- phenotyping 119
2.5.4 Yeast two-hybrid assay 120
2.5.5 Cross-linking and immunoprecipitation 121
2.5.6 Immunofluorescence Microscopy 122
2.5.7 LysoIP 123
2.5.8 Subcellular Fractionation 124
2.5.9 Computational modeling 125
2.6 Supplemental Figures 130
2.7 References 131
3 Computational modeling of Rabconnectin-3 and RAVE 137
3.1 Rabconnectin-3 and RAVE structural modeling 138
3.2 RAVE 139
3.2.1 Rav1-Rav2 139
3.2.2 Rav1-Skp1 144
3.2.3 DMXL1 and DMXL2 148
3.2.4 WDR7 151
3.2.5 WDR72 152
3.3 Rabconnectin-3/ROGDI complex 154
3.4 References 159
4 Discussion and Future Directions 160
4.1 ROGDI as a Rav2 homolog and Rabconnectin-3 subunit 161
4.2 DMXL1 lysosomal localization 165

4.3 Rav2 function investigation 166
4.4 Generation of a ROGDI knockout cell line 167
4.5 Investigation of Skp1 mutant 168
4.6 Generation of a Rabconnectin-3 structure 169
4.7 References 171
5 Chapter 5- Appendix 173
5.1 ROGDI and Rav2 are structurally homologous 173
5.2 References 175

Acknowledgments

I want to express my deepest gratitude to Dr. Patricia Kane, my doctoral advisor and guide on this journey. She always knows when and how far to push me and how to cultivate a positive environment in the lab, and she is a wealth of scientific knowledge. I could not have done this without her, and I wouldn't have been half as successful in any other lab.

I am grateful for the support and friendship from my fellow lab mates, both past and present. Maureen Tarsio has been a constant positive presence and a significant support to me and the entire lab during my time here. Every member of the lab has greatly impacted me as a colleague, a student, and a scientist. I appreciate the support and friendship from everyone, and I will continue to cherish these connections.

I am deeply grateful to my thesis advisory committee members, Dr. Stephan Wilkens and Dr. Bruce Knutson, for their valuable input over the years. I would like to express my thanks to Dr. Gary Chan and Dr. Leszek Koutla for serving on my thesis defense committee. I also want to acknowledge Dr. Morris Manolson, who made the trip from the University of Toronto to serve on my thesis defense committee. Thank you all for your time and support.

Finally, I must thank my family for their endless support. My beautiful fiancée, Ella, whose belief in me never wavered, no matter what; my parents, Carol and Steve, and my brother, Will, who have always been there for me; I couldn't have done this without them. Thank you all so much.

Abstract

V-ATPases are rotary proton pumps that are extraordinarily well-conserved among eukaryotes. V-ATPases function primarily to acidify intracellular compartments, critical to maintaining cellular homeostasis. The V-ATPase-generated proton gradient provides the optimal environment for lysosomal catabolism and drives intracellular protein trafficking. V-ATPases serve important functions throughout the human body. For example, V-ATPase activity energizes the active transport of neurotransmitters into synaptic vesicles, regulates the acid/base balance in the kidney, and helps the immune system recognize invading pathogens. However, when V-ATPase activity is inappropriately increased or decreased, these processes are affected, and disease can result.

V-ATPases are composed of peripheral V_1 and integral membrane V_0 subcomplexes; V_1 hydrolyzes ATP and transmits rotation to V_0, which moves protons across a membrane. V-ATPase activity is regulated in part through the reversible association of the V_1 subcomplex and V_1C subunit from V_0. Upon disassembly, both V_1 and V_0 are catalytically inactivated. In yeast, the RAVE complex catalyzes the efficient reassembly of V-ATPases. Rabconnectin-3 is the human homolog of the RAVE complex and functions similarly. Mutations in the Rabconnectin-3 complex can reduce V-ATPase activity through decreased assembly, which leads to disease. Both Rabconnectin-3 subunits share substantial homology with the RAVE subunit Rav1. We have identified the poorly characterized protein ROGDI as the mammalian homolog of the yeast RAVE subunit, Rav2.

ROGDI shares strong functional and structural homology with yeast Rav2. Expression of ROGDI in a *rav2Δ* yeast strain partially rescues the growth phenotype characteristic of RAVE mutants. ROGDI binds to the structurally conserved N-terminal β-sheet rich domain. AlphaFold3 modeling predicts that ROGDI binds between the Rabconnectin-3 subunits. ROGDI coimmunoprecipitates with Rabconnectin-3 and V-ATPase subunits. Additionally, ROGDI is present alongside V-ATPase and Rabconnectin-3 subunits on lysosomal membranes. This indicates that, like RAVE and Rav2, Rabconnectin-3 and ROGDI localize intracellular regions rich in V-ATPases. Identifying ROGDI as a novel Rabconnectin-3 subunit is a substantial step forward in our understanding of Rabconnectin-3 and how it influences V-ATPase activity.

LIST OF FIGURES

FIGURE 1-1- STRUCTURAL COMPARISON OF EUKARYOTIC V-ATPASES 5

FIGURE 1-2 OVERVIEW OF REVERSIBLE DISASSEMBLY 32

FIGURE 1-3 V-ATPASE BINDING REGIONS OF RAV1 38

FIGURE 1-4 STEPS OF REVERSIBLE DISASSEMBLY 43

FIGURE 1-5 INTRACELLULAR SCHEMATIC OF V-ATPASE BIOSYNTHESIS 49

FIGURE 1-6 SCHEMATIC OF RABCONNECTIN-3 ISOFORMS 52

FIGURE 1-7 RABCONNECTIN-3 RELATED DISEASE 58

FIGURE 2-1 HUMAN ROGDI AND YEAST RAV2 DISPLAY STRUCTURAL AND FUNCTIONAL HOMOLOGY. 93

FIGURE 2-2 ROGDI INTERACTS WITH CONSERVED B-PROPELLER REGION OF RAV1 AND RABCONNECTIN-3 97

FIGURE 2-3 ALPHAFOLD3 MODEL OF ROGDI BINDING TO N-TERMINAL DOMAINS OF RABCONNECTIN-3A AND B 100

FIGURE 2-4 DMXL1 CO-IMMUNOPRECIPITATES ROGDI, WDR7, AND V_1 SUBUNIT A 102

FIGURE 2-5 ROGDI PARTIALLY LOCALIZES WITH V_1A ON PERINUCLEAR LYSOSOMES 108

FIGURE 2-6- S1 TMEM192-FLAG-HA LOCALIZES TO LYSOSOMES 129

FIGURE 2-7- S2 ALPHAFOLD3 MODEL OF RABCONNECTIN-3 130

FIGURE 3-1- ALPHAFOLD3 MODEL OF RAV1 AND RAV2 BINDING 142

FIGURE 3-2 HYDROPHOBIC BINDING OF RAV2 TO RAV1. 143

FIGURE 3-3- ALPHAFOLD3 MODEL OF RAV1-SKP1 BINDING. 146

FIGURE 3-4 CRYOEM STRUCTURE OF RAVE-V1 (PARTIAL) 147

FIGURE 3-5 ALPHAFOLD3 MODEL OF DMXL1. 150

FIGURE 3-6 ALPHAFOLD3 MODEL OF HUMAN WDR7 AND WDR72. 153

FIGURE 3-7 ROGDI BINDING TO DMXL1 AND WDR7 158

FIGURE 4-1 ROGDI AS PART OF REVERSIBLE DISASSEMBLY 163

List of Tables

TABLE 2-1- YEAST STRAINS USED 126

TABLE 2-2 OLIGONUCLEOTIDES USED 128

Abbreviations

- **V-ATPase** - Vacuolar-type ATPase
- **AMPK** - AMP-activated protein kinase
- **mTORC** - Mechanistic target of rapamycin complex
- **GEF** - Guanine nucleotide exchange factor
- **TRPV** - Transient receptor potential V
- **LBK1** - Liver kinase B1
- **MMPs** - Matrix metalloproteinases
- **SCF** - Skp, Cullin, F-box containing complex
- **RAVE** - Regulator of H+-ATPases of Vacuolar and Endosomal membranes
- **DMXL** - DmX-like
- **WDR** - WD repeat domain
- **PI(4)P** - Phosphatidylinositol 4-phosphate
- **PI(3)P** - Phosphatidylinositol 3-phosphate
- **PI(3,5)P2** - Phosphatidylinositol 3,5-bisphosphate
- **PI(4,5)P2** - Phosphatidylinositol 4,5-bisphosphate
- **PIP** - Phosphoinositide phosphate
- **dRTA** - Distal renal tubular acidosis
- **AI** – Amelogenesis Imperfecta
- **ER**- Endoplasmic Reticulum

Chapter 1

Introduction

1.1 V-ATPase structure and function

V-ATPases are highly conserved rotary proton pumps present among all eukaryotes. V-ATPases are primarily located on intracellular membranes. V-ATPases are composed of two distinct subcomplexes: V_1 and V_0. V_0 is an integral membrane complex, while V_1 is peripheral and extends into the cytosol. V-ATPases use the free energy released through ATP hydrolysis to move protons across a membrane. The active transport of protons enables the regulated acidification of intracellular compartments and generates a proton-based electrochemical gradient. The low pH in the lumen of lysosomes and vacuoles provides an appropriate environment for resident acid hydrolases. V-ATPases heavily influence lysosomal activity through the effect of pH on lysosomal enzymes. The pH sensitivity of acid hydrolases couples V-ATPase activity to the overall catabolic activity of the lysosome. This allows for changes to lysosomal activity to change to match cellular needs. For example, a V-ATPase-driven increase in lysosomal catabolic activity has been observed as a defining event in the maturation of dendritic cells (Trombetta, Ebersold et al. 2003, Liberman, Bond et al. 2014).

The spectrum of luminal pH across intracellular compartments is one driver of biosynthetic endosomal trafficking. The luminal pH of intracellular compartments decreases from the Golgi to late endosomes and lysosomes. As materials travel through endosomal compartments, the decreasing pH leads to conformational changes that release ligands when they encounter a certain pH (Elkin, Lakoduk et al. 2016). For example, the mannose 6-phosphate receptor transports proteins to endosomal compartments by binding mannose 6-phosphate tagged proteins in the trans-Golgi (pH 6.5) and will release

proteins later in the endolysosomal pathway as the pH decreases (Olson, Hindsgaul et al. 2008). V-ATPase mutations that impair activity and impact the ability to generate a pH gradient result in protein mislocalization. Membrane fusion also depends on V-ATPase-driven endosomal acidification. Yeast strains that carry loss of function V-ATPase mutations contained substantially more vacuoles than WT (Coonrod, Graham et al. 2013). Restoration of the pH gradient over endosomal membranes using a non-V-ATPase proton pump rescued membrane fusion, illustrating the dependence of membrane fusion of the V-ATPase generated electrochemical gradient (Coonrod, Graham et al. 2013).

V-ATPases are part of the emerging lysosomal signaling hub (Eaton, Merkulova et al. 2020). Two major nutrient sensing pathways function through the V-ATPase, mTORC and AMPK. When amino acids are abundant, mTORC is activated; when amino acids are scarce, mTORC is inactivated (Saxton and Sabatini 2017). AMPK is activated when the AMP/ATP ratio is high and is inactivated when the AMP/ATP ratio is lower (Hardie 2014). V-ATPases interact with mTORC indirectly through the Rag-Ragulator complex (Zhang, Jiang et al. 2014). The Rag-Ragulator complex is a protein scaffold and GEF (Guanine nucleotide exchange factor) for mTORC, enabling its activation. The interaction between V-ATPase and the Rag-Ragulator complex is amino acid sensitive and is a prerequisite for mTORC localization to the lysosomal membrane. Decreased amino acid availability (mTORC inactivation) results in increased V-ATPase assembly and a similar result can be attained by pharmacological mTORC inhibition (Eaton, Merkulova et al. 2020, Ratto, Chowdhury et al. 2022). AMPK functions in opposition to mTORC through aldolase-TRPV and axin-LBK1 complexes when in the presence of glucose. In the presence of glucose, aldolase activity is increased, and TRPV and axin-

LBK1 are recruited into the lysosomal membrane. They interact with the Rag-Ragulator complex, activating AMPK and inactivating mTORC (Eaton, Merkulova et al. 2020).

In multicellular organisms, V-ATPases have been adapted to perform specialized functions. In the kidney V-ATPases are localized to the plasma membrane, and instead of pumping protons into endosomal compartments, acidifying the urine (Brown, Paunescu et al. 2009). Decreases in the activity of these plasma membrane V-ATPases due to mutations result in distal renal tubular acidosis (dRTA) (Zhang, Fuster et al. 2014, Esmail, Kartner et al. 2018). Conversely, increased activity of plasma membrane V-ATPases results in increased invasiveness of some cancers (Capecci and Forgac 2013). V-ATPases conventionally used for specialized functions can be misused in some disease states. As a result, the global alteration of V-ATPase activity to treat disease may result in substantial side effects. An attempt to inhibit V_0a4-containing V-ATPases on the plasma membrane in some cancers could inhibit kidney V-ATPases containing the same isoform. These specialized functions will be discussed in more depth later.

1.1.1 V_1

V_1, the peripheral and soluble subcomplex, extends away from V_0 and the membrane into the cytosol. V_1 contains the following subunits: three A, three B, C, D, three E, three G, F, and H (Abbas, Wu et al. 2020). Subunits within V_1 are written in capital letters. V_1 is principally responsible for hydrolyzing ATP and creating rotation of a central stalk that is transmitted to V_0. The V_1A and V_1B subunits form a hexameric ring composed of alternating V_1A and V_1B subunits. There are 3 catalytic sites located at every other interface between the V_1A and V_1B subunits.

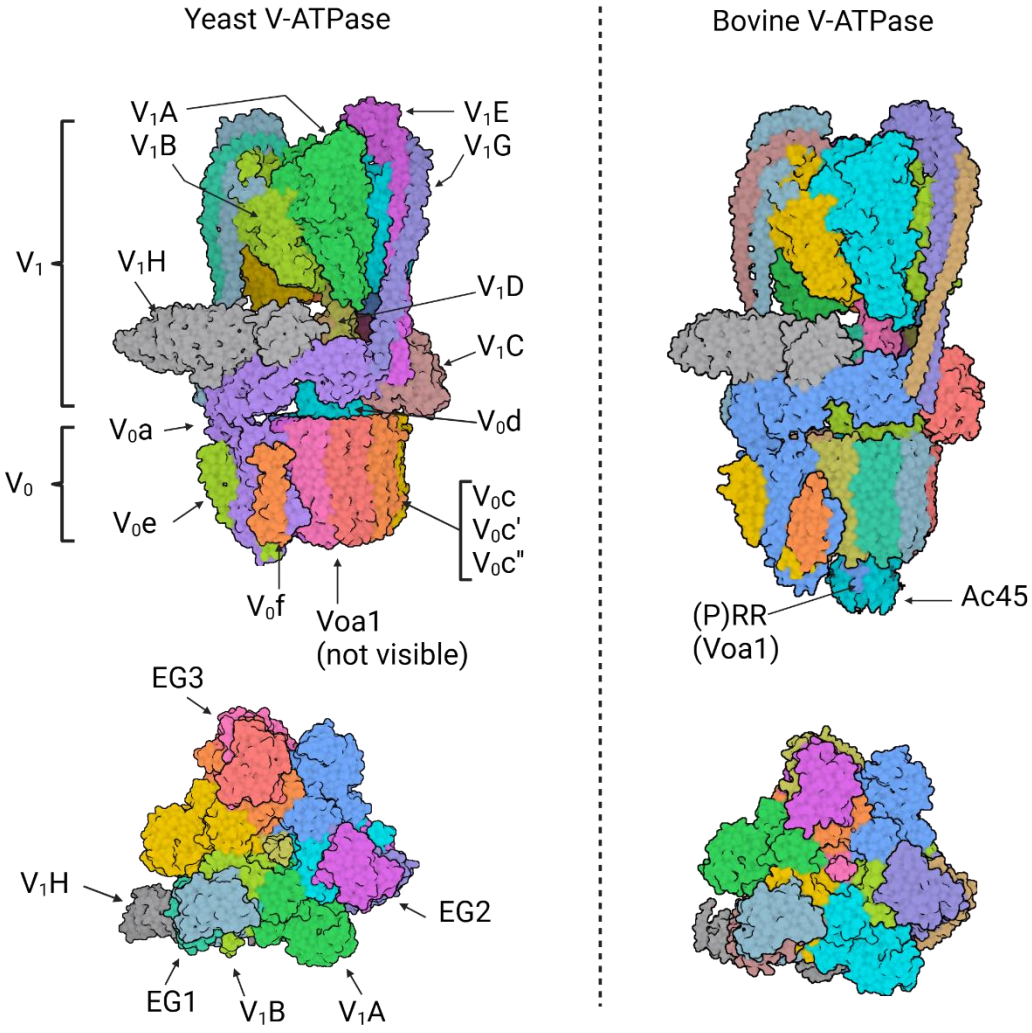

Figure 1-1- Structural comparison of eukaryotic V-ATPases

Yeast V-ATPase (left, PDB ID: 7FDA) and bovine brain V-ATPase (right, PDB ID:6XBW).

The V_1A/V_1B hexamer and catalytic cycle

At the core of V_1 is the alternating heterohexamer formed by alternating V_1A, B subunits. Recent work by Nakanishi et al (2018, 2022) shed light on the structural differences within V_1 during the catalytic cycle. At any point in the catalytic cycle, the catalytic sites take one of three conformations. There is an 'open' catalytic site which doesn't contain any bound ATP or ADP (Nakanishi, Kishikawa et al. 2018). A second catalytic site has a 'semi-closed' conformation and contains Mg-ATP. The final catalytic site takes a 'closed' conformation that contains ADP+Pi. This is the catalytic site that hydrolyzed ATP most recently. The closed conformation prevents the dissociation of ADP and inorganic phosphate from the binding site. The conformations that the catalytic sites take within V_1 are interchangeable; as a result, the conformation of catalytic sites 'rotate' clockwise (Kishikawa, Nakanishi et al. 2022) This rotation within V_1 is transmitted to V_o through the central stalk, resulting in the rotation of the V_oc proteolipid ring. There are three possible arrangements of catalytic site conformations: rotation states 1-3. A total 360° rotation results in the sequential adoption of each rotation state (Zhao, Benlekbir et al. 2015).

1.1.1.1 V_1D/F central stalk

As the catalytic cycle progresses within V_1, the central stalk (V_1D and V_1F) subunits rotate (Kishikawa, Nakanishi et al. 2022). V_1D inserts into the center of the bottom of the A/B hexamer and rotates with the conformational changes driven by ATP hydrolysis. V_1F binds to the end of V_1D stalk and connects to V_o (Wang, Wu et al. 2020).

1.1.1.2 V_1E/G peripheral stalk

The EG stalks function as stators, bracing V_1 against V_o and holding V_1 and V_o together. All three EG stalks contact the top of the A/B hexamer on one end and subunits at the V_1/V_o interface on the other. EG peripheral stalk 1 (EG1) binds to the interface between V_1H and V_oa. EG2 contacts the interface between the N-terminal domain of V_oa and the foot domain of V_1C. EG3 contacts the head domain of V_1C (Rahman, Yamato et al. 2013). The sum of the relatively weak interactions between the peripheral stalks and V_1 subunits holds V_1 to V_o (Oot and Wilkens 2012, Stam and Wilkens 2017). The V_1EG subunits are also flexible, allowing for small movements between V_1 and V_o resulting from the substantial conformational changes associated with V-ATPase activity.

1.1.1.3 V_1H Subunit

The V_1H subunit is a globular protein that contains distinct C-terminal and N-terminal domains connected by a flexible linker (Sagermann, Stevens et al. 2001). The larger N-terminal domain binds to the interface between the EG3 peripheral stalk and V_oa. Upon disassociation of V_1 from V_o, V_1H remains bound to V_1. One function of V_1H as a V-ATPase subunit is to stabilize the auto-inhibited form of V_1 following the dissociation of V_1 from V_o. Cytosolic V_1 from yeast strains that contain mutations in the gene encoding V_1H (VMA13) have significantly higher ATPase activity levels than wild-type strains (Parra, Keenan et al. 2000). Subsequent structural investigation has found that the V_1H c-terminal domain binds to the V_oa N-terminal domain under assembled conditions. Upon disassembly, The V_1H c-terminal domain releases from V_1H and binds to the V_1A/B

catalytic hexamer, stabilizing an ADP autoinhibited conformation in V_1 (Oot, Kane et al. 2016).

1.1.1.4 V1C subunit

The V_1C subunit is a 42 kDa dumbbell-shaped protein with a coiled-coil center and globular ends encoded by the yeast *Vma5* gene. The globular ends are asymmetrical; one domain is larger than the other. The larger domain is referred to as the 'foot' while the smaller region is the 'head' (Drory, Frolow et al. 2004). V_1C functions as a flexible stator, binding to the V_oa/EG2 interface with the foot domain and EG3 with the head domain (Zhang, Zheng et al. 2008, Oot and Wilkens 2012). V_1C binding to EG2 and EG3 aids in connecting the peripheral stalks with V_oa for their function as stators. Additionally, the binding between V_1C and the EG peripheral stalks and V_oa are relatively weak on their own but, when added together, are strong enough to hold V_1 to V_o (Oot and Wilkens 2012). It is thought that the use of several individually weak interactions enables the V-ATPase to disassemble by individually breaking the weak bonds between subunits (Oot and Wilkens 2012) V_1C is a unique V_1 subunit in that when V-ATPases are disassembled, V_1 is not associated with the V_1 or V_o subunits. Instead, V_1C dissociates independently. Due to this, V-ATPase disassembly is often referred to as 'tripartite disassembly.'

1.1.2 V_o

V_o is the subcomplex responsible for translocating protons across the membrane in which the V-ATPase is embedded. Overall, V_o structure is similar between mammalian and yeast V-ATPases, but there are minor differences in subunit composition. Human V-

ATPases contain: a, c9, c'', f (RNaseK), e, d, ATP6AP1, and ATP6AP2 (Abbas, Wu et al. 2020). Yeast V-ATPases contain a slightly different V_o composition, containing a, c8, c', c'', e, f, d, and Voa1p (Roh, Stam et al. 2018).

1.1.2.1 V_oc proteoplipid ring and coupling to V_1

Within V_o is a proteolipid subunit ring composed of V_oc subunits. The proteolipid ring is not symmetrical in either yeast or mammalian V-ATPases. Yeast V-ATPases contain eight c subunits, one c' subunit, and c'' subunit (Mazhab-Jafari, Rohou et al. 2016). The c' structurally resembles the V_oc subunit, while V_oc'' contains an additional N-terminal transmembrane helix with a linker that allows for its positioning in the center of the proteolipid ring (Roh, Stam et al. 2018). Although V_oc' and V_oc'' have slightly different structures, they are still functional for proton transport like other V_oc subunits. The V_oc and V_oc' subunits form a structure where every other α-helix on the outer surface of the proteolipid ring contains a glutamate residue that can be protonated and used for proton transport. The V_oc'' subunit breaks this pattern, placing a helix containing a glutamic acid directly adjacent to the glutamate-containing helix of the next V_oc subunit (Mazhab-Jafari, Rohou et al. 2016). This change in glutamic acid position serves as the position from where V_o can undergo reversible disassembly and prevents the free rotation of the proteolipid ring (Mazhab-Jafari, Rohou et al. 2016, Roh, Shekhar et al. 2020).

The V_1 D, F central stalk couples to V_o through V_od subunit, which binds the center of the proteolipid V_oc ring. The V_od subunit serves to couple rotation in the V_1D, F central stalk to the proteolipid ring. Study of a bacterial V-ATPase homolog from *Enterococcus hirae* revealed information about V_o function. Since there are a total of 10 total (eight V_oc, one c', one and c'') subunits comprising the proteolipid ring, there is a

step size of 36°, contrasting with the 120° step size within V_1 (Otomo, Iida et al. 2022). V_1 is rigidly coupled to V_o through the V_1D, F-V_od interactions. Incompatibility in step size between V_1 and V_o is alleviated through momentary pauses every 120°, which functionally decreases the V_o step size to less than 36° (Otomo, Iida et al. 2022). However, these findings were from a bacterial V-ATPase homolog, so there may be differences in eukaryotic V-ATPases.

Recently, a novel function for the V_oc subunit has emerged: initiating the non-canonical autophagic pathway CASM (**C**onjugation of **A**tg8 to **S**ingle **M**embranes). The CASM pathway is a mechanism where damaged endocytic compartments, often containing pathogens like viruses and bacteria, are labeled with lapidated Atg8/LC3 and fused with lysosomes (Wang, Ramos et al. 2022). Many pathogens infect cells by entering through the endocytic pathway and then escaping from these compartments into the cytosol as the vesicle becomes more acidic (Wang, Ramos et al. 2022). As a result, one of the major signals to initiate this pathway is through a substantial disruption of the pH gradient across a membrane. This process begins with an interaction between an ATG16L1-ATG5-12 complex and the V_oc subunit of fully assembled V-ATPase (Fischer, Wang et al. 2020). Upon binding of ATG16L1 to V_oc, LC3 (Atg8) is then lipidated and inserted into the affected membrane. The lipidated LC3 conjugated to the damaged membrane serves as a signal for the destruction of the labeled vesicle. Bacterial effector proteins interfere with this process, demonstrating the importance of the CASM pathway and the VATPase-ATG16L1 interaction. The *Salmonella* protein SopF has been found to act as a ribosyl-transferase that catalyzes the ribosylation of the ATG16L1 binding site on V_oc, preventing the initial induction of CASM (Xu, Cheng et al. 2022). A second protein

produced by *Legionella,* RavZ, catalyzes the irreversible de-lipidation of LC3/Atg8, effectively halting CASM (Choy, Dancourt et al. 2012). The evolution of both proteins illustrates the importance of the V-ATPase and CASM in cellular defense against pathogens.

1.1.2.2 V_0a subunit

The V_oa subunit contains a cytosolic N-terminal and transmembrane C-terminal domains. The V_oa NT subunit resembles a coiled-coil that runs parallel to the membrane at a 90° angle to the C-terminal domain. The C-terminal domain primarily functions to catalyze the transport of protons. The V_oa N-terminal domain serves as part of the interface between V_o and V_1 and binds to the V_1H, V_1EG, and V_1C subunits (Zhang, Zheng et al. 2008).

The C-terminal domain (CT) spans the width of the membrane and is positioned adjacent to the proteolipid ring. It contains two half channels; one directs protons from the cytosol into the space between V_oa and the V_oc ring. The second half channel is on the luminal side of the membrane and allows protons to exit the V_oa subunit. (Mazhab-Jafari, Rohou et al. 2016). Two key arginine residues (R735, R799) at the interface between V_oa and the V_oc ring facilitate the protonation of a glutamic acid residue (E137) on each c subunit of the proteolipid ring using protons that enter through the half-channel (Mazhab-Jafari, Rohou et al. 2016, Roh, Stam et al. 2018). The V_oc ring rotates clockwise, moving the newly protonated glutamic acid away from V_oa through the hydrophobic core of the membrane (Roh, Stam et al. 2018). After making a full rotation through the membrane, the protonated glutamic acid residue again reaches V_oa CT, where the second half channel

allows for the deprotonation of the glutamic acid and the release of the proton into the vesicular lumen (or extracellularly) (Mazhab-Jafari, Rohou et al. 2016).

1.1.2.3 V_{o}e subunit

The V_{o}e subunit is encoded by the *VMA9* gene in *S. cerevisiae* and the ATP6V$_{0}$E gene in humans. V_{o}e is a small (8.4 kDa) hydrophobic integral membrane protein that binds to the V_{o}a subunit within the membrane leaflet (Roh, Stam et al. 2018). Little is known about the function of V_{o}e; however, it appears to be essential for the proper V-ATPase function (Sambade and Kane 2004). Loss of V_{o}e results in a substantial decrease in protein levels of other V_{o} subunits (Compton, Graham et al. 2006), indicative of defective biosynthetic assembly. However, when V_{o}c is removed from the already formed V-ATPase by detergent solubilization, V-ATPase proton pumping activity functioned as before V_{o}e removal (Bueler and Rubinstein 2015). This highlights that the main function of V_{o}c in yeast may be during biosynthetic assembly and not during typical catalytic activity. A recent study has identified a novel function for V_{o}e in mammalian synaptic vesicles. The synaptic vesicle protein synaptophysin binds to the interface between V_{o}a and V_{o}e within the membrane leaflet (Coupland, Karimi et al. 2024, Wang, Jiang et al. 2024). This will be discussed in more depth later.

1.1.2.4 V_{o}f (RNase K) subunit

The V_{o}f subunit is also referred to as RNaseK and associates with V_{o}a, V_{o}c, and V_{o}e within the membrane leaflet (Roh, Stam et al. 2018). Like V_{o}e, relatively little is known about the function of V_{o}f as part of the V-ATPase. RNaseK was initially identified

as a part of a screen seeking to identify genes that impacted human rhinovirus (HRV) replication. Loss of RNAseK expression interfered with HRV replication, impaired clathrin-dependent and independent endocytosis, and impacted endosomal acidification (Perreira, Aker et al. 2015). RNaseK interacts with other V_o subunits, including V_oc'' and ATP6AP1, and may regulate their activity (Perreira, Aker et al. 2015). Further study is needed to better understand the function of RNaseK as part of the V-ATPase.

1.1.2.5 ATP6AP1, ATP6AP2, and Voa1p subunits

ATP6AP1, also called Ac45, is one of two accessory proteins found in mammalian V-ATPases. ATP6AP1 is a globular protein that binds to the luminal face of V_o. ATP6AP1 folds into a transmembrane α-helix connected to a β-prism connected. The helix inserts into the center of the proteolipid V_oc ring and interacts with the V_od subunit (Adams, Robinson et al. 2006, Abbas, Wu et al. 2020, Wang, Wu et al. 2020). The globular domain resides exterior to the V_oc ring on the luminal side of the membrane, contacting the V_oc subunits and ATP6AP2. ATP6AP1 shares homology with the LAMP (**L**ysosome **A**ssociated **M**embrane **P**rotein) family of proteins. LAMP is the most abundant lysosomal protein and is thought to partially protect the lysosomal membrane from luminal contents. Mutations in ATP6AP1 result in immunodeficiency, hepatopathy, cognitive impairment, protein glycosylation defects, and granular cell tumors (Jansen, Timal et al. 2016, Pareja, Brandes et al. 2018). These mutations are thought to manifest through the destabilization of ATP6AP1 and reduction in V-ATPase activity (Wang, Wu et al. 2020).

ATP6AP2 is a truncated form of the (pro)renin-receptor that traditionally functions in the renin-angiotensin signaling pathway and is the homolog of the yeast protein Voa1. ATP6AP2 is a small polypeptide that binds to the luminal face of V_o, interacting with ATP6AP1, V_oc, and V_oc'' (Wang, Wu et al. 2020). ATP6AP2 is homologous to the yeast protein Voa1p, which is necessary for proper V-ATPase biosynthetic assembly (Ryan, Graham et al. 2008). ATP6AP2 appears to function similarly in mammalian cells (Guida, Hermle et al. 2018). Loss of ATP6AP1 results in lethality in mouse cardiomyocytes through a mechanism that appears to result from impaired lysosomal activity (Kinouchi, Ichihara et al. 2010). Other studies have found that loss of ATP6AP2 in other tissues results in impaired endocytosis, V-ATPase activity, and lysosomal function (Trepiccione, Gerber et al. 2016, Figueiredo, Daryadel et al. 2021).

1.2 V-ATPase function in normal physiology

V-ATPases in multicellular organisms have been adapted to serve in specialized roles in addition to acidifying intracellular compartments that are different from maintaining homeostasis. V-ATPases within the membranes of synaptic vesicles use a V-ATPase-generated electrochemical gradient to sequester neurotransmitters within the vesicles. Within the kidney, plasma membrane V-ATPases work alongside other anion transport proteins to regulate acidifying the urine and control the acid/base equilibrium for the rest of the body. Within the immune system, V-ATPase activity and expression heavily influence the activity of lysosomes in phagocytic cells and, specifically, professional antigen-presenting cells, enabling the induction of the adaptive immune system. This is not an exhaustive list, but instead, a few examples that will be relevant later. All three of these mechanisms use the pH gradient (and its associated electrical component) in different ways to enable complex life.

1.2.1 V-ATPases in the synaptic vesicle cycle

The nervous system is an interconnected network of neurons that communicate with each other primarily through neurotransmitters. Individual neurons are separated from each other by small gaps called synapses. Within the synapse, neurotransmitters are released by pre-synaptic neurons diffuse throughout the synapse. Receptors on the surface of the post-synaptic neuron bind to the neurotransmitter and trigger the propagation of the signal. Synaptic vesicles go through a series of well-defined steps within the presynaptic neuron termed the synaptic vesicle cycle. The synaptic vesicles' journey within the presynaptic region can be broken down into well-defined steps: 1. Acidification and neurotransmitter loading, 2. Docking and priming with the presynaptic

membrane, 3. Fusion with the presynaptic membrane, 4. Endocytosis and recycling (Chanaday, Cousin et al. 2019). V-ATPases influence each step of the cycle in different ways.

As mentioned earlier, the canonical proton pumping activity of V-ATPases generates an electrochemical gradient across the membrane in which it is located. This electrochemical gradient ($\Delta\mu_{H+}$) is a sum of two components: a pH gradient (ΔpH) and an electrical gradient ($\Delta\Psi$) (Wieczorek, Brown et al. 1999). The high concentration of neurotransmitters present in synaptic vesicles requires active transport to achieve. The active transport of neurotransmitters into synaptic vesicles uses the V-ATPase-generated electrochemical gradient (Farsi, Jahn et al. 2017). Neurotransmitters use different aspects of the electrochemical gradient depending on their type.

Acetylcholine and monoamine neurotransmitters are transported using VMAT transporters and depend primarily on the ΔpH component (Anderson, King et al. 1982). Acetylcholine and monoamines are positively charged at physiological pH, contrasting with the vesicle lumen's positive charge. Two luminal protons are exchanged for each neurotransmitter molecule through VMAT transport proteins (Blakely and Edwards 2012).

Glutamate and ATP are another group of similarly behaving neurotransmitters. Glutamate is transported into synaptic vesicles through the VGLUT family of transporters while VNUT transporters transport ATP. Glutamate holds a negative charge at physiological pH, which complements the positive charge in the vesicle lumen. As a result, glutamate does not oppose the electrical component of the electrochemical gradient like acetylcholine. VGLUT transporters use a combination of the electrical

gradient ($\Delta\Psi$) and variable proton exchange (ΔpH) to move glutamate into synaptic vesicles (Martineau, Guzman et al. 2017, Kolen, Borghans et al. 2023).

The Vesicular GABA transporter (VGAT) transports GABA (gamma-aminobutyric acid) and glycine into synaptic vesicles. VGAT depends on both the pH and electrical components of the electrochemical gradient. VGAT, like VGLUT, exchanges luminal protons for neurotransmitters, but the dissipation of ΔpH does not abolish the uptake of neurotransmitters, indicating some dependence on $\Delta\Psi$ (Farsi, Jahn et al. 2017).

Following the V-ATPase-dependent uptake of neurotransmitters into synaptic vesicles, the vesicles migrate toward the presynaptic membrane. Synaptic vesicles undergo docking and priming, which is the partial binding with membrane fusion machinery like SNARE proteins, to facilitate rapid fusion with the presynaptic membrane (Chanaday, Cousin et al. 2019). The competency of synaptic vesicles to fuse with the presynaptic membrane is influenced by the presence of assembled V-ATPases on synaptic vesicles. V_1 is a large peripheral protein complex and is thought to sterically interfere with the ultimate fusion with the presynaptic membrane (Bodzęta, Kahms et al. 2017). As a result, V-ATPases must disassemble after neurotransmitter loading but before fusion with the presynaptic membrane. The signal for V-ATPase disassembly within the synaptic vesicle cycle is the luminal pH of the vesicle; synaptic vesicles with a more neutral pH display a higher proportion of assembled V-ATPases compared to vesicles with a more acidic pH (Poëa-Guyon, Ammar et al. 2013, Bodzęta, Kahms et al. 2017). The low pH of an acidified synaptic vesicle serves as a marker to trigger V-ATPase disassembly, allowing a particular synaptic vesicle to progress to the next step of the cycle (priming, fusion).

Recent studies have discovered a novel association between synaptic vesicle V-ATPases and the synaptophysin (Coupland, Karimi et al. 2024, Wang, Jiang et al. 2024). The function of synaptophysin is not precisely known, but it makes a stable complex with V-ATPases in synaptic vesicle membranes. The V-ATPase-synaptophysin interaction is mediated through the V_oe2 and V_oa subunits on the luminal side of the synaptic vesicle membrane (Wang, Jiang et al. 2024). The interaction between synaptophysin and V-ATPases appears to regulate the V-ATPase copy number on synaptic vesicles. Synaptophysin-null synaptic vesicles contained a 2.1-fold increase in the number of assembled V-ATPases and a 1.7-fold increase in only the V_o subcomplex. Synaptophysin-null mice exhibit heightened susceptibility to seizures induced by kainic acid (an excitatory neurotransmitter mimetic) compared to wild-type mice. This indicates that synaptophysin plays a vital role in synaptic regulation, possibly through regulation of V-ATPase number per synaptic vesicle (Wang, Jiang et al. 2024).

Following the fusion of synaptic vesicles with the presynaptic membrane, membrane material must be endocytosed to reform synaptic vesicles. Two main mechanisms accomplish this: clathrin-mediated endocytosis and ultrafast endocytosis (Watanabe, Rost et al. 2013, Milosevic 2018). During clathrin-mediated endocytosis, invaginations form on the presynaptic membrane which are coated with a clathrin protein coat (Kaksonen and Roux 2018). Vesicles will eventually separate from the cell membrane and enter the cell. Endocytosed clathrin-coated vesicles are uncoated and are either directly reacidified V-ATPases or merged with larger endosomal compartments and reform into new synaptic vesicles later (Kaksonen and Roux 2018). It has been found that V-ATPases strongly influence clathrin-mediated endocytosis through the trafficking of

cholesterol to the plasma membrane (Kozik, Hodson et al. 2013). When V-ATPase activity is disrupted, so is cholesterol trafficking to the plasma membrane. Cholesterol is thought to facilitate the formation of clathrin-coated vesicles by lowering the energy required for membrane scission (Kozik, Hodson et al. 2013).

1.2.2 V-ATPase function in the kidney

Within the kidney, the nephron is the functional unit responsible for blood filtration and urine production. The nephron is a series of tubes that allow for the secretion of waste and the absorption of needed material. One part of the nephron, the distal tubule, is lined with epithelia made of intercalated cells. There are two types of intercalated cells in the nephron: type A (A-IC) intercalated cells and type B intercalated (B-IC) cells (Brown, Paunescu et al. 2009). Both types of intercalated cells are rich in plasma membrane V-ATPases (Brown, Paunescu et al. 2009). A-ICs express V-ATPases have V-ATPases expressed on the apical membrane and AE1 (anion exchanger 1) on the basolateral membrane (Brown, Hirscht et al. 1988, Brown, Paunescu et al. 2009). B-ICs localize V-ATPases to both the basolateral and apical membranes and express the apical anion exchanger pendrin (Brown, Hirscht et al. 1988, Royaux, Wall et al. 2001, Brown, Paunescu et al. 2009). Both type A and type B intercalated cells express carbonic anhydrase, which catalyzes a reaction between water and carbon dioxide that forms bicarbonate and a free proton. V-ATPases on the apical surface pump protons into the nephron lumen while AE1 moves bicarbonate across the basolateral face, reabsorbing it into the body (Roy, Al-bataineh et al. 2015).

Given the importance of V-ATPase activity in intercalated cells, reducing V-ATPase activity impacts the kidney's acid/base regulation. Mutations in Voa, V_1B, and V_1C subunit isoforms reduce V-ATPase proton pumping activity and result in hypokalemic (Type 1) distal renal tubular acidosis (dRTA) (Zhang, Fuster et al. 2014, Esmail, Kartner et al. 2018, Fuster and Moe 2018, Jobst-Schwan, Klämbt et al. 2020). (Imai, Kaneko et al. 2016). Distal renal tubular acidosis is a disease state that results from insufficient plasma membrane V-ATPase activity on type A intercalated cells within the collecting duct (Wagner, Unwin et al. 2023). Acid resulting from carbonic anhydrase activity and other metabolic processes are not exported from the cell into the urine. As a result, individuals with hypokalemic dRTA retain more acid within the body and are more susceptible to bone disease, nephrocalcinosis, and nephrolithiasis (Fuster and Moe 2018). The increased acid results in poor absorption of calcium from the urine and increased absorption from bone and dietary sources of calcium, resulting in hypercalcinuria and bone disease (Fuster and Moe 2018). The combination of hypercalciuria and high urine pH results in the deposition of calcium phosphate stones in the kidney.

1.2.3 V-ATPases as part of immunity

Phagocytic immune cells, including neutrophils, macrophages, and dendritic cells, function in part to engulf extracellular material and digest it. Phagocytic cells are an essential component of the innate immune system, serving as a first line of defense against pathogens. Phagocytic cells engulf and degrade pathogens using a specialized compartment called the phagosome. The phagosome begins as an early phagosome with a pH of approximately 5.5 (Flannagan, Jaumouillé et al. 2012). Early phagosomes fuse with early endosomes and multivesicular bodies, incorporating endosomal proteins,

including V-ATPases. Phagosomes eventually fuse with lysosomes, creating a phagolysosome (Flannagan, Jaumouillé et al. 2012). Phagolysosomes contain acid hydrolases characteristic of lysosomes, enabling the endocytosed material's breakdown. A small subset of phagocytic cells, called antigen-presenting cells, can present peptides that originated as phagocytosed cargo to other immune cells to activate the adaptive immune system (Sprent 1995). The dependence of phagocytic cells on lysosomal activity means that V-ATPases heavily influence the activity of these cells. For example, dendritic cell maturation includes the upregulation of lysosomal activity. Maturation triggers lysosomes to become more acidic, increase acid hydrolase content, and stabilize V-ATPase assembly on lysosomal membranes (Trombetta, Ebersold et al. 2003, Liberman, Bond et al. 2014). MHC class II are proteins used by the immune system to identify foreign proteins and trigger the appropriate immune response. Following initial MHC class II synthesis endoplasmic reticulum, MHC II are transported to a late endosomal compartment where the MHC II are further processed and bound to a peptide (Neefjes, Jongsma et al. 2011). The MHC II-peptide complex is then transported to the cell surface, where the antigen is presented to other immune cells.

In addition to influencing phagocytosis and antigen presentation, V-ATPase activity influences viral infection and the viral life cycle. Some viruses, including the influenza virus, invade cells by binding to surface receptors, are endocytosed, and then escape from an endocytic vesicle to infect the cell. In the case of the influenza virus, the decrease in endosomal pH that occurs as endocytic compartments mature serves as a trigger that enables conformation changes in viral proteins, which allow its escape from the endosome (Marjuki, Gornitzky et al. 2011).

1.2.4 V-ATPases in cancer

V-ATPase activity has been implicated in the development, progression, and treatment of cancer. As a result, V-ATPases have emerged as a target for cancer therapy. However, given their essential function, global inhibition is not a viable option.

A well-established hallmark of cancer is the dysregulation of pH. Typically, cell cytosol is tightly regulated to a pH of 7.2, which contrasts with the extracellular pH of 7.4 (Casey, Grinstein et al. 2010). However, cancer cells are observed to have a cytosolic pH greater than 7.2 with an extracellular pH below 7.1 (Webb, Chimenti et al. 2011). The increase in cytosolic pH results from increased acid secretion from cells using proton pumps at the cell surface. V-ATPases are one of the classes of enzymes observed to be responsible for this shift in acid balance. The increased cytosolic pH has numerous downstream effects, including increasing the rate of cell division by encouraging faster progression through the cell cycle and inhibiting cell death through apoptosis (Webb, Chimenti et al. 2011). Increased cytosolic pH increases the activity of CDK1, which governs the entrance to the G2/M phase of the cell cycle (Putney and Barber 2003). At the same time, many caspases that are responsible for propagating the signaling cascades responsible for apoptosis function ideally in an acidic environment, the alkaline pH of cancer cells effectively inhibits the pro-apoptotic activity of caspases (Matsuyama, Llopis et al. 2000). The alterations in both processes contribute to the rapid, uncontrolled growth seen in most types of cancer.

A common metabolic change that cancer cells undergo is shifting from typical aerobic metabolism towards ‘aerobic glycolysis’ or the Warburg effect (Gatenby and

Gillies 2004). The Warburg effect describes that cancer cells prefer fermentative glycolysis for most ATP generation, even though oxygen is present. The dramatic increase in glycolysis followed by lactic acid fermentation increases the accumulation of lactic acid, which would decrease cytosolic pH if not dealt with. The rise in acid production is at odds with the earlier mentioned alkalinity of cytosolic pH of cancer cells. The solution is that acid produced as part of glycolysis is secreted from cells into the extracellular space, causing the characteristic acidic cancer microenvironment (Gatenby and Gillies 2004). Additionally, glycolysis is partially regulated in part by cytosolic pH, using the production of lactic acid as a negative feedback mechanism (Ui 1966, Webb, Chimenti et al. 2011). Increases in cytosolic pH effectively eliminate this regulatory mechanism, which results in even more lactic acid production and further acidification of the extracellular space.

The acidification of the extracellular space contributes to mobility and increases the metastatic potential of cancer. This is accomplished by activating extracellular proteases and exocytosis of lysosomal proteases like cathepsins (Hinton, 2009 #26}. More invasive cancer cell lines contain more V-ATPase at the plasma membrane when compared to less invasive cell lines, indicating that plasma membrane V-ATPase activity contributes to invasiveness (Sennoune, Bakunts et al. 2004). Subsequent research has found that MB231 cell lines (an invasive human breast cancer cell line) contained substantially higher levels of V_oa3 and V_oa4 compared to the MCF7 cell line (a less invasive human breast cancer cell line) (Hinton, Sennoune et al. 2009). The V_oa3 and V_oa4 subunits have been documented as translocated to the plasma membrane in some cancers (Cotter, Liberman et al. 2016, McGuire, Collins et al. 2019). Knockdown of V_oa3

expression in another invasive breast cancer cell line (MCF10CA1a) resulted in a decrease in invasiveness alongside the reduction of V_0a3 expression; similar results were seen by treatment with concanamycin-A (Capecci and Forgac 2013). It is hypothesized that the increased V-ATPase activity at the plasma membrane substantially contributes to the decreased extracellular pH, increasing the activity of extracellular proteases (Chen, Kang et al. 2022). The activity of the proteases impacts the integrity of the extracellular matrix surrounding the tumor, allowing cells to escape the primary tumor site and metastasize to other tissues.

1.3 V-ATPase regulation

V-ATPase regulation is multifaceted and integrates several regulatory signals that influence V-ATPase activity. Over time, it has been discovered that no single regulatory pathway completely controls V-ATPase activity. Instead, several distinct mechanisms work together to influence V-ATPase activity. Reversible disassembly is a process where the V_1 subdomain separates from V_0, and both become catalytically inactive. When proper conditions are met, the V_1 subcomplex reassociates with V_0, and activity resumes. V-ATPases are also sensitive to the membrane's local phosphoinositide content. Binding with the appropriate phosphoinositide lipid enhances V-ATPase activity and aids in intracellular localization. Lastly, V-ATPases also have more than one isoform for some subunits. The expression of subunit isoforms enables organellar and tissue-specific V-ATPase activity.

1.3.1 Subunit composition

In *S. cerevisiae,* only one subunit has more than one isoform. The yeast V_oa isoforms are Vph1 and Stv1 (Manolson, Proteau et al. 1992, Manolson, Wu et al. 1994). Vph1 containing V-ATPases localizes to the vacuole (Manolson, Proteau et al. 1992), enabling the enzyme to undergo reversible disassembly (Smardon, Diab et al. 2014). Stv1 containing V-ATPases localizes to the Golgi (Manolson, Wu et al. 1994, Finnigan, Cronan et al. 2012) and does not undergo reversible disassembly (Qi, Wang et al. 2007, Smardon, Diab et al. 2014). Expression of different V_oa isoforms allows for subpopulations of V-ATPases with different properties and localization to different intracellular locations. Mammalian V-ATPases contain a substantially greater number and variety of isoforms. In humans, four V_oa isoforms localize to different cellular compartments based on the PIP binding preference of each V_oa isoform (Chu, Zirngibl et al. 2021, Chu, Yao et al. 2023, Mitra, Winkley et al. 2023). It is not currently known which isoforms can undergo reversible disassembly (Tuli and Kane 2023). Humans contain the following additional isoforms for V_1 subunits: V_1B1, V_1B2, V_1C1, V_1C2, V_1E1, V_1E2, V_1G1, V_1G2, and V_1G3. In addition to the V_oa1-V_oa4 isoforms, there are V_od1, V_od2, V_oe1, and V_oe2 (Toei, Saum et al. 2010).

V-ATPase subunit isoforms display varying tissue and cell enrichment, enabling specialized V-ATPase function and fine-grained regulation. For example, the V_oa1 isoform is highly expressed in neurons (specifically the brain) and is localizes to synaptic vesicles (Wang, Jiang et al. 2024) but is expressed at a basal level in all cells. The V_oa4 isoform is primarily expressed in the kidney and some secretory tissues like salivary glands (Oka, Murata et al. 2001). V-ATPase isoforms that, under normal conditions, show

tissue enrichment can be misused and mislocalized by cancers and contribute to cancer invasiveness (Collins and Forgac 2020). Overexpression and mislocalization of V_0a3 and V_0a4 containing V-ATPases to the plasma membrane increase the invasiveness of some cancers (Capecci and Forgac 2013, Cotter, Capecci et al. 2015).

The V_1B2 isoform is the predominant isoform and is expressed widely without tissue specificity. V_1B1, on the other hand, shares an expression pattern with the V_0a4 subunit isoform and is most highly expressed in the kidney and salivary gland (Uhlén, Fagerberg et al. 2015).

The V_1G1 subunit isoform is the isoform that is the most widely expressed, while the V_1G2 and V_1G3 isoforms display specificities to neurons and the kidney, respectively (Kawamura, Sun-Wada et al. 2015). Based on their importance to the process (which will be discussed later), the V_1G isoforms are hypothesized to influence regulation by reversible disassembly. Little is known about the function of the other peripheral stalk isoforms, V_1E1 and V_1E2.

Both V_1C1 and V_1C2 are widely expressed genes. V_1C2 has been implicated as a genetic cause of dRTA, showing particular importance in the kidney. This is consistent with other V-ATPase subunits that have kidney enrichment or isoforms. It is not known what the functional differences are between the two V_1C isoforms. However, it is possible that, like V_1G, the different V_1C isoforms may impact reversible disassembly. Based on the stator function of the V_1C subunit, the different V_1C subunits may have structural differences, like different flexibility, which confer functional differences to V-ATPases containing them.

Little is known about the functional differences that the different V_oe and V_od isoforms confer to V-ATPases.

1.3.2 Reversible Disassembly

V-ATPases have a characteristic ability for the V_1 subcomplex to reversibly separate from the membrane-embedded V_o, causing catalytic inactivation of both subcomplexes (Figure 1-2). V-ATPase regulation by reversible disassembly is the regulated separation and reassociation of the V_1 and V_o subcomplexes. This process was initially observed in yeast (Kane 1995) and insects (Sumner, Dow et al. 1995) but well conserved among eukaryotes, including humans (Trombetta, Ebersold et al. 2003). Reversible disassembly is best understood in *S. cerevisiae* because of the wealth of existing V-ATPase knowledge. Reversible disassembly in *S. cerevisiae* is very sensitive to glucose (Kane 1995). Depriving yeast cells of glucose results in the rapid disassembly of V_1 from vacuole membrane-bound V_o, while the reintroduction of glucose triggers the rapid reassembly and reactivation of the complex. However, the precise signal that the V-ATPase receives is not known (Kane 1995, Parra and Kane 1998). While the signaling cascade is not fully understood, several proteins have been observed to influence V-ATPase activity when deleted. Three proteins, Ira1 and Ira2 (GAP in the Ras/cAMP pathway), Sch9 (S6K ortholog and TORC1 substrate), and PFK2 (Phosphofructokinase β subunit), have been found to impair different aspects of V-ATPase assembly. *Ira1*Δ and *ira2*Δ strains have a higher level of V-ATPase assembly when glucose is deprived, indicating that the activation of the Ras/cAMP/PKA pathway promotes V-ATPase assembly (Bond and Forgac 2008). V-ATPases in *sch9*Δ mutants are less responsive to

glucose deprivation; V-ATPases remain more assembled when glucose is deprived compared to wild type (Wilms, Swinnen et al. 2017). On the other hand, V-ATPases in *pfk2*Δ strains disassemble like wild type when glucose is removed, but do not reassemble when glucose is reintroduced (Chan, Dominguez et al. 2016). Replicative aging has also been observed to impact V-ATPase assembly. Cells with higher replicative ages have lower V-ATPase assembly basal levels than younger cells (Hashmi and Kane 2024). This is reversed by growing cells under caloric restrictive conditions.

Other eukaryotes have been observed to respond to different sets of signals in addition to glucose. Mammalian cells respond strongly to amino acid availability (Stransky and Forgac 2015, Collins, Stransky et al. 2020), glucose starvation (McGuire and Forgac 2018), and luminal pH (Rienmüller, Dreyer et al. 2012). While the basis for glucose sensitivity in yeast is not yet well understood, mechanisms underlying mammalian V-ATPase sensitivity to glucose and amino acids are relatively better known. Changes in assembly state response to amino acid levels are mediated through mTORC1. When the cell is replete with amino acids, mTORC1 is active and decreases V-ATPase assembly. However, the inactivation of mTORC1, either through a decrease in amino acid availability or pharmacologically (e.g., Torin-1), results in increased V-ATPase assembly and lysosomal catabolic activity (Ratto, Chowdhury et al. 2022). In HEK293T, a human kidney cell line, V-ATPase assembly state is sensitive to AMPK activity. When cellular energy levels drop, AMPK is active and increases V-ATPase activity. Pharmacological inhibition of AMPK prevents this increase in V-ATPase assembly (McGuire and Forgac 2018). The rise in V-ATPase assembly in response to a decrease in nutrient availability is paradoxical compared to yeast. It is thought that the response seen in mammalian cells is

to increase autophagic activity and lysosomal proteolysis during times of low nutrient availability (Mijaljica, Prescott et al. 2011). Luminal pH has been observed to influence V-ATPase assembly in mammalian systems (Poëa-Guyon, Ammar et al. 2013).

A relatively new group of proteins containing a TLDc domain have emerged as regulators of V-ATPase assembly (Eaton, Brown et al. 2021, Wilkens, Khan et al. 2023). Yeast contains two TLDc proteins, Oxr1 and Rtc5, while humans contain six TLDc proteins: NCOA7, OXR1, mEAK7, TBC1D24, IFI44, and TLDC2 (Wilkens, Khan et al. 2023). Oxr1 promotes V-ATPase disassembly in yeast, functionally counteracting efforts to reassemble V-ATPases (Khan and Wilkens 2024). Less is known about Rtc5 compared to Oxr1, the influence that Rtc5 has on V-ATPase assembly is still a matter of debate (Klössel, Zhu et al. 2024). All human TLDc proteins promote V-ATPase disassembly like yeast Oxr1, except for mEAK7 which stabilize assembled V-ATPases and increases activity (Oot and Wilkens 2024). TLDc proteins represent a substantial new mechanism to alter V-ATPase assembly. Increasing the activity of TLDc proteins (aside from mEAK7) would allow for a decrease in V-ATPase activity without inhibiting V-ATPase activity globally. Similarly, the development of an inhibitor for TLDc-V-ATPase binding may be able to increase V-ATPase assembly. This would benefit individuals with dRTA, increasing V-ATPase activity within intercalated cells and improving kidney function.

As mentioned earlier, V-ATPase results in the inhibition of both the V_o and V_1 sectors. Both ATP hydrolysis by V_1 and proton transport of V_o are paused in disassembled V-ATPases (Sumner, Dow et al. 1995, Gräf, Harvey et al. 1996). Uncontrolled hydrolysis of ATP by V_1 would seriously impact cellular ATP pools. Additionally, an unlocked proton pore would allow for the escape of protons from endosomal compartments,

allowing for the dissipation of the proton gradient. Dissipation of the electrochemical gradient would have knock-on effects, impairing intracellular protein trafficking, lysosomal storage disorders, and general impacts on cellular homeostasis. To avoid these scenarios, both V_1 and V_o have unique mechanisms that control catalytic activity in the disassembled complex.

V_1 activity is regulated through a combination of substrate-meditated inhibition by ADP binding (Kettner, Obermeyer et al. 2003, Huss and Wieczorek 2007), rotational state incompatibility with V_o (Abbas, Wu et al. 2020), and conformational changes by the V_1H subunit (Parra, Keenan et al. 2000, Diab, Ohira et al. 2009, Vasanthakumar, Keon et al. 2021). The binding of ADP to the catalytic sites within V_1 inhibits activity by preventing the binding of hydrolyzable Mg-ATP. V_1H binds to V_1 primarily through its N-terminal domain (NT), which interacts with the EG1 peripheral stalk (Diab, Ohira et al. 2009, Sharma, Oot et al. 2018). When V-ATPases are catalytically active, the C-terminal domain (CT) of V_1H is not tightly associated with V_1 and binds to Voa-NT (Sharma, Oot et al. 2018). Upon dissociation of V_1 from V_o, V_1H undergoes a conformational change, causing V_1H CT to release from V_oa NT and bind to the membrane face of the A/B hexamer, inhibiting V_1 activity (Oot, Kane et al. 2016). The conformational change of V_1H contributes to product-mediated inhibition by stabilizing a conformation of V_1A/B, which encourages ADP binding over ATP binding (Oot, Kane et al. 2016). This is due to a preference of V_1H CT for V_1 in rotation state 2. In this rotation state, the catalytic site V_1H interacts with is in the 'open' conformation. V_1H stabilizes state 2 and the open binding pocket, allowing for the binding of ADP (Oot, Kane et al. 2016). V_1 rotation state 2 is achieved following disassembly by interactions between V_1C and the V_1F subunit

following dissociation from V_o (Vasanthakumar, Keon et al. 2021). This enables the binding of V_1H to V_1 and subsequent inhibition to occur quickly after disassembly. In addition to binding to the V_1A/B catalytic subunits, V_1H CT binds to EG2, pulling the membrane end of EG2 towards V_1H and EG1 (Vasanthakumar, Keon et al. 2021). This interaction between EG2 and V_1H CT constrains the available conformation of V_1A and V_1B, preventing the hydrolysis of ATP and advancement from rotation state 2 to 3, providing another mechanism that pauses the V_1 catalytic cycle in state 2.

Autoinhibition of V_o upon disassembly is comparatively less understood compared to V_1. Upon dissociation of V_1 from V_o, the V_oa subunit (Vhp1) undergoes a conformational change where the N-terminal region contacts V_od (Couoh-Cardel, Milgrom et al. 2015). This interaction is not solely responsible for V_o inhibition but may be one of several mechanisms. A second mechanism is through the asymmetry of the proteolipid c-ring. As mentioned earlier, there is an asymmetry of V_oc subunits within V_o. In yeast, there are c' and c'' subunit isoforms in addition to c subunit. Mammals contain a single c'' in addition to the normal c subunits. The structural differences between the V_oc' and V_oc'' compared to V_oc may prevent reverse rotation of the proteolipid ring and proton leakage (Couoh-Cardel, Milgrom et al. 2015, Oot, Couoh-Cardel et al. 2017). Both mechanisms prevent the passive rotation of V_o and keep V_o locked in rotation state 3. The incompatibility between V_o (state 3) and V_1 (state 2) would also discourage passive V-ATPase reassembly (Stam and Wilkens 2017). The realignment of rotation states between V_1 and V_o serves as an additional barrier to V-ATPase assembly.

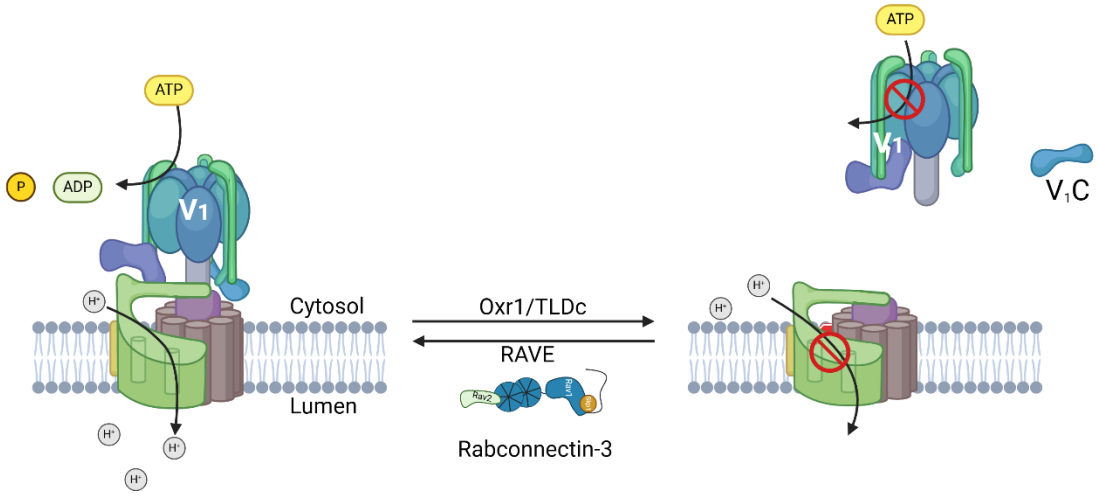

Figure 1-2 Overview of Reversible Disassembly

Under certain conditions V-ATPases will reversibly disassemble. The V_1 subcomplex and V_1C subunit disassociate from V_0 and both subcomplexes become inactive (Right). When conditions are met, V_1 and V_0 will reassemble with V_0 and both subcomplexes will resume catalytic activity (Left). V-ATPase disassembly is catalyzed by Oxr1 and other TLDc domain-containing proteins, while reassembly is catalyzed by RAVE.

1.3.3 Phosphoinositide lipids

Phosphoinositide Phosphate lipids (PIP) make up a small fraction of the total lipid content in cells. Still, they are essential in distinguishing intracellular compartments and modulating protein activity (Posor, Jang et al. 2022). PIP lipids are a subclass of phospholipids with an inositol headgroup that can be differentially phosphorylated, changing their identity. Specific lipid kinases and phosphatases catalyze the addition and removal of phosphate groups from the inositol ring, allowing for the interconversion of PIP lipids in membrane compartments as they move throughout the cell. For example, PI(4)P is enriched within the Golgi while endosomes and lysosomes are rich in PI3P and PI(3,5)P2, and the plasma membrane is rich in PI(4,5)P2 (Posor, Jang et al. 2022). Proteins contain PIP lipid-interacting domains that aid intracellular localization and modulating activity (Stahelin, Scott et al. 2014, Posor, Jang et al. 2022). For example, under starvation conditions, lysosomes that are traditionally located in the cell periphery and contain largely PI(3,5)P2 will accumulate at the cell center, and the membrane is remodeled to contain primarily PI(4)P (Ebner, Puchkov et al. 2023). The shift from PI(3,5)P2 to PI(4)P enables a change in the proteins associated with the lysosomal membrane to support the cellular response to starvation.

V-ATPases do not contain a conventional PIP lipid-binding motif like a pleckstrin homology domain (Lemmon 2007), but do interact with a subset of PIP lipids. Vph1 containing V-ATPases interact with the lysosomal/vacuolar PI(3,5)P2 lipid (Li, Diakov et al. 2014). Binding of PI(3,5)P2 stabilizes the interaction between V_1 and V_o, promoting assembly, and increasing V-ATPase activity (Li, Diakov et al. 2014, Banerjee, Clapp et al. 2019). Stv1 containing V-ATPases interact with PI4P, facilitating its Golgi retention

(Banerjee and Kane 2017). Like Vph1, Stv1 activity is increased by binding to PI(4)P, its corresponding PIP lipid (Vasanthakumar, Bueler et al. 2019). Mammalian V0a isoforms also display binding preferences to PIP lipids. Human V0a1 interacts with PI(3)P and PI(3,5)P2 and V$_O$a2 interacts with PI(4)P (Banerjee and Kane 2017, Mitra, Winkley et al. 2023, Chu, Yao et al. 2024). The human V$_O$a4 isoform binds to PI(4,5), a plasma membrane-enriched PI lipid (Chu, Yao et al. 2023). This is consistent with the plasma membrane localization of V$_O$a4 Like in yeast, mammalian V$_O$a isoform localization is influenced by PIP lipid localization (Chu, Yao et al. 2023, Chu, Yao et al. 2024). The preferential binding of V$_O$a isoforms to specific PIP lipids adds a layer of regulation beyond the binary activation and inactivation of the entire complex through reversible disassembly.

1.3.4 RAVE Complex - **R**egulator of H+-**A**TPases of **V**acuolar and **E**ndosomal membranes

The RAVE complex was first formally identified by Seol et al. in 2001. RAVE was an incidental finding while searching for novel Skp1 binding partners involved in Skp1-Cullin-F-box ubiquitin ligases (Seol, Shevchenko et al. 2001). RAVE is a heterotrimer with three subunits: Rav1, Rav2, and Skp1 (Seol, Shevchenko et al. 2001). RAVE has since been shown to function both in the biosynthetic assembly of V-ATPases following their exit from the endoplasmic reticulum and the reversible disassembly of V-ATPases on the vacuolar membrane (Seol, Shevchenko et al. 2001, Smardon, Tarsio et al. 2002, Smardon and Kane 2007). Strains carrying RAVE mutations display a partial Vma- phenotype termed a Rav- phenotype. The similarity between the Vma- and Rav- phenotypes stems from V-ATPase assembly defects in RAVE mutants. The resulting

decrease in V-ATPase activity resulting from RAVE mutations phenocopy V-ATPase mutations that result in reduced activity. RAVE mutants only display a partial Vma- phenotype because RAVE is an isoform-specific complex; RAVE only catalyzes the reassembly of Vph1 containing V-ATPases. Stv1p containing V-ATPases are insensitive to RAVE-catalyzed reassembly (Smardon, Diab et al. 2014). Strains carrying RAVE mutations have a growth phenotype that is sensitive to elevated pH, the presence of calcium and zinc, and elevated temperature (Seol, Shevchenko et al. 2001, Smardon, Tarsio et al. 2002) that parallels the Vma- phenotype (Nelson and Nelson 1990). This is because RAVE mutations directly result in impaired V-ATPase activity. In addition to defective growth under certain conditions, isolated vacuoles displayed both lower V-ATPase assembly and concanamycin-A sensitive ATPase activity (Smardon, Tarsio et al. 2002), consistent with Vph1 containing V-ATPases being affected by RAVE activity.

1.3.4.1 Rav1

Rav1 can be thought of as the backbone of the RAVE complex. It is the largest of the three RAVE subunits at 156 kDa. A cryo-EM structure of RAVE-V_1 has only recently been published (Wang, Tarsio et al. 2024), previous work has used homology and predictive modeling to identify structurally distinct domains. There are 4 broad regions that Rav1 can be divided up into N-terminal β-propellers (1-725), a flexible partially-folded linker (679-898), an α-solenoid domain (840-1125), and a disordered C-terminal tail (1125-1357) (Figure 1-3) (Smardon, Nasab et al. 2015). Each region contains binding sites for different RAVE or V-ATPase subunits.

The N-terminal region of Rav1 (residues 1-725) contains WD40 repeats that are modeled to fold into two β-propellers (Smardon, Nasab et al. 2015). WD40 repeats are small structural motifs that often end with tryptophan-aspartic acid (WD) amino acids. WD40 repeats form β-strands, which fold into a tertiary structure called a β-propeller (Smith, Gaitatzes et al. 1999). β-propellers, a well-conserved structural motif, are characterized by their blade count and function in part to facilitate protein-protein interactions (Chen, Chan et al. 2011). Both Rav1 N-terminal β-propellers contain seven blades each. Residues 1-240 are responsible for the Rav1-Rav2 interaction and include four of seven blades within the first propeller (Smardon, Nasab et al. 2015, Wang, Tarsio et al. 2024). The second β-propeller binds to the N-terminal end of the α-solenoid region.

Following the β-propeller domain is a partially folded linker domain (679-898) that connects the β-propellers and α-solenoid domain. A well-conserved sequence of six amino acids in this region, $L^{757}PVYHP^{762}$, is indispensable for the RAVE-Vph1 (V_0) interaction (Jaskolka and Kane 2020). Deletion of the entire sequence, or a mutation of ^{760}YH->AA, causes the RAVE complex to lose the ability to cycle to the vacuolar membrane (Jaskolka and Kane 2020). The loss of RAVE localization to the vacuolar membrane impairs RAVE-catalyzed V-ATPase reassembly. These rav1-6Δ mutants display the earlier mentioned Rav- phenotype, and isolated vacuoles displayed both decreased V-ATPase activity and a lower content of V_1 subunits. This indicates that the $L^{757}PVYHP^{762}$ motif is the primary mechanism by which RAVE localizes to the vacuolar membrane. There are no additional domains identified in RAVE that would interact with membranes. Interestingly, the available AlphaFold structures for Rav1(Jumper, Evans et al. 2021) reveal the $L^{757}PVYHP^{762}$ sequence resides away from the surface, situated

between the β-propeller and α-solenoid domains. This suggests that a substantial conformational in Rav1 is necessary to enable binding to Vph1 and subsequently localize to the vacuolar membrane. The recently available RAVE structure also shows the Vph1 binding sequence located away from the surface, reinforcing that a conformational change in Rav1 likely occurs.

The next major domain, encompassing resides 840-1125, forms an α-solenoid. A-solenoids resemble a series of alpha-helices stacked side-by-side. The α-solenoid contains binding sites for V_1 through the EG peripheral stalks and V_1C (Smardon, Nasab et al. 2015). This is the region of the RAVE complex, which is directly responsible for V_1 binding. Recent structures of RAVE bound to a partial V_1 subcomplex illustrate how RAVE binds to V_1 at what is likely the start of the reassembly process. The structure shows RAVE binding through the Rav1 α-solenoid domain to the region of V_1, which EG3 would typically occupy (Wang, Tarsio et al. 2024). The RAVE-V_1 structure has a portion of V_1, including EG3, and a single V_1A/B pair missing. Based on previous yeast 2 hybrid data that show strong interactions between Rav1 and V_1E (Smardon, Nasab et al. 2015), this is likely the correct location for RAVE-V_1 binding, although there is a region of V_1 missing.

The final region of Rav1 is the disordered C-terminal tail. This region contains the binding site for Skp1, but the functional significance of this region is not known (Smardon, Nasab et al. 2015). Overexpression of Rav1 is lethal because the increased amount of Rav1 sequesters Skp1 away from other protein complexes, impairing other cellular processes. (Brace, Parkinson et al. 2006). This indicates that Rav1 is a substantial Skp1 binding partner.

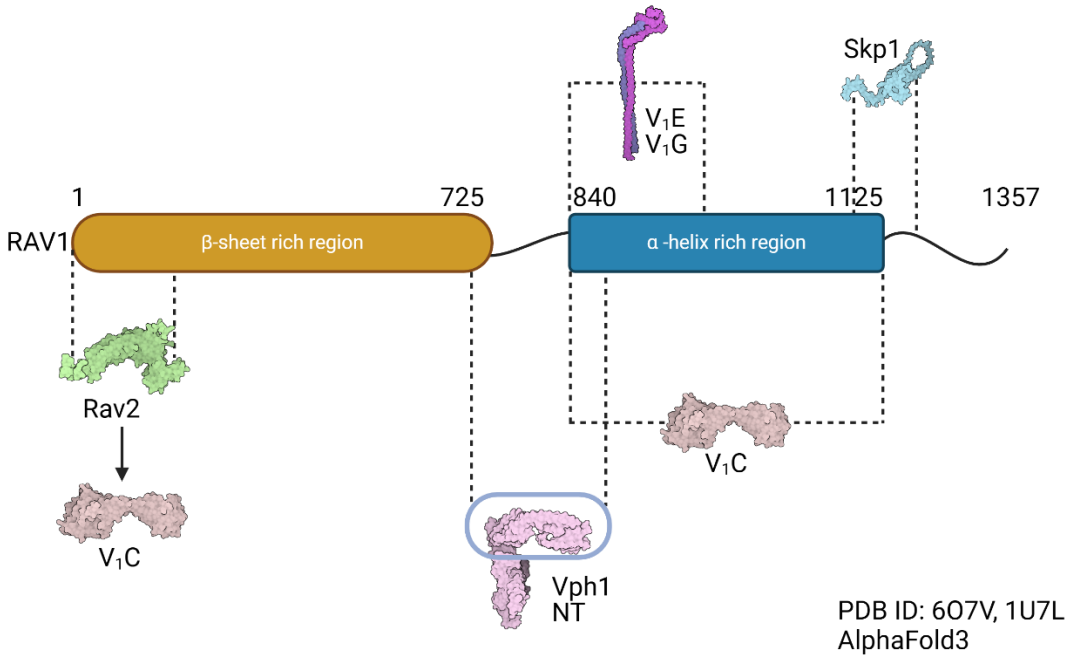

Figure 1-3 V-ATPase binding regions of Rav1

Rav1 N-terminal β sheet rich region binds Rav2; Rav2 binds to V1C. Rav1 binds Vph1 through a region between the β sheet rich region and α helix rich region. The α helix rich region binds V1E/G peripheral stalk and V1C subunit. Skp1 binds to the end of the α helix rich region and the disordered tail.

1.3.4.2 Rav2

Rav2 is the second and smallest of the V-ATPase-specific RAVE subunits. Relatively little is known about the function of Rav2 within the RAVE complex compared with Rav1. Rav2 (40kDa) is a much smaller protein compared to Rav1. It is known that Rav2 binds to V_1C and the N-terminal domain of Rav1. Like *rav1* mutations, *rav2* mutations result in a partial Vma- phenotype (Seol, Shevchenko et al. 2001). Additionally, vacuolar vesicles prepared from *rav2*Δ cells reflect lower V-ATPase activity and decreased V_1 subunit content (Smardon, Tarsio et al. 2002). Interestingly, although Rav1 contains the binding regions for V_1 and Vph1, both RAVE subunits are required for the proper intracellular localization of RAVE to the vacuolar membrane (Jaskolka and Kane 2020). The inability of *rav2* mutants to localize to the vacuolar membrane indicates that Rav2 aids in membrane localization directly, or Rav2 is essential in a step before the earlier mentioned Rav1 conformational change. The loss of Rav2 would stall the process and prevent Rav1 from binding to Vph1.

1.3.4.3 Skp1

SKP1 is an adaptor protein originally found to be connected to cellular morphology in budding yeast. Mutations in *SKP1* resulted in cells that stall during cell division. Cells stall at different points of the cell cycle depending on the specific *SKP1* mutation. Some appeared to have undergone DNA replication in S-phase, while others stalled before the checkpoint between G1 and S. It was thought at the time that this different phenotype was associated with a role related to the kinetochore, the structure responsible for separating the sister chromatids from the mother cell into the budding

daughter (Connelly and Hieter 1996). However, it was discovered later that while Skp1 is a component of the kinetochore complex, it also has a role as a subunit of the SCF ubiquitin ligase complex (Skp1, Cdc53, and various F-box proteins) (Kitagawa, Skowyra et al. 1999). Skp1 binds to both Skp2 and kinetochore subunits through an F-box motif (Bai, Sen et al. 1996). However, there is no F-box motif present in Rav1, meaning that Skp1-Rav1 binding is outside traditional SCF E3 ubiquitin ligase function (Seol, Shevchenko et al. 2001). There is limited understanding of what Skp1 does as part of the RAVE complex. A Skp1 mutant that prevented Rav1 binding showed defects in the release of RAVE from the membrane after RAVE completed catalyzing V-ATPase reassembly (Brace, Parkinson et al. 2006). Skp1 binds to RAVE and F-box proteins through distinct binding sites, allowing for the continued function of Skp1 as an SCF subunit but preventing binding to Rav1 (Wang, Tarsio et al. 2024).

1.3.5 RAVE and Reversible Disassembly

The complete process of RAVE-mediated V-ATPase reassembly is not entirely understood. However, previous work has identified possible conformational steps that RAVE and V_1 undergo before rejoining with V_o (Jaskolka, Tarsio et al. 2021). In this model, a series of conformation changes must occur to progress to the next step (Figure 1-4). It was found that V_1C binds more tightly to a RAVE-V_1 complex compared to RAVE alone (Jaskolka, Tarsio et al. 2021). This indicates a more favorable conformation in the RAVE-V_1 complex that enables V_1C binding than RAVE alone. As a result, forming a RAVE-V_1 complex is considered a prerequisite for creating the RAVE-V_1-V_1C complex. After the formation of the RAVE-V_1-C complex, the necessary components are

present for complete V-ATPase reassembly on the vacuolar membrane (Jaskolka, Tarsio et al. 2021). As mentioned earlier, early structural investigations into RAVE, specifically Rav1, suggest that a substantial conformational change is required to bind Rav1 to Vph1. This conformational change may be the result of the formation of the RAVE-V_1-V_1C complex. Given that the only identified binding partner of Rav2 is V_1C, the loss of Rav2 would likely impair the formation of this intermediate. This would result in stalling the reassembly process at forming the RAVE-V_1 complex. RAVE-V_1 wouldn't be competent for assembly, and V-ATPase assembly would occur. This provides a hypothesis for how *rav2* mutants result in impaired vacuolar localization, even without any domain that would interact with the membrane or any membrane-associated protein.

V-ATPase assembly in yeast is very sensitive to glucose; glucose deprivation results in rapid V-ATPase disassembly, and readdition results in the rapid reassembly of the complex (Kane 1995). The details of this signaling pathway are unknown, but it does not appear to depend heavily on the protein kinase C pathway (Parra and Kane 1998). Later study found that V-ATPase disassembly is sensitive to the activity of the Ras/cAMP pathway (Bond and Forgac 2008). Glucose-sensitive reassembly appears to be driven by RAVE instead of V-ATPase. RAVE cycles to and from the vacuolar membrane in a glucose-sensitive manner, irrespective of the presence of V_1 (Jaskolka and Kane 2020). This suggests that the glucose-sensitive component involved in V-ATPase reassembly is RAVE, not the V-ATPase itself. However, this explanation fails to clarify how glucose deprivation triggers V-ATPase disassembly, or the specific glucose-related signal RAVE receives. TLDc proteins may be sensitive to the signals for disassembly, while RAVE is sensitive to reassembly signals.

As mentioned earlier, when V-ATPases disassemble, there is an apparent mismatch between the rotational states of V_1 and V_o. Disassembled V_1 is locked in rotation state 2, while free V_o is locked in rotation state 3. Before V-ATPase is reassembled, the rotational states of the two subcomplexes need to be synchronized. It is thought that V_1 will adopt rotation state 3 to become competent for reassembly with V_o (Vasanthakumar, Keon et al. 2021). The mismatch in rotation states is a hurdle that needs to be overcome as part of reassembly. While there are portions of V_1 that are missing, the rotation state of V_1 can be determined. RAVE displays a preference for binding V_1 at a site near EG3 when V_1 in rotation state 3 (Wang, Tarsio et al. 2024). When V_1 dissociates from V_1, it is in rotation state 2, while V_o is in rotation state 3. The apparent mismatch in the rotational state between disassembled V_1 and V_o is considered a barrier for spontaneous reassembly that RAVE overcomes. The advancement of the V_1 catalytic cycle upon binding of RAVE aligns V_1 and V_o in rotation state 3, making V_1 competent for reassembly with V_o later.

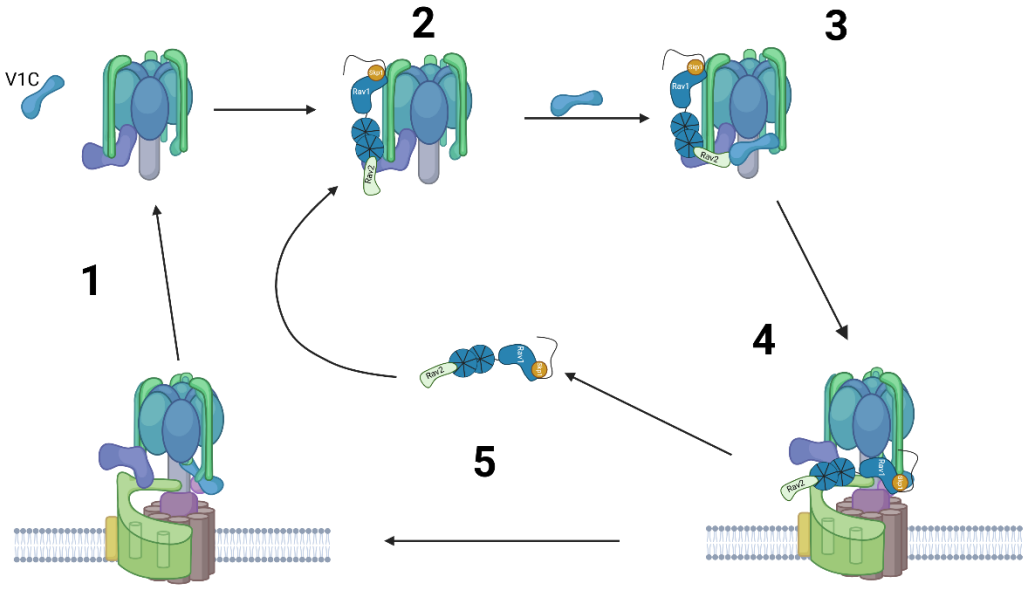

Figure 1-4 Steps of Reversible Disassembly

1- V-ATPase disassembly is catalyzed by Oxr1. Both V_1 and V_1C separate from V_o and become cytosolic. The catalytic activities of both V_1 and V_o are inactivated.

2- RAVE binds to cytosolic V_1 creating the RAVE-V_1 intermediate.

3- V_1C binds to the RAVE-V_1 complex, forming the RAVE-V_1-V_1C intermediate. This intermediate is ready for binding with V_o.

4- RAVE-V_1-V_1C localizes to the vacuolar membrane and V_1 and V_1C binds to V_o. Conformational changes within V_1 and V_o reactivate ATP catalyzed proton transport.

5- RAVE disassociates from assembled V-ATPase and becomes cytosolic, ready to begin the cycle again

1.3.6 RAVE as part of V-ATPase biosynthetic assembly

V-ATPase assembly occurs in the endoplasmic reticulum through a concerted pathway. During this process, V_0 and V_1 subunits are progressively added to the forming V-ATPase until the complex exits the endoplasmic reticulum (Figure 1-5) (Kane, Tarsio et al. 1999). Deletion of individual subunits impacts the V_1 and V_0 subcomplexes differently (Doherty and Kane 1993), indicating some separation between V_0 and V_1 biosynthesis.

The cytosolic nature of the V_1 subunits allows for the independent synthesis of individual subunits. These subunits then associate to form the complete V_1 subcomplex. As a result, deletion of either of the V_1A, V_1B, V_1E, or V_1C subunits does not impact the synthesis or stability of any of the individual subunits (Kane, Kuehn et al. 1992, Doherty and Kane 1993). However, loss of the V_1A, V_1B, or V_1E subunits results in a decreased pool of stable V_1 subcomplexes that contain all the required subunits (Doherty and Kane 1993). While the deletion of the gene encoding for an individual subunit does not impact the expression or stability of other subunits, it does affect the stability of the greater V_1 subcomplex. Based on glycerol gradient sedimentation experiments, V_1 subunits are assembled into the larger subcomplex in an order. The V_1A and V_1B subunits are among the earliest subunits to be incorporated into V_1, followed by the V_1E and V_1G peripheral stalk subunit (Doherty and Kane 1993). The V_1C subunit does not assemble with V_1 like the other subunits, owing to its ability to disassociate independently during tripartite disassembly.

Unlike the V_1 subunits, which are independently stable and synthesized independently, V_0 subunits show more interdependence on other subunits. Unlike V_1,

which can form various partially assembled subcomplexes, the loss of individual subunits during V_o assembly affects the stability of the overall subcomplex. Loss of V_oc subunit expression results in a substantial decrease in Vph1 subunit levels in whole-cell extracts and a complete absence of Vph1 in vacuolar samples (Kane, Kuehn et al. 1992). This demonstrates that Vph1 stability is dependent on the ability to properly assemble with the V_oc proteolipid core. The decrease in Vph1 levels in $V_oc\Delta$ mutants is the result of degradation in the endoplasmic reticulum (Hill and Stevens 1995). Additionally, the loss of Vph1 at the vacuole suggests that only fully assembled V_o is free to exit the endoplasmic reticulum. The loss of V_oc or Vph1 and the resulting decrease in functional vacuolar V_o results in exclusive localization of intact V_1 subunits to the cytosol since there are no functional V_o subcomplexes for V_1 to associate with on the vacuolar membrane.

While it appears that V_1 is competent to self-assemble in the cytosol independent of any additional assembly factors, V_o has been found to utilize three unique assembly factors (Vma12,21,22) in the endoplasmic reticulum that facilitate the assembly of V_o but are not present in the final assembled complex. An additional assembly factor, Voa1p (not to be confused with mammalian V_oa1 isoform), remains as a subunit post biosynthetic assembly (Ryan, Graham et al. 2008, Roh, Stam et al. 2018). Voa1p is a glycoprotein that resides in the center of the V_oc ring and contains an ER retention sequence that is blocked upon assembly (Wang, Bueler et al. 2023). Vma21 is an 8.5 kDa transmembrane protein that localizes to the endoplasmic reticulum using a retention sequence at the c-terminus (Hill and Stevens 1994). Disruption of *VMA21* results in the characteristic Vma- phenotype mentioned earlier, and purified vacuolar vesicles had no concanamycin-

sensitive V-ATPase activity. On a cellular level, *vma21*Δ mutants contain WT levels of V_1 subunits but substantially decreased levels of Vph1 (100kDa subunit). The vacuole contained very little to no Vph1 or V_1 subunits. Based on previous findings that indicate that a biosynthetic assembly defect resulting from either Vph1 or V_1C results in the degradation of V_o, it was determined that Vma21 is an assembly factor that catalyzes the initial assembly of V_o within the endoplasmic reticulum (Hill and Stevens 1994). Both Vma22 (21 kDa) and Vma12 (25 kDa) are transmembrane proteins that localize to the endoplasmic reticulum but don't have an endoplasmic reticulum retention tag like Vma21 but serve a similar function (Hirata, Umemoto et al. 1993, Hill and Stevens 1995). Loss of Vma22 and Vma12 results in Vma- phenotype like the loss of Vma21 and also results in the loss of V_o (Hirata, Umemoto et al. 1993, Hill and Stevens 1995).

Subsequent studies have revealed that Vma12 and Vma22 form a functional complex that binds to V_o during biosynthesis in the endoplasmic reticulum (Graham, Hill et al. 1998). Cryo-EM studies have shown that the Vma12-22 complex resembles a cap that binds superior to the V_od subunit where the central shaft of V_1 would connect to V_o (Wang, Bueler et al. 2023). Vma12-22 binds to both V_o with and without the Vph1, V_oe, and V_of subunits; however, it is unknown if the partial V_o-Vma12-22 structure is physiologically relevant. It is possible that this is an intermediate that occurs between Vma12-22 binding but before the recruitment of Vph1. Vma12-22 binds to the top of the V_od subunit through an interaction with the V_1F subunit (Wang, Bueler et al. 2023). V_1F primarily binds to V_1D but appears to be necessary for the binding of the Vma12-22 complex to nascent V_o. The structure of Vma12-22 resembles the V_1D subunit; together with the binding of Vma12-22 to the V_1F and V_od subunit points to its function. Vma12-

22 functions in part to prevent the association of V_1 to V_o while it is still in remains in the endoplasmic reticulum (Wang, Bueler et al. 2023). The luminal pH in the ER is neutral, with a pH of 7. The association of V_1 with V_o and activation of proton transport during synthesis would be very disruptive to ER luminal pH. In addition to preventing aberrant V-ATPase activation, Vma12-22 also catalyzes the addition of Vph1 to the V_oc proteolipid, indirectly adding V_oe and V_of to V_o (Graham, Hill et al. 1998, Wang, Bueler et al. 2023). Vma12 contains a C-terminal extension containing two transmembrane alpha helices, one of which binds directly to the N-terminal region of Vph1. This interaction between Vph1-NT and Vma12 stabilizes the association between Vph1 and the V_oc ring (Wang, Bueler et al. 2023). Following the recruitment of Vph1, V_oe, f to the V_oc ring a conformation change occurs where the V_oc ring settles into the energetically favorable conformation found in V-ATPases outside the ER. This conformational change triggers the potentially slow release of Vma12-22 from a now fully assembled V_o(Wang, Bueler et al. 2023). Vma21 binds primarily to the V_oc ring adjacent to Vph1, however there are additional weaker densities corresponding to Vma21 at other locations on the Voc ring (Wang, Bueler et al. 2023). It is not known what these additional Vma21 copies contribute to V-ATPase assembly.

Following the synthesis of V_o in the endoplasmic reticulum, it enters the biosynthetic trafficking pathway, which eventually delivers it to the vacuole (Figure 1-5). Since the Vma12-22 complex partially prevents the association between V_o and V_1 in the ER, V_1 must associate with V_o during travel through the Golgi and early endosomes to the vacuole. The initial association of V_1 with V_o during trafficking is likely catalyzed by RAVE, similar to the reversible disassembly that occurs at the vacuole (Smardon and

Kane 2007). Rav1 was independently discovered in a screen searching for genes influencing protein trafficking through the Golgi (Brace, Parkinson et al. 2006). A population of Rav1 was observed in the Golgi, an unconventional location for Rav1 based on its function on vacuole-localized V-ATPase. Given RAVE's importance in correctly assembling V-ATPases at the vacuole, it is likely that RAVE catalyzes the initial association between V_1 and V_0 as the V-ATPase travels to the lysosome.

V-ATPase biosynthetic assembly in mammalian systems is less understood than in yeast. However, some assembly factors are homologous to yeast Vma12, Vma21, and Vma22. The mammalian proteins TMEM199 and CCDC115 form a homologous complex to the Vma12-22 complex. Vma21 retains its name in mammalian cells. Disruption of the TMEM199-CCDC115 complex impacts cellular iron homeostasis through decreased V-ATPase activity (Miles, Burr et al. 2017). TMEM-199-CCDC115 localizes to the ER, suggesting that it is serving an analogous function to Vam12-22 (Miles, Burr et al. 2017). It is not currently known the mammalian RAVE homolog Rabconnectin-3 catalyzes V_1's association with V_0 following synthesis. However, based on the conservation of other aspects of V-ATPase biosynthesis, Rabconnectin-3 may function like RAVE.

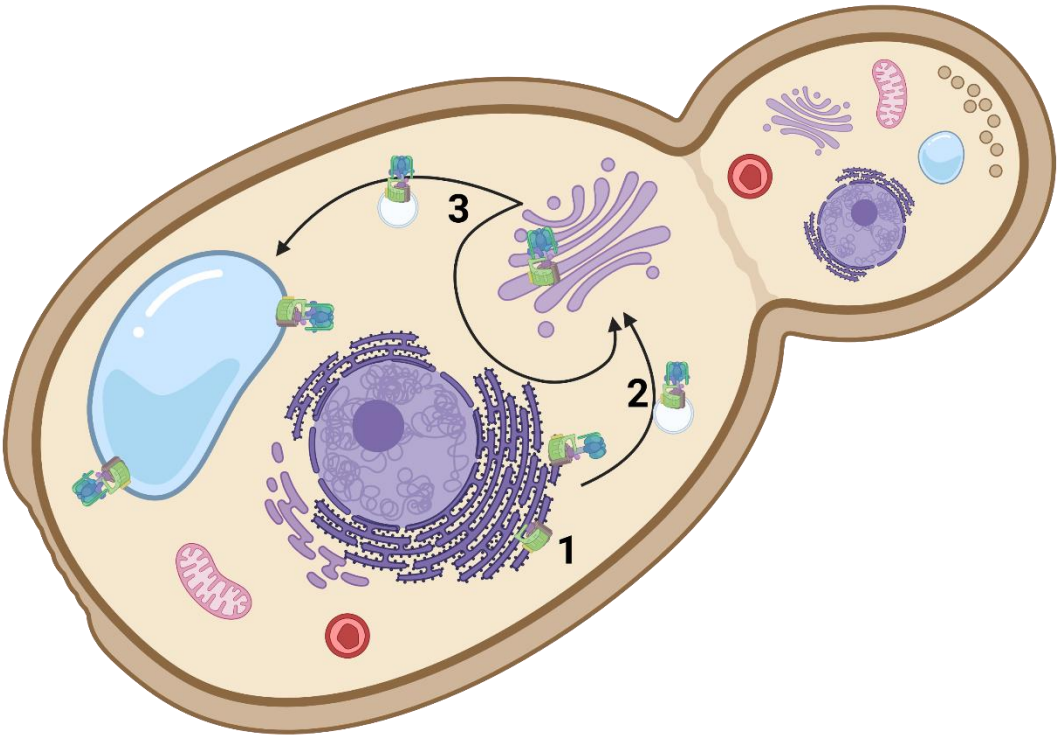

Figure 1-5 Intracellular schematic of V-ATPase biosynthesis

1. V-ATPase assembly begins in the endoplasmic reticulum. Assembly factors, including Vma12-22, Vma21, and Voa1, catalyze the assembly of V_o. V_1 subunits begin assembling with V_o subcomplexes.
2. Vma21 facilitates the exit of assembled V-ATPases from the endoplasmic reticulum. Additional V_1 subunits are recruited during trafficking to the Golgi Body.
3. While in the Golgi RAVE may catalyze the joining of V_1C with V-ATPases. Vph1 containing V-ATPases are trafficked to the vacuole, while Stv1 containing V-ATPases are retained in the Golgi.

1.3.7 Rabconnectin-3

V-ATPase regulation by reversible disassembly, like overall V-ATPase structure, is well conserved among eukaryotes. As organisms evolved to become more complex over evolutionary time, V-ATPases have taken on additional jobs beyond simply maintaining endolysosomal pH, which requires extra layers of regulation. For example, V-ATPase is the driving force behind neurotransmitter uptake into synaptic vesicles (Farsi, Jahn et al. 2017) and plasma membrane V-ATPase located in the kidney regulates urine acidification (Brown, Paunescu et al. 2009). Mammalian V-ATPases, like yeast V-ATPases, must be tightly controlled to maintain proper cellular and systemic homeostasis. Pathology can result if V-ATPase activity is disrupted by either increasing or decreasing activity. While overall V-ATPase regulation by reversible disassembly is conserved, the protein machinery that catalyzes reassembly is slightly different. Metazoans, including humans, have a protein complex called Rabconnectin-3 instead of RAVE. Rabconnectin-3 was first purified from a rat brain crude synaptic vesicle fraction and defined as a heterodimer of two proteins: DMXL2 (Rabconnectin-3α) and WDR7 (Rabconnectin-3β) (Nagano, Kawabe et al. 2002, Kawabe, Sakisaka et al. 2003). It is a stable complex with a Rabconnecin-3α-Rabconnectin-3β stoichiometry of 1:1 (Kawabe, Sakisaka et al. 2003).

Rabconnectin-3 has been found to function similarly to yeast RAVE. As mentioned earlier, RAVE mutations phenocopy V-ATPase mutations because of their direct impact on V-ATPase activity; the same is true for Rabconnectin-3. Rabconnectin-3 mutations phenocopy V-ATPases mutations that compromise catalytic activity (Yan,

Denef et al. 2009). Rabconnectin-3 mutants show decreased V-ATPase assembly and activity (Yan, Denef et al. 2009, Einhorn, Trapani et al. 2012, Eaton, Danielson et al. 2024) and endosomal trafficking defects often observed resulting from V-ATPase mutations (Marshansky and Futai 2008, Yan, Denef et al. 2009). Downstream processes that depend on endocytosis and endosomal trafficking, like Notch and Wnt signaling, are also affected (Yan, Denef et al. 2009, Tuttle, Hoffman et al. 2014).

While DMXL2/WDR7 was the first Rabconnectin-3 complex to be identified, additional isoforms were available for each subunit. Rabconnectin-3α has two isoforms DMXL1 and DMXL2 (Kraemer, Enklaar et al. 2000, Eaton, Danielson et al. 2024) while Rabconnectin-3β is speculated to include WDR7 and WDR72 (El-Sayed, Parry et al. 2009, Katsura, Nakano et al. 2022). There is substantially less data suggesting WDR72 as a Rabconnectin-3 subunit. However, WDR72 and WDR7 share homology (35% identity), and mutations in both WDR72 and kidney-enriched V-ATPase isoforms cause distal renal tubular acidosis (Jobst-Schwan, Klämbt et al. 2020). Each Rabconnectin-3 subunit has one isoform, which is more ubiquitously expressed, and another, which shows tissue-specific enrichment. DMXL1 and WDR7 are widely expressed and do not display any strong tissue specificity (Uhlén, Fagerberg et al. 2015). DMXL2 is highly enriched in the brain, neural tissues, and some glands. WDR72 is most highly expressed in the kidney and some secretory organs (Uhlén, Fagerberg et al. 2015).

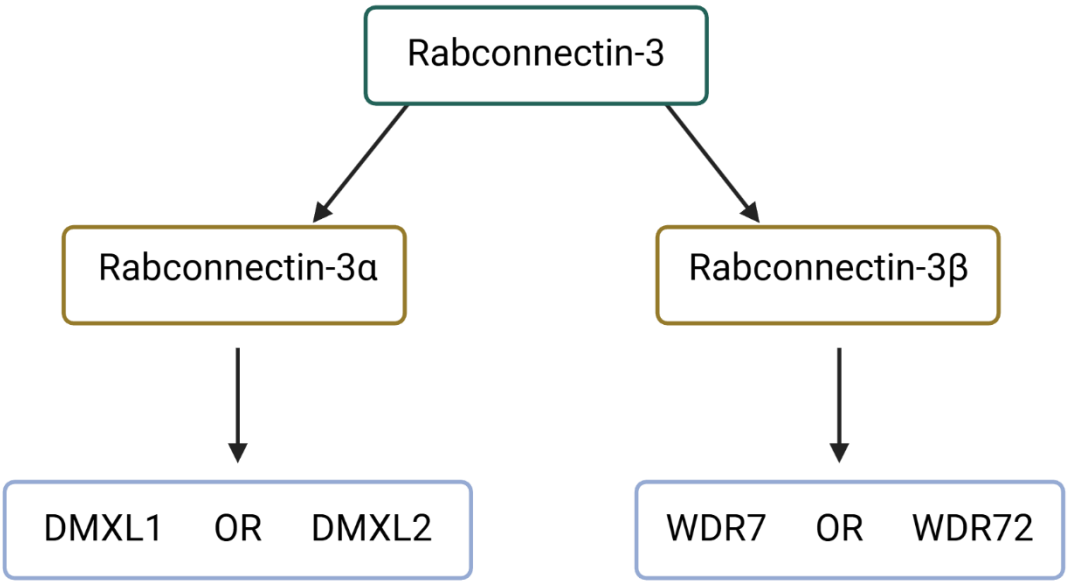

Figure 1-6 Schematic of Rabconnectin-3 isoforms

Rabconnectin-3 is a complex of two subunits: Rabconnectin-3α and Rabconnectin-3β. Rabconnectin-3α has two isoforms: DMXL1 and DMXL2. Rabconnectin-3β has two isoforms: WDR7 and WDR72. DMXL1 and WDR7 expression is not tissue specific while WDR72 and DMXL2 show tissue enrichment.

1.3.7.1 DMXL1

DMXL1 was initially discovered in *Drosophila melanogaster* and was termed *DmX* due to its discovery in *D. melanogaster* and its location on the X chromosome (Kraemer, Weil et al. 1998). DmX contains at least 30 WD repeats and 3427 amino acids, equaling about 380 kDa. It was described to be homologous to a yeast ORF of unknown function, which encodes a 155 kDa protein (Kraemer, Weil et al. 1998). This ORF would later be identified as *RAV1*. Two human homologs of the *DmX* gene were discovered one year later and termed DMXL1 and DMXL2 (DmX-like 1/2) (Kraemer, Enklaar,. DMXL1 and DMXL2 are smaller compared to *D. melanogaster* DmX. Human DMXL1 is 3,027 amino acids (338 kDa) and DMXL2 is 3,036 (340 kDa) (Kraemer, Enklaar et al. 2000). The *DmX* gene in *D. melanogaster* was later renamed to Rabconnectin-3A, following the identification of DMXL2.

1.3.7.2 DMXL2

The open reading frame and subsequent protein for DMXL2 were identified around the same time as DMXL1. However, DMXL2 has been much more thoroughly studied than DMXL1, partially due to its high expression in brain tissue. Crude synaptic vesicle fractions have historically been a preferred material to purify V-ATPase. Brain tissue is V-ATPase and Rabconnectin-3 rich compared to other tissues. DMXL2 was first functionally identified as a protein in the Rab3 interactome (Nagano, Kawabe et al. 2002). DMXL2 was found to coimmunoprecipitate with the Rab3 GAP and Rab3 GEF (GAP: GTPase activating protein; GEF: GTP/GDP exchange protein) (Nagano, Kawabe

et al. 2002). Rab3 is a small GTPase that shuttles to and from the membranes of intracellular vesicles, guiding intracellular trafficking through its GTP or GDP-bound state. Rab3 is important for the Ca^{+2} sensitive release of synaptic vesicles from the presynaptic neuron, consistent with the neuronal expression of DMXL2. DMXL2 was subsequently termed Rabconnectin-3 since it appeared to 'connect' Rab3 interacting proteins. Additionally, DMXL2/Rabconnectin-3α was highly expressed in the synaptic vesicle fraction from neurons, which is rich in Rab3. However, with time and continued study, the connection to Rab3 has become more distant.

1.3.7.3 WDR7

WDR7, also called Rabconnectin-3β, was first identified as a Rabconnectin-3α binding partner. Immunoprecipitation of DMXL2 or the Rab3 GEF or GAP from a crude synaptic vesicle fraction results in the coimmunoprecipitation of WDR7, indicating that WDR7 is a substantial binding partner of DMXL2. WDR7 is similar in size to Rav1, containing 1490 amino acids (168 kDa).

Over time, it has been found that other protein complexes interact with Rabconnectin-3 through the WDR7 subunit. CAPS1 (calcium-dependent activator protein for secretion 1) interacts with the membranes of dense core vesicles through WDR7 (Crummy, Mani et al. 2019). CAPS1 is a protein that is essential in the priming of both synaptic and dense core vesicles before fusion with the cell membrane (Jockusch, Speidel et al. 2007). Dense core vesicles are a specialized type of exocytic vesicles released from neuroendocrine cells and contain signaling peptides and other neurotransmitters. Like other intracellular vesicles, dense core vesicles depend on the pH gradient for cargo

uptake and eventual fusion with the plasma membrane. WDR7 is necessary for CAPS1 localization to dense core vesicles, and a knockdown of DMXL2, WDR7, or CAPS1 leads to dense core vesicles whose lumen is not acidic (Crummy, Mani et al. 2019).

1.3.7.4 WDR72

There is comparatively less known about WDR72 than DMXL1, DXML2, or WDR7. WDR72 is slightly smaller than WDR7; it has 1102 amino acids (123 kDa) but shares substantial homology with 37% direct homology and 58% similarity. There is little evidence currently linking WDR72 to other Rabconnectin-3 subunits, but there is more circumstantial evidence that WDR72 may function through the V-ATPase. The most substantial connection between WDR72 and the V-ATPase is through the development of dRTA. In addition to WDR72, congenital dRTA (distal renal tubular acidosis) is commonly caused by mutations in ATP6V$_0$A4, ATP6V$_1$B1, and SLC4A1 (Jobst-Schwan, Klämbt et al. 2020). ATP6V$_0$A4 encodes one V$_0$a isoform, which is enriched kidney and most highly expressed at the plasma membrane of intercalated cells of the distal tubule (Stehberger, Schulz et al. 2003). ATP6V$_1$B1 is an isoform of one of the two subunits which make up the catalytic hexamer in V$_1$. V$_1$B1 appears to enable V-ATPases containing this isoform to maintain higher levels of activity compared to V-ATPases containing V$_1$B2 (Finberg, Wagner et al. 2005). The homology between WDR72 and WDR7 and the phenotypic connections to V-ATPases highlight WDR72 as a potential Rabconnectin-3 subunit isoform.

1.3.8 Rabconnectin-3 as a regulator of V-ATPase assembly

Rabconnectin-3, like RAVE, has been found to facilitate the reassembly of V-ATPases. This is most often observed through changes in the acidification of intracellular organelles like lysosomes. However, other organelles depend on V-ATPase activity for proper function. Disruption of either Rabconnectin-3α or Rabconnectin-3β reduces LysoTracker intensity, suggesting from reduced V-ATPase activity (Yan, Denef et al. 2009, Sethi, Yan et al. 2010, Einhorn, Trapani et al. 2012). Additionally, a knockdown of DMXL1 or DMXL2 results in decreased lysosomal localized V_1B2, reflecting a decrease in V-ATPase assembly. This parallels the increase in pH seen in yeast strains carrying Rav- mutations. In addition to direct measurements of V-ATPase activity and assembly, defects in processes that depend on lysosomal acidification and endosomal trafficking have been observed. Two notable signaling processes instrumental in developmental signaling, Notch and Wnt, depend on the V-ATPase differently.

As mentioned earlier, mammalian V-ATPases alter their assembly state through Rabconnectin-3 through a variety of signals. However, unlike the Rav- phenotype observed in yeast, there is a greater variety of phenotypes when mutations occur in Rabconnectin-3 subunits.

1.4 Rabconnectin-3 related function and pathology

V-ATPases are an essential protein complex in most eukaryotes aside from baker's yeast, suggesting that V-ATPases play a role in processes that are indispensable. Like mutations in genes encoding V-ATPase subunits, Rabconnectin-3 mutations impair the function and development of a variety of tissues and organs throughout the body (Figure

1-7). Additionally, Notch and Wnt signaling are two developmental processes that depend on the V-ATPase and Rabconnectin-3. Both Notch and Wnt are pathways where a ligand binds to a receptor on the cell surface, and after intracellular processing, a transcription factor can affect the transcription of target genes. Changes in V-ATPase and Rabconnectin-3 activity can impact the downstream targets of these signaling pathways.

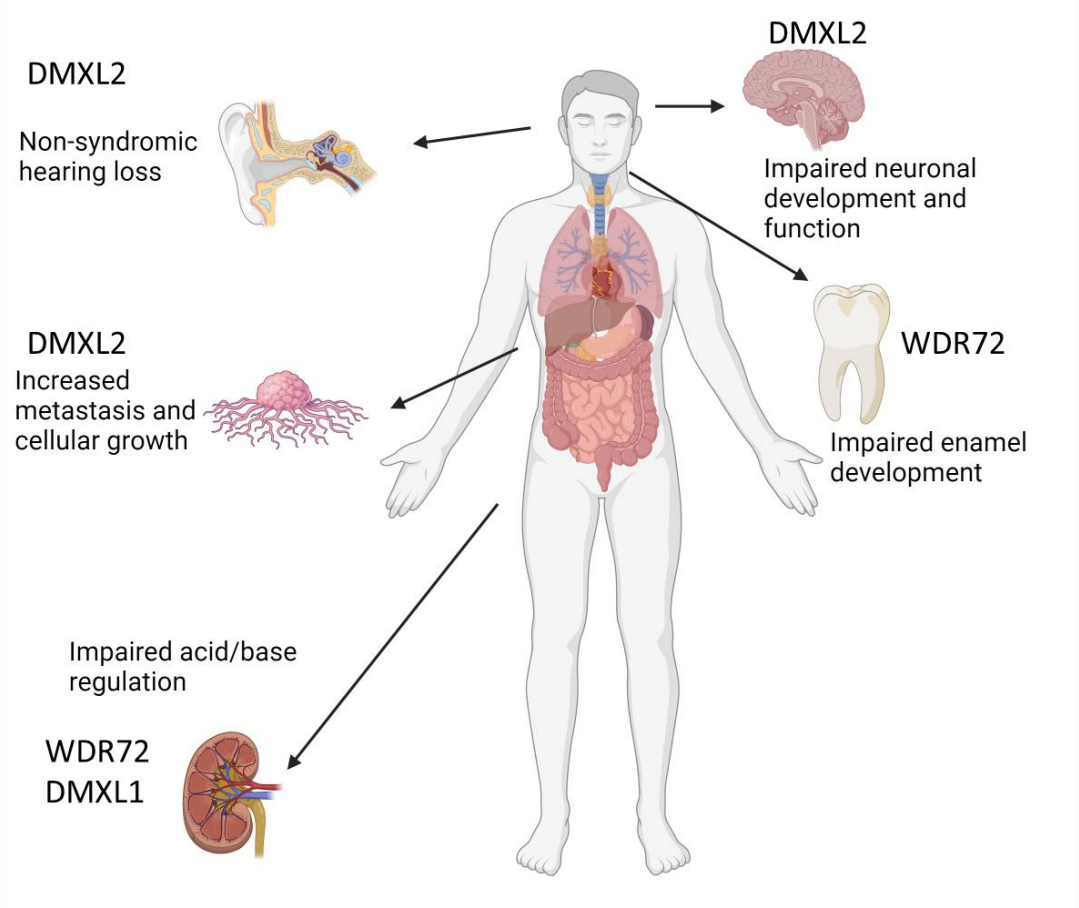

Figure 1-7 Rabconnectin-3 related disease

DMXL2 mutations result in non-syndromic hearing loss, impaired neurological development function, and cancer development and increased metastasis. Loss of DMXL1 expression results in distal renal tubular acidosis (dRTA). WDR72 mutations result in dRTA and amelogenesis imperfecta.

1.4.1 Developmental signaling

1.4.1.1 Notch signaling

Notch signaling is a cell-cell signaling system widely found across metazoans and involved in cell fate signaling, including proliferation, differentiation, and survival/death. The Notch receptor resides on the cell membrane and consists of an extracellular domain, a transmembrane domain, and an intracellular domain. Notch signaling is regulated by a series of proteolytic cleavage events called S1, S2, and S3. S1 cleavage occurs between the transmembrane region and the extracellular domain during trafficking in the Golgi. S2 cleavage occurs at the plasma membrane, and S3 cleavage by γ-secretase occurs in an endocytic compartment after binding of a Notch ligand (Kopan 2012). In *D. melanogaster* cells, the knockdown of Rabconnectin-3α results in a decrease in the expression of Notch-controlled genes. This is because the S3 cleavage occurs in an endocytic compartment, which is acidified by the V-ATPase (Vaccari, Lu et al. 2008). γ-secretase is a pH-sensitive enzyme that functions best in an acidic (LysoTracker positive) environment (Maesako, Houser et al. 2022). Rabconnectin-3 and V-ATPase defects increase the pH of this compartment. The catalytic activity of γ-secretase would then be decreased because of the alkaline conditions, reducing the activation of Notch sensitive effector genes (Sethi, Yan et al. 2010). Notch signaling has been found to be altered in many cancers, and overactive notch signaling promotes tumorigenesis and metastasis (Li, Tang et al. 2017). DMXL2 has been found to be aberrantly expressed in some breast cancers and heavily influences Notch signaling activity. Knocking down DMXL2 decreases Notch signaling and downregulates the epithelial-to-mesenchymal transition associated with cancer metastasis(Faronato, Nguyen et al. 2015).

1.4.1.2 Wnt signaling

Wnt signaling, like Notch signaling, depends on proper endosomal trafficking. Wnt ligands bind to the receptor complex on the plasma membrane and are then endocytosed into a 'signaling endosome.' In this signaling endosome, conformational changes within the Wnt receptor-signaling complex allow for further transduction and target gene activation. The V-ATPase accessory subunit ATP6AP2, also known as the pro-renin receptor, is important for the maturation of the Wnt signaling complex. V-ATPase inhibition through bafilomycin inhibited Wnt signaling, suggesting that the proton pumping activity of the V-ATPase is necessary for proper Wnt signalosome maturation (Cruciat, Ohkawara et al. 2010). Rabconnectin-3α (DMXL2) mutations have been shown to cause defects in Wnt signaling, resulting in improper development in zebrafish embryos and reducing transcription of Wnt target genes (Tuttle, Hoffman et al. 2014). Altered Wnt signaling has been implicated in the development of many cancers, including colorectal cancers, melanomas, and breast cancers, and contributes to the epithelial to mesenchymal transition (Zhan, Rindtorff et al. 2017).

1.4.2 DMXL1 mutations and pathology

Very few DMXL1 mutations have been identified in the literature. However, a recent study successfully generated a partial DMXL1 knockout mouse model where DMXL1 is not expressed in kidney-intercalated cells (Eaton, Danielson et al. 2024). Complete loss of DMXL1 expression appears to result in lethality, based on the absence

of homozygous DMXL1-null mice (Eaton, Danielson et al. 2024). This is consistent with embryonic lethality resulting from V-ATPase mutations (Inoue, Noumi et al. 1999).

As mentioned earlier in 'V-ATPase function in the kidney', V-ATPases play a critical role in the function of the kidney and acid/base regulation. DMXL1 KO mice have an impaired response to the acid challenge, resulting in lower venous pH and higher urine pH (Eaton, Danielson et al. 2024). V-ATPases in DMXL1 KO intercalated cells display V-ATPase abnormalities accompanying the altered pH. DMXL1 KO results in decreased expression of V_1 subunits, mislocalization of V-ATPase to intracellular membranes instead of the apical plasma membrane, decreased V-ATPase assembly, and changes in intercalated cell morphology (Eaton, Danielson et al. 2024).

1.4.3 DMXL2 mutations and pathology

Like the V-ATPases, complete loss of function mutations are lethal in higher eukaryotes. However, DMXL2 mutations result in neonatal death instead of embryonic death, which occurs with V-ATPase mutations (Sun-Wada, Murata et al. 2000, Gobe, Elzaiat et al. 2019). This discrepancy is likely because of the tissue specificity of DMXL2 compared to DMXL1. DMXL1 may facilitate V-ATPase in the embryonic stage and is sufficient for most development. DMXL2, however, is expressed more narrowly, potentially delaying lethality until after birth when the organism must function independently.

DMXL2 mutations are associated with several neurological pathologies, including Ohtahara syndrome, non-syndromic hearing loss, and infertility (Tata, Huijbregts et al.

2014, Chen, Liu et al. 2017, Esposito, Falace et al. 2019). Ohtahara syndrome, also called early infantile epileptic encephalopathy, is where infants present with myoclonic seizures within 3 months of birth. Seizures are about 10 seconds but can occur hundreds of times per day. The relatively benign myoclonic seizures can progress into more severe convulsions, including tonic-clonic seizures. As a result, the prognosis is poor, and afflicted infants often will not live beyond several months of age; however, in some cases, individuals can reach adulthood (Beal, Cherian et al. 2012).

DMXL2 mutations are associated with non-syndromic hearing loss. Non-syndromic hearing loss is hearing loss that is not accompanied by other symptoms, meaning that individuals have only impaired hearing. DMXL2 has been observed to localize to the basal region of hair cells in zebrafish (Einhorn, Trapani et al. 2012). Hair cells are specialized cells that convert mechanical stimulus into an action potential transmitted to the nervous system (Hudspeth 1985). The region of the hair cell that DMXL2 was found to localize to is the synaptic vesicle-containing region (Einhorn, Trapani et al. 2012). DMXL2-mutant zebrafish contained decreased V_1A on synaptic vesicles and decreased synaptic vesicle pH. This is reflective of impaired V-ATPase assembly and reduced activity on synaptic vesicles. The decreased activity results in impaired neurotransmission, resulting in the mechanical signals from hair cells not being passed to the nervous system. Individuals with DMXL2-related non-syndromic hearing loss present with a phenotype similar to that of zebrafish (Chen, Liu et al. 2017). A recent condition knockout of DMXL2 in hair cells results in partial hearing loss, mirroring the result of DMXL2 mutations in humans (Peng, Wang et al. 2024). Loss of DMXL2 impairs synaptic vesicle exocytosis under sustained stimulation. This reflects decreased

endocytosis and recycling of synaptic vesicles. These findings are consistent with the role that V-ATPase plays during the recycling of synaptic vesicles. Under a model where the disassembly of V-ATPases following acidification of neurotransmitter uptake influences the ability of synaptic vesicles to associate with the presynaptic membrane (Bodzęta, Kahms et al. 2017), synaptic vesicles that are unable to acidify due to impaired V-ATPase assembly would not move ahead and prime. The loss of DMXL2 in the conditional knockout mice appears to result in a dramatic decrease in WDR7 expression (Peng, Wang et al. 2024). Beyond the V-ATPase assembling function of Rabconnectin-3, WDR7 has been found to associate with priming proteins like CAPS-1 (Crummy, Mani et al. 2019) within the active zone of neurons. The reduction of docked and primed synaptic vesicles in the DMXL2 conditional knockout could be through interactions with WDR7 instead of just the function of DMXL2.

1.4.4 WDR72 mutations and pathology

In addition to dRTA, mutations in WDR72 cause amelogenesis imperfecta (AI) (El-Sayed, Parry et al. 2009). AI is a condition where the dental enamel, the most external layer of the teeth, does not form properly during development (Crawford, Aldred et al. 2007). The result is yellow/brown teeth with either an abnormally thin or poorly mineralized enamel, indicative of issues during the maturation phase of amelogenesis (Crawford, Aldred et al. 2007). The maturation phase of amelogenesis includes the removal of a proteinaceous matrix and replacement with mineralized enamel (Wang, Hu et al. 2015). Digestion of the proteinaceous membrane requires the enzyme KLK4, a serine protease that functions optimally at pH 6. Plasma membrane V-ATPase likely

maintains this optimal pH. During the maturation phase, V-ATPase subunit expression is strongly upregulated and robust localization to the cell surface (Sarkar, Wen et al. 2016). WDR72 mutations result in the loss of extracellular acidification that is typically observed during amelogenesis (Wang, Hu et al. 2015). Given that KLK4 functions best in a slightly acidic environment, it is possible the loss of extracellular acidification results in decreased protease activity (Wang, Hu et al. 2015). Together with the endocytic defects observed in WDR72 mutants (Katsura, Nakano et al. 2022), it is also possible that loss of WDR72 impairs the removal of the protein matrix and prevents later mineralization.

Interestingly, mutations in WDR72 also cause a loss of the typical ruffled border found in maturation-stage ameloblasts and lead to a general dysregulation of the microtubule network. It is thought that the microtubule dysfunction may be the cause of both the altered physiology and the impaired vesicular trafficking (Katsura, Nakano et al. 2022). However, this explanation for how WDR72 mutations cause amelogenesis imperfecta does not explain how the same mutation can also cause dRTA. WDR72 also shares strong homology with the beta-COP subunit and may be involved in membrane deformation (Katsura, Horst et al. 2014). This is consistent with endocytic and early endosome trafficking defects but does not explain the microtubule defects.

The inclusion of WDR72 as a novel Rabconnectin-3β isoform explains the effect that WDR72 has on urine acidification and enamel matrix pH. Since the two pathologies are related to WDR72 and involve the activity of plasma membrane V-ATPases, WDR72 may catalyze the assembly of V-ATPases containing V_oa3 and V_oa4 isoforms at the plasma membrane. Loss of WDR72 expression would impair the assembly and activity of these V-ATPases, resulting in disease.

1.4.5 Kohschutter-Tonz sydrome

Kohlschutter-Tonz syndrome (KTS) is a condition characterized by early onset epilepsy, amelogenesis imperfecta, psychomotor regression, and recently, nephrocalcinosis (Schossig, Wolf et al. 2012, Liepina, Kalnina et al. 2021). Kohlschutter-Tonz syndrome is caused by loss of function mutations in the gene encoding the protein ROGDI. ROGDI is a protein with a previously unknown function, but we have found that ROGDI shares substantial homology with the yeast RAVE subunit Rav2. This will be discussed in greater detail in Chapter 2.

KTS follows an autosomal recessive inheritance pattern where two mutated alleles are required to develop KTS. As a result, KTS is particularly common in populations with low genetic diversity. Although KTS is uncommon, genetic information is available for multiple KTS families. Mutations observed are nonsense, frameshift, or splice mutations (Liepina, Kalnina et al. 2021). These mutations lead to the production of a protein that is unstable, non-functional, or prone to degradation. While Kohlscutter-Tonz syndrome almost always presents epilepsy, developmental delay, and amelogenesis imperfecta, there is variation in the overall severity of the disease (Liepina, Kalnina et al. 2021). Individuals respond differently to anti-epileptic drugs, severity and type of seizures, severity of developmental delay, age of epileptic onset, and lifespan (Liepina, Kalnina et al. 2021). SLC13A5 is a second gene identified to cause Kohlschutter-Tonz syndrome(Schossig, Bloch-Zupan et al. 2017), it is possible that there are other genetic contributors to disease characteristics and severity.

Recent studies, including a mouse model of KTS, have shed light on additional consequences from the loss of ROGDI (Jimenez-Armijo, Morkmued et al. 2024). A ROGDI mouse model was generated using a design where *ROGDI* exons 6-11 are deleted, comparable to the frameshift and nonsense mutations seen in humans (Jimenez-Armijo, Morkmued et al. 2024). ROGDI KO mice displayed the typical KTS phenotypes, including amelogenesis imperfecta, epilepsy, and psychomotor regression (Jimenez-Armijo, Morkmued et al. 2024). In addition, the mice showed memory defects and hyperactivity previously seen in a *D. melanogaster* ROGDI model system (Kim, Jang et al. 2017). ROGDI KO mice also displayed alterations to stomach size and function, kidney morphology, and liver morphology. Stomachs in KO mice were substantially larger, and the contents had a pH of 6 compared to the wild type with a pH of 3. ROGDI KO mice display hepatomegaly (enlarged liver) and discolored kidneys (Jimenez-Armijo, Morkmued et al. 2024).

The phenotypes of KTS intersect with the phenotypes of Rabconnectin-3, V-ATPase, and WDR72 mutations. Amelogenesis imperfecta and dRTA/nephrocalcinosis are caused by both ROGDI and WDR72 mutations. Mutations in the V-ATPase subunits V_0a4, V_1B1, and V_1C2 have also been found to cause distal renal tubular acidosis (Stover, Borthwick et al. 2002, Jobst-Schwan, Klämbt et al. 2020). Both KTS and Ohtahara syndrome are considered epileptic encephalopathies. Mutations have also been found in V-ATPase subunits, including the V_0a1 and V_0c, that lead to neurological phenotypes (Bott, Forouhan et al. 2021, Mattison, Tossing et al. 2023).

1.5 Dissertation objectives

Rabconnectin-3 is required to reassemble mammalian V-ATPases efficiently, and reductions in Rabconnectin-3 activity result in disease. Included in this are neurological and kidney dysfunction. However, the details surrounding the Rabconnectin-3 function are not well understood. This deficit in the literature includes what proteins are part of the Rabconnectin-3 complex and what functions they serve. We identified ROGDI as a possible homolog of the yeast protein Rav2. Loss of function mutations in ROGDI cause Kohlschutter-Tonz syndrome, a disease characterized by epileptic encephalopathy with amelogenesis imperfecta. Based on the extensive homology between ROGDI and Rav2 and the connections between V-ATPase mutations, DRTA, and neurological disease, we hypothesize that KTS is a disease of the V-ATPase. Part of this hypothesis is that loss of ROGDI impairs V-ATPase activity, leading to the phenotypes seen in KTS. **Chapter 2** highlights our work investigating ROGDI as a novel Rabconnecin-3 subunit and V-ATPase regulator. ROGDI shares functional and structural homology with the yeast RAVE subunit Rav2. ROGDI is associated with DMXL1, WDR7, and V_1 in mammalian cells. ROGDI localizes to lysosomes at the cell center and periphery. These lysosomes also contain DMXL1 and V_1A. This illustrates that ROGDI localizes intracellularly with V-ATPase and Rabconnectin-3 subunits, analogously to Rav2 in yeast. **Chapter 3** includes predictive AlphaFold3 models of the Rabconnectin-3 and RAVE complexes. Predictive modeling of the Rabconnectin-3-ROGDI complex has been very helpful in developing a model for how Rabconnectin-3 interacts with ROGDI and how disease can result from mutations in individual subunits. Modeling of RAVE has provided additional insights into structural changes that must occur during the reassembly process. Improving

our understanding of the structure and function of RAVE and Rabconnectin-3 is foundational to understanding how they impact V-ATPase activity.

1.6 References

Abbas, Y. M., et al. (2020). "Structure of V-ATPase from the mammalian brain." Science **367**(6483): 1240-1246.

Adams, D. S., et al. (2006). "Early, H+-V-ATPase-dependent proton flux is necessary for consistent left-right patterning of non-mammalian vertebrates." Development **133**(9): 1657-1671.

Anderson, D., et al. (1982). "Proton gradient linkage to active uptake of [3H] acetylcholine by Torpedo electric organ synaptic vesicles." Biochemistry **21**(13): 3037-3043.

Bai, C., et al. (1996). "SKP1 connects cell cycle regulators to the ubiquitin proteolysis machinery through a novel motif, the F-box." Cell **86**(2): 263-274.

Banerjee, S., et al. (2019). "Interaction of the late endo-lysosomal lipid PI (3, 5) P2 with the Vph1 isoform of yeast V-ATPase increases its activity and cellular stress tolerance." Journal of Biological Chemistry **294**(23): 9161-9171.

Banerjee, S. and P. M. Kane (2017). "Direct interaction of the Golgi V-ATPase a-subunit isoform with PI (4) P drives localization of Golgi V-ATPases in yeast." Molecular biology of the cell **28**(19): 2518-2530.

Beal, J. C., et al. (2012). "Early-onset epileptic encephalopathies: Ohtahara syndrome and early myoclonic encephalopathy." Pediatric neurology **47**(5): 317-323.

Blakely, R. D. and R. H. Edwards (2012). "Vesicular and plasma membrane transporters for neurotransmitters." Cold Spring Harbor perspectives in biology **4**(2): a005595.

Bodzęta, A., et al. (2017). "The presynaptic v-ATPase reversibly disassembles and thereby modulates exocytosis but is not part of the fusion machinery." Cell reports **20**(6): 1348-1359.

Bond, S. and M. Forgac (2008). "The Ras/cAMP/protein kinase A pathway regulates glucose-dependent assembly of the vacuolar (H+)-ATPase in yeast." Journal of Biological Chemistry **283**(52): 36513-36521.

Bott, L. C., et al. (2021). "Variants in ATP6V0A1 cause progressive myoclonus epilepsy and developmental and epileptic encephalopathy." Brain communications **3**(4): fcab245.

Brace, E., et al. (2006). "Skp1p regulates Soi3p/Rav1p association with endosomal membranes but is not required for vacuolar ATPase assembly." Eukaryotic cell **5**(12): 2104-2113.

Brown, D., et al. (1988). "An H+-ATPase in opposite plasma membrane domains in kidney epithelial cell subpopulations." Nature **331**(6157): 622-624.

Brown, D., et al. (2009). "Regulation of the V-ATPase in kidney epithelial cells: dual role in acid–base homeostasis and vesicle trafficking." Journal of Experimental Biology **212**(11): 1762-1772.

Bueler, S. A. and J. L. Rubinstein (2015). "Vma9p need not be associated with the yeast V-ATPase for fully-coupled proton pumping activity in vitro." Biochemistry **54**(3): 853-858.

Capecci, J. and M. Forgac (2013). "The function of vacuolar ATPase (V-ATPase) a subunit isoforms in invasiveness of MCF10a and MCF10CA1a human breast cancer cells." Journal of Biological Chemistry **288**(45): 32731-32741.

Casey, J. R., et al. (2010). "Sensors and regulators of intracellular pH." Nature reviews Molecular cell biology **11**(1): 50-61.

Chan, C.-Y., et al. (2016). "Regulation of vacuolar H+-ATPase (V-ATPase) reassembly by glycolysis flow in 6-phosphofructo-1-kinase (PFK-1)-deficient yeast cells." Journal of Biological Chemistry **291**(30): 15820-15829.

Chanaday, N. L., et al. (2019). "The synaptic vesicle cycle revisited: new insights into the modes and mechanisms." Journal of Neuroscience **39**(42): 8209-8216.

Chen, C. K.-M., et al. (2011). "The many blades of the β-propeller proteins: conserved but versatile." Trends in Biochemical Sciences **36**(10): 553-561.

Chen, D.-Y., et al. (2017). "A dominant variant in DMXL2 is linked to nonsyndromic hearing loss." Genetics in Medicine **19**(5): 553-558.

Chen, F., et al. (2022). "The V-ATPases in cancer and cell death." Cancer gene therapy **29**(11): 1529-1541.

Choy, A., et al. (2012). "The Legionella effector RavZ inhibits host autophagy through irreversible Atg8 deconjugation." Science **338**(6110): 1072-1076.

Chu, A., et al. (2024). "The Human Mutation K237_V238del in a Putative Lipid Binding Motif within the V-ATPase a2 Isoform Suggests a Molecular Mechanism Underlying Cutis Laxa." International Journal of Molecular Sciences **25**(4): 2170.

Chu, A., et al. (2023). "Characterization of a PIP Binding Site in the N-Terminal Domain of V-ATPase a4 and Its Role in Plasma Membrane Association." International Journal of Molecular Sciences **24**(5): 4867.

Chu, A., et al. (2021). "The V-ATPase a 3 Subunit: Structure, Function and Therapeutic Potential of an Essential Biomolecule in Osteoclastic Bone Resorption." International Journal of Molecular Sciences **22**(13): 6934.

Collins, M. P. and M. Forgac (2020). "Regulation and function of V-ATPases in physiology and disease." Biochimica et Biophysica Acta (BBA)-Biomembranes **1862**(12): 183341.

Collins, M. P., et al. (2020). "AKT Ser/Thr kinase increases V-ATPase–dependent lysosomal acidification in response to amino acid starvation in mammalian cells." Journal of Biological Chemistry: jbc. RA120. 013223.

Compton, M. A., et al. (2006). "Vma9p (subunit e) is an integral membrane V0 subunit of the yeast V-ATPase." Journal of Biological Chemistry **281**(22): 15312-15319.

Connelly, C. and P. Hieter (1996). "Budding yeast SKP1 encodes an evolutionarily conserved kinetochore protein required for cell cycle progression." Cell **86**(2): 275-285.

Coonrod, E. M., et al. (2013). "Homotypic vacuole fusion in yeast requires organelle acidification and not the V-ATPase membrane domain." Developmental cell **27**(4): 462-468.

Cotter, K., et al. (2015). "Activity of plasma membrane V-ATPases is critical for the invasion of MDA-MB231 breast cancer cells." Journal of Biological Chemistry **290**(6): 3680-3692.

Cotter, K., et al. (2016). "The a3 isoform of subunit a of the vacuolar ATPase localizes to the plasma membrane of invasive breast tumor cells and is overexpressed in human breast cancer." Oncotarget **7**(29): 46142.

Couoh-Cardel, S., et al. (2015). "Affinity purification and structural features of the yeast vacuolar ATPase Vo membrane sector." Journal of Biological Chemistry **290**(46): 27959-27971.

Coupland, C. E., et al. (2024). "High-resolution electron cryomicroscopy of V-ATPase in native synaptic vesicles." Science: eadp5577.

Crawford, P. J., et al. (2007). "Amelogenesis imperfecta." Orphanet journal of rare diseases **2**: 1-11.

Cruciat, C.-M., et al. (2010). "Requirement of prorenin receptor and vacuolar H+-ATPase–mediated acidification for Wnt signaling." Science **327**(5964): 459-463.

Crummy, E., et al. (2019). "The priming factor CAPS1 regulates dense-core vesicle acidification by interacting with rabconnectin3β/WDR7 in neuroendocrine cells." Journal of Biological Chemistry **294**(24): 9402-9415.

Diab, H., et al. (2009). "Subunit interactions and requirements for inhibition of the yeast V1-ATPase." Journal of Biological Chemistry **284**(20): 13316-13325.

Doherty, R. and P. Kane (1993). "Partial assembly of the yeast vacuolar H (+)-ATPase in mutants lacking one subunit of the enzyme." Journal of Biological Chemistry **268**(22): 16845-16851.

Drory, O., et al. (2004). "Crystal structure of yeast V-ATPase subunit C reveals its stator function." EMBO reports **5**(12): 1148-1152.

Eaton, A. F., et al. (2021). "The evolutionary conserved TLDc domain defines a new class of (H+) V-ATPase interacting proteins." Scientific reports **11**(1): 22654.

Eaton, A. F., et al. (2024). "Dmxl1 is an Essential Mammalian Gene that is Required for V-ATPase Assembly and Function In Vivo." Function: zqae025.

Eaton, A. F., et al. (2020). "The H+ ATPase (V-ATPase): from proton pump to signaling complex in health and disease." American Journal of Physiology-Cell Physiology.

Ebner, M., et al. (2023). "Nutrient-regulated control of lysosome function by signaling lipid conversion." Cell **186**(24): 5328-5346. e5326.

Einhorn, Z., et al. (2012). "Rabconnectin3α promotes stable activity of the H+ pump on synaptic vesicles in hair cells." Journal of Neuroscience **32**(32): 11144-11156.

El-Sayed, W., et al. (2009). "Mutations in the beta propeller WDR72 cause autosomal-recessive hypomaturation amelogenesis imperfecta." The American Journal of Human Genetics **85**(5): 699-705.

Elkin, S. R., et al. (2016). "Endocytic pathways and endosomal trafficking: a primer." Wiener Medizinische Wochenschrift **166**: 196-204.

Esmail, S., et al. (2018). "Molecular mechanisms of cutis laxa–and distal renal tubular acidosis–causing mutations in V-ATPase a subunits, ATP6V0A2 and ATP6V0A4." Journal of Biological Chemistry **293**(8): 2787-2800.

Esposito, A., et al. (2019). "Biallelic DMXL2 mutations impair autophagy and cause Ohtahara syndrome with progressive course." Brain **142**(12): 3876-3891.

Faronato, M., et al. (2015). "DMXL2 drives epithelial to mesenchymal transition in hormonal therapy resistant breast cancer through Notch hyper-activation." Oncotarget **6**(26): 22467.

Farsi, Z., et al. (2017). "Proton electrochemical gradient: driving and regulating neurotransmitter uptake." Bioessays **39**(5): 1600240.

Figueiredo, M., et al. (2021). "The (pro) renin receptor (ATP6ap2) facilitates receptor-mediated endocytosis and lysosomal function in the renal proximal tubule." Pflügers Archiv-European Journal of Physiology **473**: 1229-1246.

Finberg, K. E., et al. (2005). "The B1-subunit of the H+ ATPase is required for maximal urinary acidification." Proceedings of the National Academy of Sciences **102**(38): 13616-13621.

Finnigan, G. C., et al. (2012). "Sorting of the Yeast Vacuolar-type, Proton-translocating ATPase Enzyme Complex (V-ATPase) IDENTIFICATION OF A NECESSARY AND SUFFICIENT GOLGI/ENDOSOMAL RETENTION SIGNAL IN Stv1p." Journal of Biological Chemistry **287**(23): 19487-19500.

Fischer, T. D., et al. (2020). "STING induces LC3B lipidation onto single-membrane vesicles via the V-ATPase and ATG16L1-WD40 domain." Journal of Cell Biology **219**(12): e202009128.

Flannagan, R. S., et al. (2012). "The cell biology of phagocytosis." Annual Review of Pathology: Mechanisms of Disease **7**(1): 61-98.

Fuster, D. G. and O. W. Moe (2018). "Incomplete distal renal tubular acidosis and kidney stones." Advances in chronic kidney disease **25**(4): 366-374.

Gatenby, R. A. and R. J. Gillies (2004). "Why do cancers have high aerobic glycolysis?" Nature Reviews Cancer **4**(11): 891-899.

Gobe, C., et al. (2019). "Dual role of DMXL2 in olfactory information transmission and the first wave of spermatogenesis." PLoS genetics **15**(2): e1007909.

Gräf, R., et al. (1996). "Purification and properties of a cytosolic V1-ATPase." Journal of Biological Chemistry **271**(34): 20908-20913.

Graham, L. A., et al. (1998). "Assembly of the yeast vacuolar H+-ATPase occurs in the endoplasmic reticulum and requires a Vma12p/Vma22p assembly complex." The Journal of cell biology **142**(1): 39-49.

Guida, M. C., et al. (2018). "ATP6AP2 functions as a V-ATPase assembly factor in the endoplasmic reticulum." Molecular biology of the cell **29**(18): 2156-2164.

Hardie, D. G. (2014). "AMPK—sensing energy while talking to other signaling pathways." Cell metabolism **20**(6): 939-952.

Hashmi, F. and P. M. Kane (2024). "V-ATPase Disassembly at the Yeast Lysosome-Like Vacuole Is a Phenotypic Driver of Lysosome Dysfunction in Replicative Aging." bioRxiv.

Hill, K. J. and T. H. Stevens (1994). "Vma21p is a yeast membrane protein retained in the endoplasmic reticulum by a di-lysine motif and is required for the assembly of the vacuolar H (+)-ATPase complex." Molecular biology of the cell **5**(9): 1039-1050.

Hill, K. J. and T. H. Stevens (1995). "Vma22p is a novel endoplasmic reticulum-associated protein required for assembly of the yeast vacuolar H+-ATPase complex." Journal of Biological Chemistry **270**(38): 22329-22336.

Hinton, A., et al. (2009). "Function of a subunit isoforms of the V-ATPase in pH homeostasis and in vitro invasion of MDA-MB231 human breast cancer cells." Journal of Biological Chemistry **284**(24): 16400-16408.

Hirata, R., et al. (1993). "VMA12 is essential for assembly of the vacuolar H (+)-ATPase subunits onto the vacuolar membrane in Saccharomyces cerevisiae." Journal of Biological Chemistry **268**(2): 961-967.

Hudspeth, A. (1985). "The cellular basis of hearing: the biophysics of hair cells." Science **230**(4727): 745-752.

Huss, M. and H. Wieczorek (2007). "Influence of ATP and ADP on dissociation of the V-ATPase into its V1 and VO complexes." FEBS letters **581**(29): 5566-5572.

Imai, E., et al. (2016). "A novel heterozygous mutation in the ATP6V0A4 gene encoding the V-ATPase a4 subunit in an adult patient with incomplete distal renal tubular acidosis." Clinical kidney journal **9**(3): 424-428.

Inoue, H., et al. (1999). "Targeted disruption of the gene encoding the proteolipid subunit of mouse vacuolar H+-ATPase leads to early embryonic lethality." Biochimica et Biophysica Acta (BBA)-Bioenergetics **1413**(3): 130-138.

Jansen, E. J., et al. (2016). "ATP6AP1 deficiency causes an immunodeficiency with hepatopathy, cognitive impairment and abnormal protein glycosylation." Nature communications **7**(1): 11600.

Jaskolka, M. C. and P. M. Kane (2020). "Interaction between the yeast RAVE complex and Vph1-containing Vo sectors is a central glucose-sensitive interaction required for V-ATPase reassembly." Journal of Biological Chemistry **295**(8): 2259-2269.

Jaskolka, M. C., et al. (2021). "Defining steps in RAVE-catalyzed V-ATPase assembly using purified RAVE and V-ATPase subcomplexes." Journal of Biological Chemistry **296**.

Jimenez-Armijo, A., et al. (2024). "The Rogdi knockout mouse is a model for Kohlschütter–Tönz syndrome." Scientific reports **14**(1): 445.

Jobst-Schwan, T., et al. (2020). "Whole exome sequencing identified ATP6V1C2 as a novel candidate gene for recessive distal renal tubular acidosis." Kidney international **97**(3): 567-579.

Jockusch, W. J., et al. (2007). "CAPS-1 and CAPS-2 are essential synaptic vesicle priming proteins." Cell **131**(4): 796-808.

Jumper, J., et al. (2021). "Highly accurate protein structure prediction with AlphaFold." Nature **596**(7873): 583-589.

Kaksonen, M. and A. Roux (2018). "Mechanisms of clathrin-mediated endocytosis." Nature reviews Molecular cell biology **19**(5): 313-326.

Kane, P., et al. (1992). "Assembly and targeting of peripheral and integral membrane subunits of the yeast vacuolar H (+)-ATPase." Journal of Biological Chemistry **267**(1): 447-454.

Kane, P. M. (1995). "Disassembly and reassembly of the yeast vacuolar H+-ATPase in vivo." Journal of Biological Chemistry **270**(28): 17025-17032.

Kane, P. M., et al. (1999). "Early steps in assembly of the yeast vacuolar H+-ATPase." Journal of Biological Chemistry **274**(24): 17275-17283.

Katsura, K., et al. (2014). "WDR72 models of structure and function: A stage-specific regulator of enamel mineralization." Matrix Biology **38**: 48-58.

Katsura, K., et al. (2022). "WDR72 regulates vesicle trafficking in ameloblasts." Scientific reports **12**(1): 1-12.

Kawabe, H., et al. (2003). "A novel rabconnectin-3-binding protein that directly binds a GDP/GTP exchange protein for Rab3A small G protein implicated in Ca2+-dependent exocytosis of neurotransmitter." Genes to Cells **8**(6): 537-546.

Kawamura, N., et al. (2015). "Loss of G 2 subunit of vacuolar-type proton transporting ATPase leads to G 1 subunit upregulation in the brain." Scientific reports **5**(1): 14027.

Kettner, C., et al. (2003). "Inhibition of the yeast V-type ATPase by cytosolic ADP." FEBS letters **535**(1-3): 119-124.

Khan, M. M. and S. Wilkens (2024). "Molecular mechanism of Oxr1p mediated disassembly of yeast V-ATPase." EMBO reports **25**(5): 2323-2347.

Kim, M., et al. (2017). "Rogdi Defines GABAergic Control of a Wake-promoting Dopaminergic Pathway to Sustain Sleep in Drosophila." Scientific reports **7**(1): 1-14.

Kinouchi, K., et al. (2010). "The (pro) renin receptor/ATP6AP2 is essential for vacuolar H+-ATPase assembly in murine cardiomyocytes." Circulation research **107**(1): 30-34.

Kishikawa, J., et al. (2022). "Structural snapshots of V/A-ATPase reveal the rotary catalytic mechanism of rotary ATPases." Nature communications **13**(1): 1213.

Kitagawa, K., et al. (1999). "SGT1 encodes an essential component of the yeast kinetochore assembly pathway and a novel subunit of the SCF ubiquitin ligase complex." Molecular Cell **4**(1): 21-33.

Klössel, S., et al. (2024). "Yeast TLDc domain proteins regulate assembly state and subcellular localization of the V-ATPase." The EMBO journal **43**(9): 1870-1897.

Kolen, B., et al. (2023). "Vesicular glutamate transporters are H+-anion exchangers that operate at variable stoichiometry." Nature communications **14**(1): 2723.

Kopan, R. (2012). "Notch signaling." Cold Spring Harbor perspectives in biology **4**(10): a011213.

Kozik, P., et al. (2013). "A human genome-wide screen for regulators of clathrin-coated vesicle formation reveals an unexpected role for the V-ATPase." Nature cell biology **15**(1): 50-60.

Kraemer, C., et al. (2000). "Mapping and structure of DMXL1, a human homologue of the DmX gene from Drosophila melanogaster coding for a WD repeat protein." Genomics **64**(1): 97-101.

Kraemer, C., et al. (1998). "The new gene DmX from Drosophila melanogaster encodes a novel WD-repeat protein." Gene **216**(2): 267-276.

Lemmon, M. A. (2007). Pleckstrin homology (PH) domains and phosphoinositides. Biochemical Society Symposia, Portland Press Ltd.

Li, L., et al. (2017). "Notch signaling pathway networks in cancer metastasis: a new target for cancer therapy." Medical oncology **34**: 1-10.

Li, S. C., et al. (2014). "The signaling lipid PI (3, 5) P2 stabilizes V1–Vo sector interactions and activates the V-ATPase." Molecular biology of the cell **25**(8): 1251-1262.

Liberman, R., et al. (2014). "Regulated assembly of vacuolar ATPase is increased during cluster disruption-induced maturation of dendritic cells through a phosphatidylinositol 3-kinase/mTOR-dependent pathway." Journal of Biological Chemistry **289**(3): 1355-1363.

Liepina, L., et al. (2021). "Kohlschütter–Tönz syndrome: Case report with novel feature and detailed review of features associated with ROGDI variants." American Journal of Medical Genetics Part A.

Maesako, M., et al. (2022). "Presenilin/γ-secretase activity is located in acidic compartments of live neurons." Journal of Neuroscience **42**(1): 145-154.

Manolson, M. F., et al. (1992). "The VPH1 gene encodes a 95-kDa integral membrane polypeptide required for in vivo assembly and activity of the yeast vacuolar H (+)-ATPase." Journal of Biological Chemistry **267**(20): 14294-14303.

Manolson, M. F., et al. (1994). "STV1 gene encodes functional homologue of 95-kDa yeast vacuolar H (+)-ATPase subunit Vph1p." Journal of Biological Chemistry **269**(19): 14064-14074.

Marjuki, H., et al. (2011). "Influenza A virus-induced early activation of ERK and PI3K mediates V-ATPase-dependent intracellular pH change required for fusion." Cellular microbiology **13**(4): 587-601.

Marshansky, V. and M. Futai (2008). "The V-type H+-ATPase in vesicular trafficking: targeting, regulation and function." Current opinion in cell biology **20**(4): 415-426.

Martineau, M., et al. (2017). "VGLUT1 functions as a glutamate/proton exchanger with chloride channel activity in hippocampal glutamatergic synapses." Nature communications **8**(1): 2279.

Matsuyama, S., et al. (2000). "Changes in intramitochondrial and cytosolic pH: early events that modulate caspase activation during apoptosis." Nature cell biology **2**(6): 318-325.

Mattison, K. A., et al. (2023). "ATP6V0C variants impair V-ATPase function causing a neurodevelopmental disorder often associated with epilepsy." Brain **146**(4): 1357-1372.

Mazhab-Jafari, M. T., et al. (2016). "Atomic model for the membrane-embedded VO motor of a eukaryotic V-ATPase." Nature **539**(7627): 118-122.

McGuire, C. M., et al. (2019). "Isoform-specific gene disruptions reveal a role for the V-ATPase subunit a4 isoform in the invasiveness of 4T1-12B breast cancer cells." Journal of Biological Chemistry **294**(29): 11248-11258.

McGuire, C. M. and M. Forgac (2018). "Glucose starvation increases V-ATPase assembly and activity in mammalian cells through AMP kinase and phosphatidylinositide 3-kinase/Akt signaling." Journal of Biological Chemistry **293**(23): 9113-9123.

Mijaljica, D., et al. (2011). "V-ATPase engagement in autophagic processes." Autophagy **7**(6): 666-668.

Miles, A. L., et al. (2017). "The vacuolar-ATPase complex and assembly factors, TMEM199 and CCDC115, control HIF1α prolyl hydroxylation by regulating cellular iron levels." Elife **6**: e22693.

Milosevic, I. (2018). "Revisiting the role of clathrin-mediated endoytosis in synaptic vesicle recycling." Frontiers in Cellular Neuroscience **12**: 27.

Mitra, C., et al. (2023). "Human V-ATPase a-subunit isoforms bind specifically to distinct phosphoinositide phospholipids." Journal of Biological Chemistry **299**(12).

Nagano, F., et al. (2002). "Rabconnectin-3, a novel protein that binds both GDP/GTP exchange protein and GTPase-activating protein for Rab3 small G protein family." Journal of Biological Chemistry **277**(12): 9629-9632.

Nakanishi, A., et al. (2018). "Cryo EM structure of intact rotary H+-ATPase/synthase from Thermus thermophilus." Nature communications **9**(1): 89.

Neefjes, J., et al. (2011). "Towards a systems understanding of MHC class I and MHC class II antigen presentation." Nature reviews immunology **11**(12): 823-836.

Nelson, H. and N. Nelson (1990). "Disruption of genes encoding subunits of yeast vacuolar H (+)-ATPase causes conditional lethality." Proceedings of the National Academy of Sciences **87**(9): 3503-3507.

Oka, T., et al. (2001). "a4, a unique kidney-specific isoform of mouse vacuolar H+-ATPase subunit a." Journal of Biological Chemistry **276**(43): 40050-40054.

Olson, L. J., et al. (2008). "Structural insights into the mechanism of pH-dependent ligand binding and release by the cation-dependent mannose 6-phosphate receptor." Journal of Biological Chemistry **283**(15): 10124-10134.

Oot, R. A., et al. (2017). "Breaking up and making up: the secret life of the vacuolar H+-ATPase." Protein Science **26**(5): 896-909.

Oot, R. A., et al. (2016). "Crystal structure of yeast V1-ATP ase in the autoinhibited state." The EMBO journal **35**(15): 1694-1706.

Oot, R. A. and S. Wilkens (2012). "Subunit interactions at the V1-Vo interface in yeast vacuolar ATPase." Journal of Biological Chemistry **287**(16): 13396-13406.

Oot, R. A. and S. Wilkens (2024). "Human V-ATPase function is positively and negatively regulated by TLDc proteins." Structure.

Otomo, A., et al. (2022). "Direct observation of stepping rotation of V-ATPase reveals rigid component in coupling between Vo and V1 motors." Proceedings of the National Academy of Sciences **119**(42): e2210204119.

Pareja, F., et al. (2018). "Loss-of-function mutations in ATP6AP1 and ATP6AP2 in granular cell tumors." Nature communications **9**(1): 3533.

Parra, K. J. and P. M. Kane (1998). "Reversible association between the V1and V0 domains of yeast vacuolar H+-ATPase is an unconventional glucose-induced effect." Molecular and cellular biology.

Parra, K. J., et al. (2000). "The H subunit (Vma13p) of the yeast V-ATPase inhibits the ATPase activity of cytosolic V1 complexes." Journal of Biological Chemistry **275**(28): 21761-21767.

Peng, H., et al. (2024). "DMXL2 is required for endocytosis and recycling of synaptic vesicles in auditory hair cells." Journal of Neuroscience.

Perreira, J. M., et al. (2015). "RNASEK is a V-ATPase-associated factor required for endocytosis and the replication of rhinovirus, influenza A virus, and dengue virus." Cell reports **12**(5): 850-863.

Poëa-Guyon, S., et al. (2013). "The V-ATPase membrane domain is a sensor of granular pH that controls the exocytotic machinery." Journal of Cell Biology **203**(2): 283-298.

Posor, Y., et al. (2022). "Phosphoinositides as membrane organizers." Nature reviews Molecular cell biology **23**(12): 797-816.

Putney, L. K. and D. L. Barber (2003). "Na-H exchange-dependent increase in intracellular pH times G2/M entry and transition." Journal of Biological Chemistry **278**(45): 44645-44649.

Qi, J., et al. (2007). "The vacuolar (H+)-ATPase: subunit arrangement and in vivo regulation." Journal of bioenergetics and biomembranes **39**: 423-426.

Rahman, S., et al. (2013). "Biochemical and biophysical properties of interactions between subunits of the peripheral stalk region of human V-ATPase." PloS one **8**(2): e55704.

Ratto, E., et al. (2022). "Direct control of lysosomal catabolic activity by mTORC1 through regulation of V-ATPase assembly." Nature communications **13**(1): 4848.

Rienmüller, F., et al. (2012). "Luminal and cytosolic pH feedback on proton pump activity and ATP affinity of V-type ATPase from Arabidopsis." Journal of Biological Chemistry **287**(12): 8986-8993.

Roh, S.-H., et al. (2020). "Cryo-EM and MD infer water-mediated proton transport and autoinhibition mechanisms of Vo complex." Science Advances **6**(41): eabb9605.

Roh, S.-H., et al. (2018). "The 3.5-Å CryoEM structure of nanodisc-reconstituted yeast vacuolar ATPase Vo proton channel." Molecular Cell **69**(6): 993-1004. e1003.

Roy, A., et al. (2015). "Collecting duct intercalated cell function and regulation." Clinical Journal of the American Society of Nephrology **10**(2): 305-324.

Royaux, I. E., et al. (2001). "Pendrin, encoded by the Pendred syndrome gene, resides in the apical region of renal intercalated cells and mediates bicarbonate secretion." Proceedings of the National Academy of Sciences **98**(7): 4221-4226.

Ryan, M., et al. (2008). "Voa1p functions in V-ATPase assembly in the yeast endoplasmic reticulum." Molecular biology of the cell **19**(12): 5131-5142.

Sagermann, M., et al. (2001). "Crystal structure of the regulatory subunit H of the V-type ATPase of Saccharomyces cerevisiae." Proceedings of the National Academy of Sciences **98**(13): 7134-7139.

Sambade, M. and P. M. Kane (2004). "The yeast vacuolar proton-translocating ATPase contains a subunit homologous to the Manduca sexta and bovine e subunits that is essential for function." Journal of Biological Chemistry **279**(17): 17361-17365.

Sarkar, J., et al. (2016). "V-type ATPase proton pump expression during enamel formation." Matrix Biology **52**: 234-245.

Saxton, R. A. and D. M. Sabatini (2017). "mTOR signaling in growth, metabolism, and disease." Cell **168**(6): 960-976.

Schossig, A., et al. (2017). "SLC13A5 is the second gene associated with Kohlschütter–Tönz syndrome." Journal of medical genetics **54**(1): 54-62.

Schossig, A., et al. (2012). "Mutations in ROGDI cause Kohlschütter-Tönz syndrome." The American Journal of Human Genetics **90**(4): 701-707.

Sennoune, S. R., et al. (2004). "Vacuolar H+-ATPase in human breast cancer cells with distinct metastatic potential: distribution and functional activity." American Journal of Physiology-Cell Physiology **286**(6): C1443-C1452.

Seol, J. H., et al. (2001). "Skp1 forms multiple protein complexes, including RAVE, a regulator of V-ATPase assembly." Nature cell biology **3**(4): 384-391.

Sethi, N., et al. (2010). "Rabconnectin-3 is a functional regulator of mammalian Notch signaling." Journal of Biological Chemistry **285**(45): 34757-34764.

Sharma, S., et al. (2018). "MgATP hydrolysis destabilizes the interaction between subunit H and yeast V1-ATPase, highlighting H's role in V-ATPase regulation by reversible disassembly." Journal of Biological Chemistry **293**(27): 10718-10730.

Smardon, A. M., et al. (2014). "The RAVE complex is an isoform-specific V-ATPase assembly factor in yeast." Molecular biology of the cell **25**(3): 356-367.

Smardon, A. M. and P. M. Kane (2007). "RAVE is essential for the efficient assembly of the C subunit with the vacuolar H+-ATPase." Journal of Biological Chemistry **282**(36): 26185-26194.

Smardon, A. M., et al. (2015). "Molecular interactions and cellular itinerary of the yeast RAVE (regulator of the H+-ATPase of vacuolar and endosomal membranes) complex." Journal of Biological Chemistry **290**(46): 27511-27523.

Smardon, A. M., et al. (2002). "The RAVE complex is essential for stable assembly of the yeast V-ATPase." Journal of Biological Chemistry **277**(16): 13831-13839.

Smith, T. F., et al. (1999). "The WD repeat: a common architecture for diverse functions." Trends in Biochemical Sciences **24**(5): 181-185.

Sprent, J. (1995). "Antigen-presenting cells: professionals and amateurs." Current Biology **5**(10): 1095-1097.

Stahelin, R. V., et al. (2014). "Cellular and molecular interactions of phosphoinositides and peripheral proteins." Chemistry and physics of lipids **182**: 3-18.

Stam, N. J. and S. Wilkens (2017). "Structure of the lipid nanodisc-reconstituted vacuolar ATPase proton channel: definition of the interaction of rotor and stator and implications for enzyme regulation by reversible dissociation." Journal of Biological Chemistry **292**(5): 1749-1761.

Stehberger, P. A., et al. (2003). "Localization and regulation of the ATP6V0A4 (a4) vacuolar H+-ATPase subunit defective in an inherited form of distal renal tubular acidosis." Journal of the American Society of Nephrology **14**(12): 3027-3038.

Stover, E., et al. (2002). "Novel ATP6V1B1 and ATP6V0A4 mutations in autosomal recessive distal renal tubular acidosis with new evidence for hearing loss." Journal of medical genetics **39**(11): 796-803.

Stransky, L. A. and M. Forgac (2015). "Amino acid availability modulates vacuolar H+-ATPase assembly." Journal of Biological Chemistry **290**(45): 27360-27369.

Sumner, J.-P., et al. (1995). "Regulation of plasma membrane V-ATPase activity by dissociation of peripheral subunits." Journal of Biological Chemistry **270**(10): 5649-5653.

Sun-Wada, G.-H., et al. (2000). "Acidic endomembrane organelles are required for mouse postimplantation development." Developmental biology **228**(2): 315-325.

Tata, B., et al. (2014). "Haploinsufficiency of Dmxl2, encoding a synaptic protein, causes infertility associated with a loss of GnRH neurons in mouse." PLoS biology **12**(9): e1001952.

Toei, M., et al. (2010). "Regulation and isoform function of the V-ATPases." Biochemistry **49**(23): 4715-4723.

Trepiccione, F., et al. (2016). "Renal Atp6ap2/(Pro) renin receptor is required for normal vacuolar H+-ATPase function but not for the renin-angiotensin system." Journal of the American Society of Nephrology **27**(11): 3320-3330.

Trombetta, E. S., et al. (2003). "Activation of lysosomal function during dendritic cell maturation." Science **299**(5611): 1400-1403.

Tuli, F. and P. M. Kane (2023). "The cytosolic N-terminal domain of V-ATPase a-subunits is a regulatory hub targeted by multiple signals." Frontiers in Molecular Biosciences **10**: 1168680.

Tuttle, A. M., et al. (2014). "Rabconnectin-3a regulates vesicle endocytosis and canonical Wnt signaling in zebrafish neural crest migration." PLoS biology **12**(5).

Uhlén, M., et al. (2015). "Tissue-based map of the human proteome." Science **347**(6220): 1260419.

Ui, M. (1966). "A role of phosphofructokinase in pH-dependent regulation of glycolysis." Biochimica et Biophysica Acta (BBA)-General Subjects **124**(2): 310-322.

Vaccari, T., et al. (2008). "Endosomal entry regulates Notch receptor activation in Drosophila melanogaster." The Journal of cell biology **180**(4): 755-762.

Vasanthakumar, T., et al. (2019). "Structural comparison of the vacuolar and Golgi V-ATPases from Saccharomyces cerevisiae." Proceedings of the National Academy of Sciences **116**(15): 7272-7277.

Vasanthakumar, T., et al. (2021). "Coordinated conformational changes in the V1 complex during V-ATPase reversible dissociation."

Wagner, C. A., et al. (2023). "The pathophysiology of distal renal tubular acidosis." Nature Reviews Nephrology **19**(6): 384-400.

Wang, C., et al. (2024). "Structure and topography of the synaptic V-ATPase–synaptophysin complex." Nature: 1-3.

Wang, H., et al. (2023). "Structural basis of V-ATPase VO region assembly by Vma12p, 21p, and 22p." Proceedings of the National Academy of Sciences **120**(6): e2217181120.

Wang, H., et al. (2024). "Structure of yeast RAVE bound to a partial V1 complex." bioRxiv: 2024.2007. 2018.604153.

Wang, L., et al. (2020). "Structures of a complete human V-ATPase reveal mechanisms of its assembly." Molecular Cell **80**(3): 501-511. e503.

Wang, S. K., et al. (2015). "Critical roles for WDR 72 in calcium transport and matrix protein removal during enamel maturation." Molecular genetics & genomic medicine **3**(4): 302-319.

Wang, Y., et al. (2022). "Control of infection by LC3-associated phagocytosis, CASM, and detection of raised vacuolar pH by the V-ATPase-ATG16L1 axis." Science Advances **8**(43): eabn3298.

Watanabe, S., et al. (2013). "Ultrafast endocytosis at mouse hippocampal synapses." Nature **504**(7479): 242-247.

Webb, B. A., et al. (2011). "Dysregulated pH: a perfect storm for cancer progression." Nature Reviews Cancer **11**(9): 671-677.

Wieczorek, H., et al. (1999). "Animal plasma membrane energization by proton-motive V-ATPases." Bioessays **21**(8): 637-648.

Wilkens, S., et al. (2023). "Tender love and disassembly: How a TLDc domain protein breaks the V-ATPase." Bioessays **45**(7): 2200251.

Wilms, T., et al. (2017). "The yeast protein kinase Sch9 adjusts V-ATPase assembly/disassembly to control pH homeostasis and longevity in response to glucose availability." PLoS genetics **13**(6): e1006835.

Xu, Y., et al. (2022). "ARF GTPases activate Salmonella effector SopF to ADP-ribosylate host V-ATPase and inhibit endomembrane damage-induced autophagy." Nature structural & molecular biology **29**(1): 67-77.

Yan, Y., et al. (2009). "The vacuolar proton pump, V-ATPase, is required for notch signaling and endosomal trafficking in Drosophila." Developmental cell **17**(3): 387-402.

Zhan, T., et al. (2017). "Wnt signaling in cancer." Oncogene **36**(11): 1461-1473.

Zhang, C.-S., et al. (2014). "The lysosomal v-ATPase-Ragulator complex is a common activator for AMPK and mTORC1, acting as a switch between catabolism and anabolism." Cell metabolism **20**(3): 526-540.

Zhang, J., et al. (2014). "Incomplete distal renal tubular acidosis from a heterozygous mutation of the V-ATPase B1 subunit." American Journal of Physiology-Renal Physiology **307**(9): F1063-F1071.

Zhang, Z., et al. (2008). "Structure of the yeast vacuolar ATPase." Journal of Biological Chemistry **283**(51): 35983-35995.

Zhao, J., et al. (2015). "Electron cryomicroscopy observation of rotational states in a eukaryotic V-ATPase." Nature **521**(7551): 241-245.

Chapter 2

The ROGDI protein mutated in Kohlschutter-Tonz syndrome is a novel subunit of the Rabconnectin-3 complex implicated in V-ATPase assembly.

Samuel Winkley and Patricia Kane

This chapter is under revision for the Journal of Biological Chemistry

2.1 ABSTRACT

V-ATPases are highly conserved ATP driven rotary proton pumps found widely among eukaryotes. V-ATPases are composed of two subcomplexes: V_1 and V_0. V-ATPase activity is regulated in part through a process called reversible disassembly, during which V_1 physically separates from V_0 and both subcomplexes become inactive. Reassociation of V_1 to V_0 reactivates the complex for ATP-driven proton pumping and organelle acidification. V-ATPase reassembly in *S. cerevisiae* requires the RAVE complex (Rav1, Rav2, and Skp1) and higher eukaryotes, including humans, utilize the Rabconnectin-3 complex. Mammalian Rabconnectin-3 has two subunits: Rabconnectin-3α and Rabconnectin-3β. Rabconnectin-3 α isoforms are homologous to Rav1, but there is no known Rav2 homolog and the molecular basis of the interaction between the Rabconnectin-3α and β subunits is unknown. We identified ROGDI as a Rav2 homolog and novel Rabconnectin-3 subunit. ROGDI mutations cause Kohlschutter-Tonz syndrome, an epileptic encephalopathy with amelogenesis imperfecta that has parallels to V-ATPase-related disease. ROGDI shares extensive structural homology with yeast Rav2 and binds to the N-terminal domains of both Rabconnectin-3 α and β in a manner similar to Rav2 binding to Rav1. Molecular modeling suggests that ROGDI may bridge the two Rabconnectin-3 subunits. ROGDI co-immunoprecipitates with Rabconnectin-3 subunits from detergent solubilized lysates and is present with them in immunopurified lysosomes. In immunofluorescence microscopy, ROGDI partially localizes with Rabconnectin-3a in highly acidic, perinuclear lysosomes. The discovery of ROGDI as a novel Rabconnectin-3 interactor sheds new light on both Kohlschutter-Tonz syndrome and the mechanisms behind mammalian V-ATPase regulation.

2.2 INTRODUCTION

V-ATPases are rotary motors that couple the hydrolysis of ATP to the movement of protons across biological membranes. V-ATPases are composed broadly of two subcomplexes, V_1 and V_0. V_0 resides in a membrane and is responsible for the translation of the rotational force from V_1 into proton translocation across the membrane. V_1, which is oriented toward the cytosol and peripheral to the V_0 subcomplex, hydrolyzes ATP, creating rotation of a central stalk that is transmitted to V_0. V-ATPase activity is essential in higher eukaryotes, and conditionally lethal in yeast (Nelson and Nelson 1990, Inoue, Noumi et al. 1999). V-ATPases are highly conserved among eukaryotes, including mammals. This broad conservation allows *S. cerevisiae* to be used as a model system for studying the V-ATPase. V-ATPase activity has been shown to be important for viral entry into cells, vesicular loading and trafficking, lysosomal/vacuolar degradation, and the progression of some cancers (Santos-Pereira, Rodrigues et al. 2021). Given the important roles that V-ATPases play, proper regulation of V-ATPase activity is essential. Several different regulatory mechanisms have been identified including membrane phosphoinositide lipid content, subunit composition, and reversible disassembly (Kane 1995, Kawasaki-Nishi, Nishi et al. 2001, Banerjee, Clapp et al. 2019).

In cells, V-ATPases are present as both fully assembled, active complexes and disassembled, inactive V_1 and V_0 subcomplexes. Conversion between these states can depend on multiple signals and is termed reversible disassembly. In *S. cerevisiae,* glucose deprivation triggers V-ATPase disassembly while the presence of glucose triggers rapid reassembly (Kane 1995, Parra, Keenan et al. 2000). When the proper conditions are met,

V_1 reassembles with V_o and catalytic activity resumes. The assembly state of mammalian V-ATPases has been found to respond to glucose, amino acids, and luminal pH (Nakamura 2004, Zoncu, Bar-Peled et al. 2011, Bodzęta, Kahms et al. 2017, McGuire and Forgac 2018).

In yeast, the RAVE complex (composed of Rav1, Rav2, and Skp1) catalyzes V-ATPase assembly (Seol, Shevchenko et al. 2001, Smardon, Tarsio et al. 2002). Rav1 is the backbone of the RAVE complex, and binds to Rav2, Skp1, V_1 subunits (V_1E and G, V_1C), and Vph1 (V_oa) (Smardon, Nasab et al. 2015). Comparatively less is known about Rav2; it binds to the N-terminal end of Rav1 (2-240) and has been shown to also bind to Vma5 (Wang, Tarsio et al. 2024) (Smardon, Nasab et al. 2015). The current model of RAVE-catalyzed reassembly suggests that RAVE binds to cytosolic V_1, creating a RAVE-V_1 complex. The RAVE/V_1 complex then binds to cytosolic V_1C and then reunites V_1 and V_1C with V_o on the vacuolar membrane (Jaskolka, Tarsio et al. 2021). Upon reassembly on the vacuolar membrane the catalytic activity of both domains resume.

The process of reversible disassembly, like V-ATPase structure, is well conserved among eukaryotes(Sautin, Lu et al. 2005, Collins and Forgac 2020). The RAVE complex homolog in higher eukaryotes is Rabconnectin-3. RAVE and Rabconnectin-3 are both required for efficient V-ATPase reassembly but respond to different signals for assembly and disassembly (Sethi, Yan et al. 2010, Einhorn, Trapani et al. 2012, Tuttle, Hoffman et al. 2014, Ratto, Chowdhury et al. 2022). Rabconnectin-3 is a heterodimer composed of two subunits: Rabconnectin-3α and Rabconnectin-3β(Nagano, Kawabe et al. 2002, Kawabe, Sakisaka et al. 2003). Each Rabconnectin-3 subunit has two isoforms in mammals. Rabconnectin-3α includes DMXL1 and DMXL2 and Rabconnectin-3β

includes WDR7 and possibly WDR72. Based on published expression data, the isoforms for each subunit appear to be expressed differently based on tissue type (Uhlén, Fagerberg et al. 2015). Both Rabconnectin-3α and Rabconnectin-3β share some structural similarity to Rav1 (Jaskolka, Winkley et al. 2021) although Rabconnectin-3α shares additional sequence homology.

We show here that the relatively poorly characterized protein ROGDI is the higher eukaryotic homolog of yeast Rav2. ROGDI mutations cause Kohlschutter-Tonz syndrome (KTS), a homozygous recessive condition characterized by amelogenesis imperfecta, epilepsy and psychomotor regression (Schossig, Wolf et al. 2012). We found that ROGDI interacts with the N-terminal region of Rabconnectin-3 subunits and co-immunoprecipitates with DMXL1, WDR7 and the V_1A subunit. ROGDI strongly colocalizes with V_1A and partially colocalizes DMXL1 and lysosomes. We speculate that Kohlschutter-Tonz syndrome is a disease resulting from impaired V-ATPase activity; ROGDI mutations impair the activity of the Rabconnectin-3 complex which in turn results in decreased V-ATPase assembly and activity.

2.3 RESULTS

2.3.1 Mammalian ROGDI shares structural and functional homology with yeast Rav2

Although Rav2 is essential for RAVE function in yeast (Smardon, Tarsio et al. 2002) Rabconnectin-3 has long been characterized as a heterodimer with no subunit equivalent to yeast Rav2. Mutations in the ROGDI protein are associated with Kohlschutter-Tonz syndrome, but its molecular function was unknown (Schossig, Wolf et al. 2012). However, the Phyre2 homology server (Kelley, Mezulis et al. 2015) modelled

most of the Rav2 sequence onto a crystal structure of ROGDI (Lee, Jeong et al. 2017) with high confidence. In addition, ROGDI has been identified in co-precipitates with the V-ATPase and Rabconnectin-3 subunits by mass spectrometry (Merkulova, Păunescu et al. 2015, Coupland, Karimi et al. 2024). A recent ROGDI knockout mouse both recapitulates the symptoms of Kohlscutter-Tonz syndrome and exhibits evidence of altered pH homeostasis (Jimenez-Armijo, Morkmued et al. 2024).

Rogdi and Rav2 are of similar sizes; ROGDI is 287 amino acids (32 kDa) and Rav2 is 351 amino acids (40 kDa). The two sequences are only 20.5% similar (11% direct identity) based on comparison by EMBOSS (Rice, Longden et al. 2000), but a superposition of the AlphaFold (Jumper, Evans et al. 2021) models for Rav2 and Rogdi shown in Figure 1a highlights striking structural similarities between the proteins. A recent structure of yeast RAVE (Wang, Tarsio et al. 2024) further supports the strong structural similarity between Rav2 and ROGDI. Both proteins contain two main domains: an α-domain which folds into an atypical leucine zipper and a β-domain which folds into a β-sandwich. Surface loops within these regions contain the most structural diversity. The additional size of Rav2 derives from a domain peripheral to the β-domain (residues 225-300). The functional consequence of these differences is not yet known. However, the substantial structural similarity between the two proteins strongly suggests a common function.

Yeast *rav1*Δ and *rav2*Δ deletion mutants exhibit a characteristically weaker version of the Vma^- phenotype arising from loss of V-ATPase activity (Seol, Shevchenko et al. 2001) The Vma^- mutants can grow at pH 5 but grow poorly at elevated pH or in the presence of multiple ions including Zn^{2+}. *vph1*Δ mutants, which lack a vacuole-specific

V-ATPase subunit isoform, show some growth at elevated pH, but fail to grow in plates containing 4 mM $ZnCl_2$. RAVE is an isoform-specific assembly factor, only catalyzing assembly of Vph1 containing V-ATPases, and *rav* mutants also fail to grow in elevated zinc concentrations (Smardon, Diab et al. 2014).

Replacement of the *RAV2* open reading frame with the human ROGDI cDNA partially rescues the Rav^- phenotype of a *rav2Δ* mutant as shown in Figure 1b. We also expressed a yeast codon-optimized ROGDI from the *RAV2* promoter (RecHu ROGDI). This further rescued the Rav^- phenotype compared to human ROGDI cDNA. Replacement of the native *RAV2* promoter, which is relatively weak, with the strong *TEF* promoter slightly improved growth. To confirm that ROGDI was acting as part of the yeast RAVE complex rather than as a bypass suppressor, we deleted RAV_1 in the TEF-RecHu ROGDI strain. In this strain, any rescue by ROGDI is abolished, indicating that ROGDI may function as part of the RAVE complex in a Rav2-like manner.

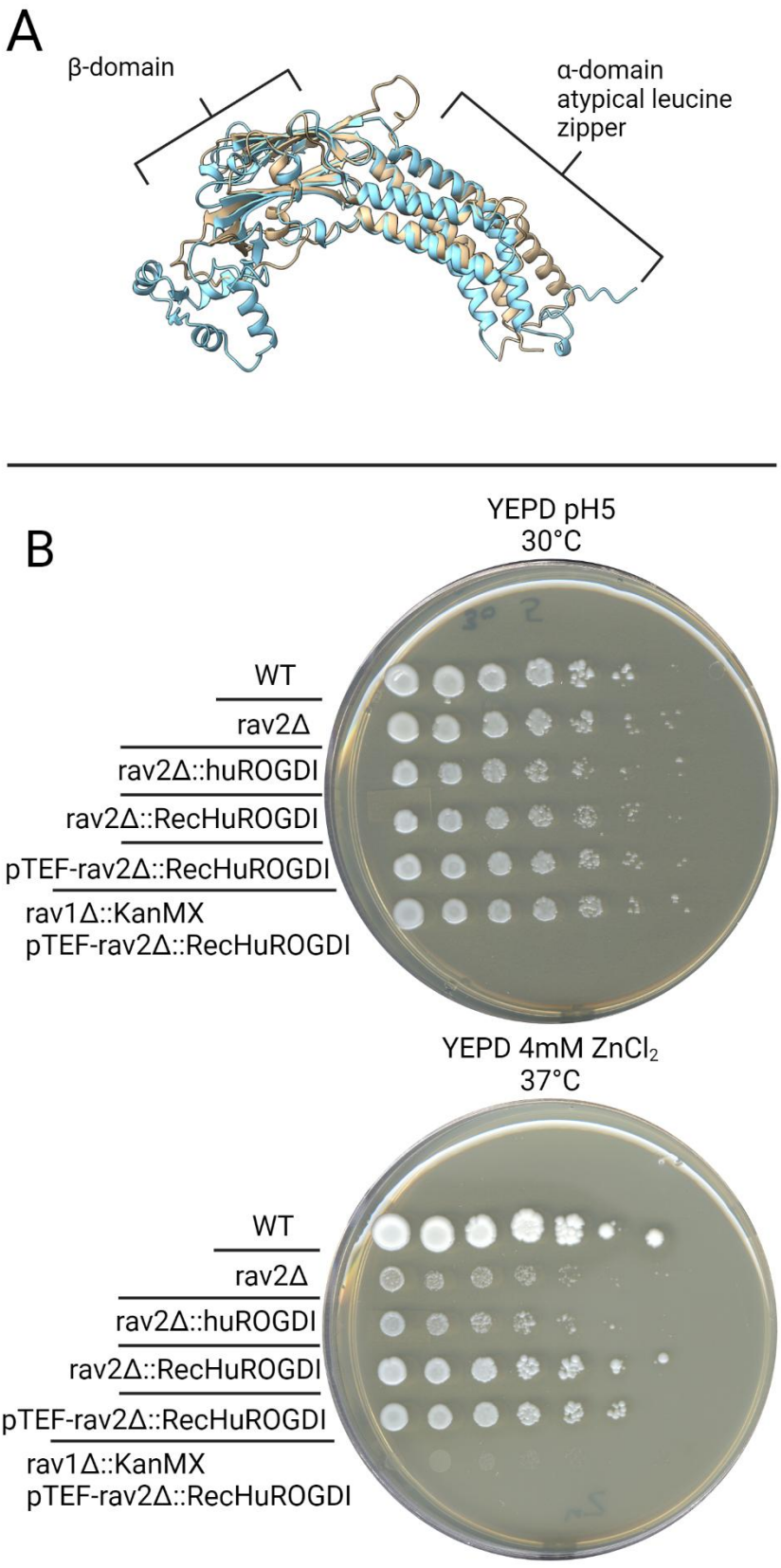
A
β-domain
α-domain
atypical leucine
zipper
B
YEPD pH5
30°C
WT
rav2Δ
rav2Δ::huROGDI
rav2Δ::RecHuROGDI
pTEF-rav2Δ::RecHuROGDI
rav1Δ::KanMX
pTEF-rav2Δ::RecHuROGDI
YEPD 4mM ZnCl2
37°C
WT
rav2Δ
rav2Δ::huROGDI
rav2Δ::RecHuROGDI
pTEF-rav2Δ::RecHuROGDI
rav1Δ::KanMX
pTEF-rav2Δ::RecHuROGDI

Figure 2-1 Human ROGDI and yeast Rav2 display structural and functional homology.

A, Superposition of AlphaFold3 models of human ROGDI (tan, uniprot ID: Q03956) and yeast Rav2 (blue, Uniprot ID: Q9GZN7). Models were superimposed with UCSF ChimeraX. Models were retrieved from the AlphaFold Protein Structure Database, identifiable by Uniprot ID. **B**, Phenotyping of *rav2*Δ and *rav2*Δ*::ROGDI* containing strains. *rav2*Δ::huROGDI encodes for human ROGDI in place of the *RAV2* open reading frame under control of the native *RAV2* promoter*; rav2*Δ*::*RecHuROGDI encodes human ROGDI recoded for yeast expression in place of the *RAV2* open reading frame; pTEF-*rav2*Δ::RecHuROGDI replaces the native *RAV2* promoter for the strong *TEF* promoter; the *rav1*Δ*::KanMX* p*TEF-rav2*Δ*::RecHuROGDI* strain carries a deletion in the RAVE backbone subunit Rav1. YEPD pH 5 at 30°C (Top) is permissive for growth of *rav* mutants, YEPD +4 mM $ZnCl_2$ at 37°C (bottom) is not permissive for the growth of *rav* mutants.

2.3.2 ROGDI interacts with structurally conserved N-terminal β-propeller in yeast two-hybrid assay

We hypothesized that ROGDI might bind to Rav1, based on the complementation of the *rav2Δ* phenotype, and possibly to one or more of the Rabconnectin-3 subunits. There are no experimental structures of Rabconnectin-3 subunits available. Secondary structure comparisons of the Rabconnectin-3 subunits to Rav1 are shown in Figure 2a. The N-terminal region of Rav1 forms two b-propellers (Wang, Tarsio et al. 2024) and both Rabconnectin-3 subunits are predicted to be rich in β-sheets and to contain WD-40 repeats which form β-propellers. Additionally, in all three proteins, following the β-propellers is an α-solenoid domain. The α-solenoid of Rav1 is responsible for binding to the V_1E and V_1G subunits (Smardon, Nasab et al. 2015). This region has the highest homology between Rav1 and Rabconnectin-3α. There are additional regions of homology within the β-propeller region and a 6 amino acid sequence necessary for Rav1 to bind to Vph1 (Jaskolka, Winkley et al. 2021). Specifically, it appears that Rav1 residues 2-240 are indispensable for Rav2 binding (Smardon, Nasab et al. 2015), and are conserved in Rabconnectin-3a. In the cryo-EM structure of RAVE-V_1, residues 2-240 localize to the first β-propeller and Rav2 binds in this region (Wang, Tarsio et al. 2024).Considering the overall structural conservation of Rogdi to Rav2 and Rav1 to Rabconnectin-3, we hypothesize that Rogdi interacts with the similar regions of Rabconnectin-3.

We generated yeast two-hybrid constructs containing the N-terminal β-propeller regions of DMXL2, WDR7, WDR72, and Rav1. With this yeast 2-hybrid system (James, Halladay et al. 1996)), fusion proteins with the Gal4 activating and binding domains

drive expression of genes under control of the GAL1 and GAL2 promoters when they interact. Growth on medium lacking adenine and histidine (SD-trp, leu, ade, his) can then be used as a readout for protein-protein interactions. Figure 2b shows growth for strains containing ROGDI and DMXL2 NT, WDR7 NT, WDR72 NT, and Rav1 NT, but there is no growth when ROGDI is combined with control vectors pACT2 and pAS1-lamin. These data indicate that ROGDI binds to the indicated N-terminal regions of DMXL2, WDR7, WDR72, and Rav1. ROGDI binding to Rav1 is consistent with the ability for ROGDI to partially rescue growth under Rav- conditions in a *rav2*Δ mutant shown in Figure 1b. Furthermore, these results suggest that ROGDI binds to both DMXL2, which has direct sequence homology with Rav1, and WDR7 and WDR72, which do not.

A

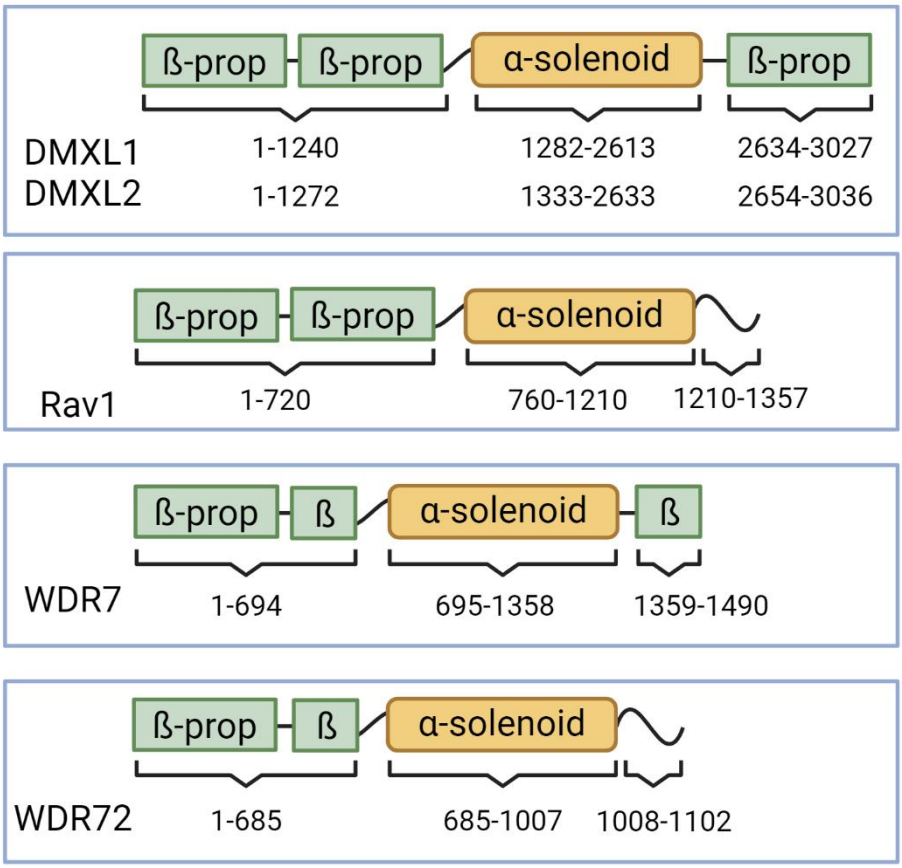

B

pACT2 ROGDI x pAS2 DMXL2 1-625
pAS2 ROGDI x pACT2 WDR7 1-596
pACT2 ROGDI x pAS2 WDR72 2-589
pACT2 ROGDI x pAS2 Rav1 NT
pACT2 ROGDI x pAS1 Lamin
pAS2 ROGDI x pACT2 E.V

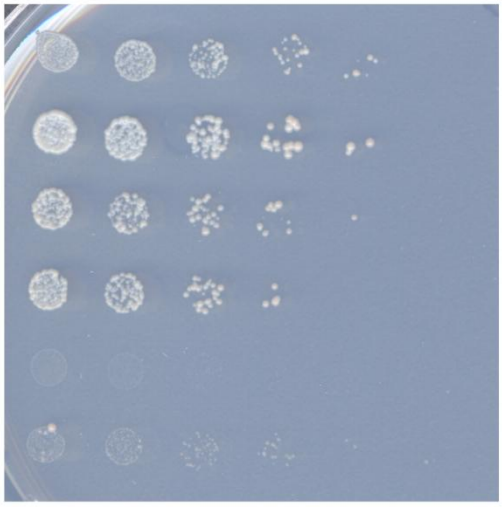

Figure 2-2 ROGDI interacts with conserved β-propeller region of Rav1 and Rabconnectin-3

A, Secondary structure comparison of Rabconnectin-3α, Rabconnectin-3β, and Rav1. Regions that are modeled to form β-propellers and α-solenoid are indicated with corresponding amino acid positions. **B**, Fusion proteins of ROGDI, DMXL2 1-625, WDR7 1-596, WDR72 1-589, and Rav1 2-720 were generated in pAS2 and pACT2 plasmids as described in Experimental Procedures. All pACT2 plasmids were transformed into the PJ69-4α two-hybrid strain and pAS2 plasmids were transformed into PJ69-4a yeast two-hybrid strain. Diploids were selected on SD media lacking leucine and tryptophan (SD-Trp, Leu). Growth on test media lacking tryptophan, leucine, histidine, and adenine (SD- trp, leu, ade, his) is shown and indicates protein-protein interactions between the fusion proteins. pACT2 vector only and pAS1-lamin were used as negative controls.

2.3.3 ROGDI is modeled to interact with both Rabconnectin-3 subunits

The molecular nature of the interaction between the Rabconnectin-3 subunits is not understood. A stable complex between Rabconnectin-3α and Rabconnectin-3β was identified by Kawabe et al in 2003 (Kawabe, Sakisaka et al. 2003). However, it is not known whether there are additional members of the complex. Since one of the major differences between human Rabconnectin-3 and yeast RAVE is the apparent duplication of the Rav1-like subunit, we are not able to look to yeast as a model system. ROGDI displays yeast two-hybrid interactions between the N-terminal domain of both Rabconnectin-3a and b subunits (Figure 2b). We speculate that ROGDI may serve a bridging function, connecting the two Rabconnectin-3 subunits. To begin investigating the interaction between ROGDI, DMXL1 NT, and WDR7 NT we used AlphaFold Multimer (Evans, O'Neill et al. 2022) to model the three proteins together. WDR7 and DMXL1 were chosen as they are the more ubiquitously expressed isoforms (Uhlén, Fagerberg et al. 2015). The top result is a model which includes ROGDI interacting with β-propellers from both DMXL1 NT and WDR7 NT (Figure 3). WDR7 is modeled to include 1.5 N-terminal propellers in the N-terminal region while DMXL1 is modeled to include 2 full propellers, like Rav1. ROGDI is positioned between the face of the full propeller of WDR7 with the half propeller contracting the ROGDI α-domain. DMXL1 is modeled to contact the ROGDI α-domain opposing WDR7, with ROGDI making contacts with first DMXL1 ß-propeller. The DMXL1-ROGDI interaction is similar to the interaction between Rav1 and Rav2 (Wang, Tarsio et al. 2024). There are few contacts modeled between DMXL1 and WDR 7; consistent with this, we have not observed

interactions between Rabconnectin-3a and b subunit isoforms in yeast 2-hybrid experiments. Further investigation is needed to experimentally confirm the details of this modeled interaction, but we sought support for a trimeric complex by immunoprecipitating DMXL1 from a mammalian cell system and probing for its partner proteins.

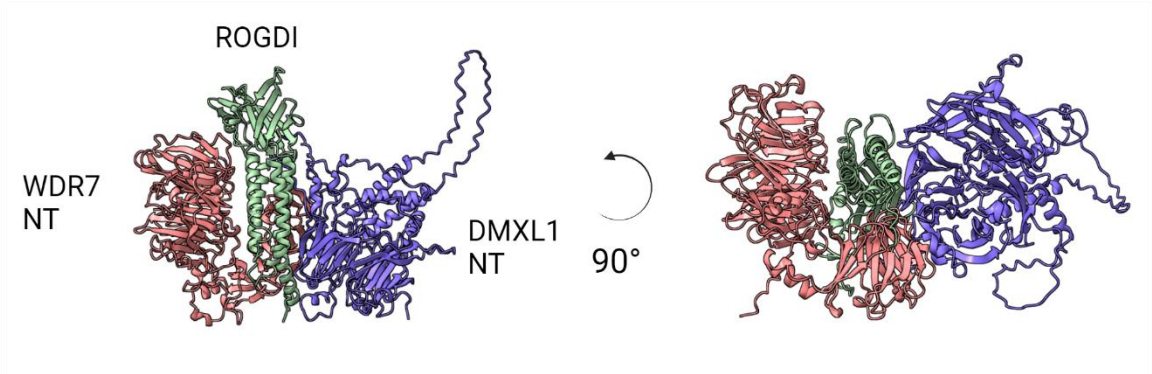

Figure 2-3 AlphaFold3 model of ROGDI binding to N-terminal domains of Rabconnectin-3α and β

AlphaFold3 model of DMXL1 NT (amino acids 1-630), WDR7 NT (1-600), and full-length ROGDI. The ipTM for this model is 0.82 and pTM is 0.81, as described in Experimental Procedures. These reflect a high confidence model.

2.3.4 DMXL1 co-immunoprecipitates WDR7, ROGDI and V_1 subuit A

Both ROGDI and the Rabconnectin-3 subunits are highly conserved among mammals. We immunoprecipitated DMXL1 from a mouse breast cancer cell line previously used to study the V-ATPase (McGuire, Collins et al. 2019) DMXL1 is a large protein (predicted molecular mass of 337 kDa) but only a ~200 kDa fragment was detectable in the input (Figure 4). However, an anti-DMXL1 polyclonal antibody immunoprecipitated both the ~200 kDa fragment and full length DMXL1. Additionally, WDR7, ROGDI, and V_1A co-immunoprecipitated with DMXL1 (Figure 4). None of these proteins was immunoprecipitated with a non-specific isotype control. These data suggest that ROGDI is present in complexes with DMXL1, WDR7, and the V-ATPase.

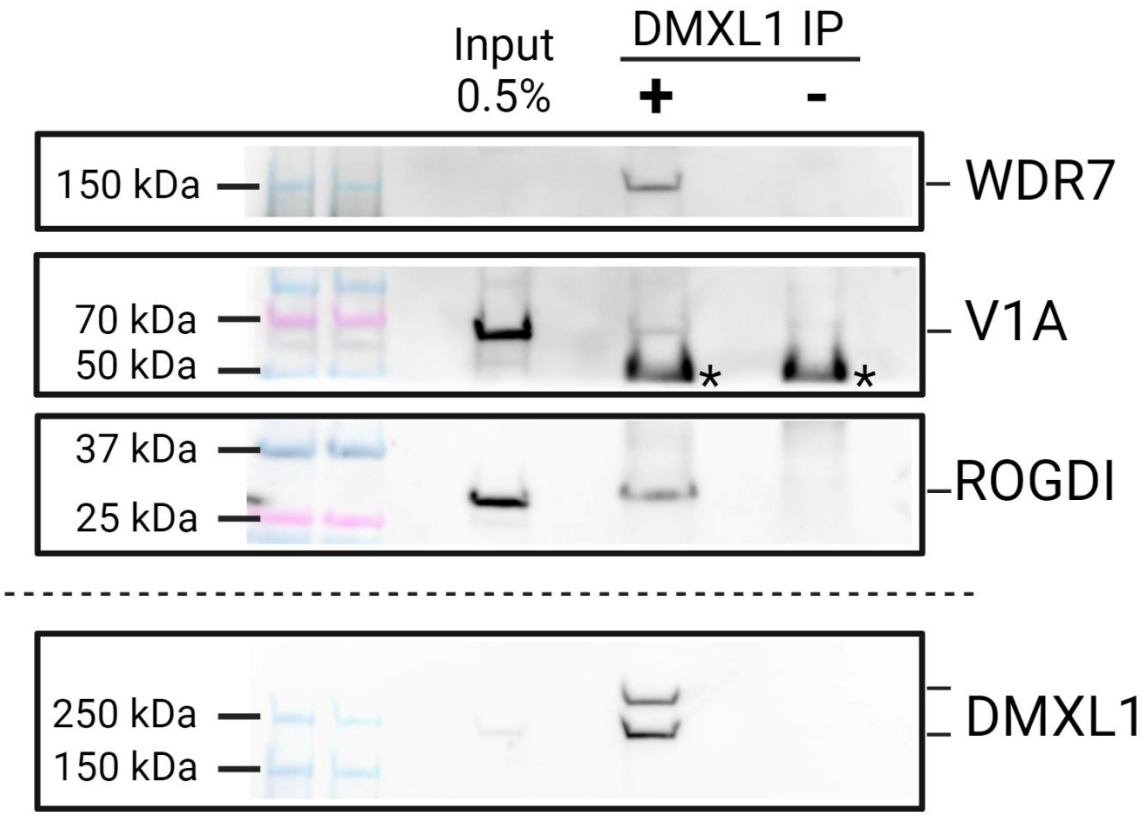

Figure 2-4 DMXL1 co-immunoprecipitates ROGDI, WDR7, and V_1 subunit A

DMXL1 immunoprecipitation from mouse 4T1 cells was performed as described in Experimental Methods. Anti-DMXL1 antibody (+) or an equal amount nonspecific rabbit IgG (-) were separately bound to equal volumes of protein-A Dynabeads. 4T1 cells were lysed and subjected to crosslinking as described in Experimental Procedures. 0.5% of the total lysate was run on the gel as indicated. The IgG-Dynabead complexes were incubated with equal volumes of 4T1 lysate at 4° with agitation. Samples were eluted from beads by heating at 98°C in the presence of cracking buffer, then analyzed by SDS-PAGE and western blotting with the indicated antibodies. The top three images

were cut from the same blot, then probed with antibodies. The bottom image is from a separate blot. Molecular mass standards are shown at the left. IgG heavy chain is denoted with an asterisk. The data shown are representative of three biological replicates.

2.3.5 Cellular localization of ROGDI and DMXL1

In *S. cerevisiae*, RAVE binds to V_1 in the cytosol and Rav1 and Rav2 are reversibly recruited to vacuolar membrane as a complex under assembly conditions (Parra and Kane 1998, Smardon, Nasab et al. 2015). We investigated the intracellular localization of ROGDI and the V-ATPase V_1A subunit using direct immunofluorescence microscopy (Figure 5a). Both ROGDI and V_1A exhibit diffuse cytosolic staining and puncta, with an enrichment in puncta adjacent to the nucleus. Merging the ROGDI and V_1A channels shows substantial overlap between ROGDI and V_1A in the perinuclear region and occasional overlap peripherally. Colocalization of the two proteins is supported by line scan profiles from the ROGDI and V_1A channels in which there is an increase in pixel intensity at similar locations along the line. It appears that, ROGDI, like Rav2, partially colocalizes with V_1 subunits on intracellular compartments. As shown in Figure 5b, the lysosomal membrane marker LAMP2 labels puncta throughout the cell (peripheral lysosomes) and is concentrated adjacent to the nucleus (perinuclear lysosomes). A similar distribution of peripheral and perinuclear lysosomes has been seen in other cell types (Johnson, Ostrowski et al. 2016, Ebner, Puchkov et al. 2023). Staining the same cells with the fixable LysoTracker Red DND-99 pH indicator, which accumulates in acidified lysosomes (Lemieux, Percival et al. 2004), reveals prominent labeling of the perinuclear LAMP2-containing lysosomes, indicating that they are strongly acidic. However, there is also labeling of peripheral lysosomes.

Figure 6a demonstrates that ROGDI also partially colocalizes with LAMP2 puncta, particularly in the perinuclear region. ROGDI/LAMP2 puncta are present

peripherally but are less numerous. However, as shown in Figure 5a, ROGDI also displays a diffuse cytosolic staining, suggesting that not all ROGDI is associated with membranes. We compared the localization of DMXL1 and LAMP2 (Figure 6b) as well. DMXL1 shows extensive co-localization with LAMP2 in both peripheral and perinuclear lysosome populations, with little cytosolic staining, suggesting it associates more strongly with lysosomes than ROGDI. Finally, we compared the localization of DMXL1 and ROGDI directly (Figure 6c). As shown in Figure 6c, there is strong overlap between ROGDI and DMXL1 in the perinuclear region. These data suggest that DMXL1 is localized generally to lysosomes throughout the cell on both peripheral and perinuclear lysosomes. ROGDI, on the other hand, localizes primarily to perinuclear lysosomes and has a diffuse cytosolic population that may not be bound to any membrane.

To investigate the subcellular distribution of ROGDI, WDR7, DMXL1, and V_1 subunit A further, we first used subcellular fractionation. Cells were lysed in the absence of detergent and the supernatant from a low-speed centrifugation was separated into membrane and soluble fractions by high-speed centrifugation. Figure 7a demonstrates that Rabconnectin-3 subunits WDR7 and DMXL1 are almost entirely in the membrane fraction with relatively little free in the cytosol (Figure 7a). In contrast, ROGDI is largely in the supernatant while a minor population is membrane associated.

We also isolated a lysosomal fraction by LysoIP, using the HA-tagged lysosomal protein TMEM192 to affinity purify lysosomes from a cell lysate (Abu-Remaileh, Wyant et al. 2017). (Supporting Information Figure 1 shows that TMEM192 localizes to the lysosomal membrane in these cells.) Both DMXL1 and ROGDI are enriched in LysoIP sample (Figure 7b), suggesting they associate with lysosomal membranes. A smaller

proportion of V_1 subunit A is also present on lysosomes; this population is likely to represent assembled V-ATPases. These results are consistent with localizations observed in Figures 5 and 6 and suggest that although ROGDI can associate with Rabconnectin-3 subunits DMXL1 and WDR7, it is not always associated with them in the cell. Like the V-ATPase V_1 subcomplex, ROGDI can be present both in the cytosol and on the lysosomal membrane.

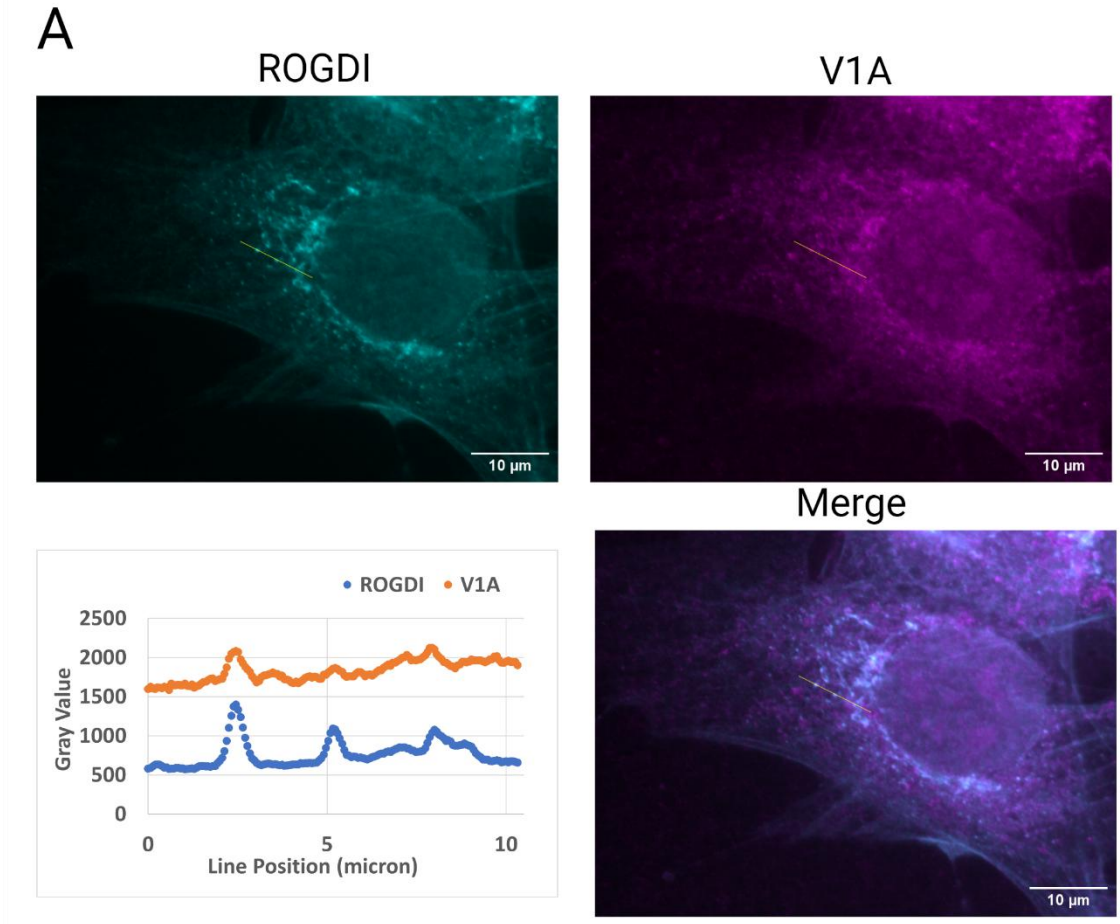
A
ROGDI
V1A
10 µm
10 µm
Merge
ROGDI
V1A
2500
2000
1500
1000
500
0
Gray Value
0
5
10
Line Position (micron)
10 µm

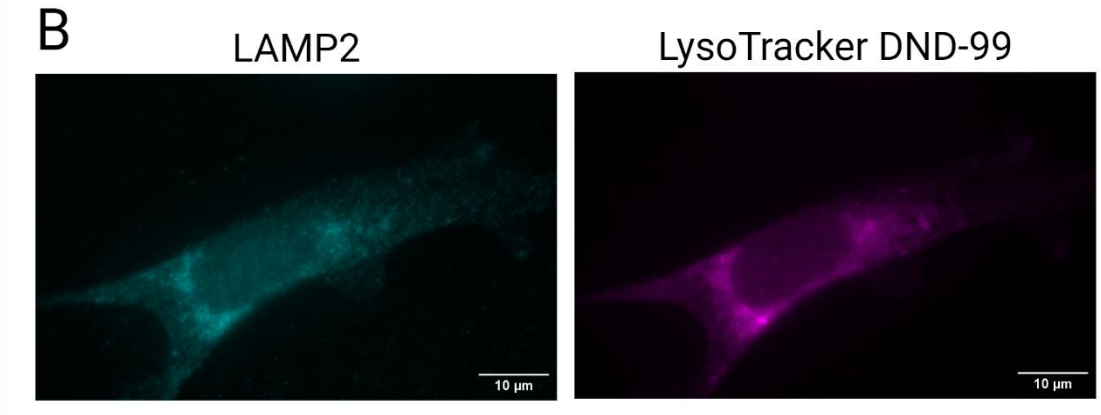
B
LAMP2
LysoTracker DND-99
10 µm
10 µm

Figure 2-5 Rogdi partially localizes with V_1A on perinuclear lysosomes

A, immunofluorescence micrograph of 4T1 cells co-stained with directly labeled anti-V_1 A subunit (magenta) and anti-ROGDI (cyan) antibodies as described in Experimental Procedures. A yellow line was drawn through ROGDI puncta using FIJI to evaluate the distribution of fluorescence intensity between ROGDI and V_1A channels. Fluorescence intensity for ROGDI is plotted in blue and V_1A is plotted in orange. A merged image combining the ROGDI and V_1A channels is present to the right of the linescan plot. **B**, immunofluorescence micrograph of 4T1 cells co-stained with anti-LAMP2 (cyan) antibody and fixable LysoTracker DND-99 (magenta), an indicator of lysosomal acidification. Cells were stained with LysoTracker DND-99 immediately prior to fixation and permeabilization. Permeabilization and fixation were performed as in Figure 5a. Images shown are representative of images from three separate biological replicates.

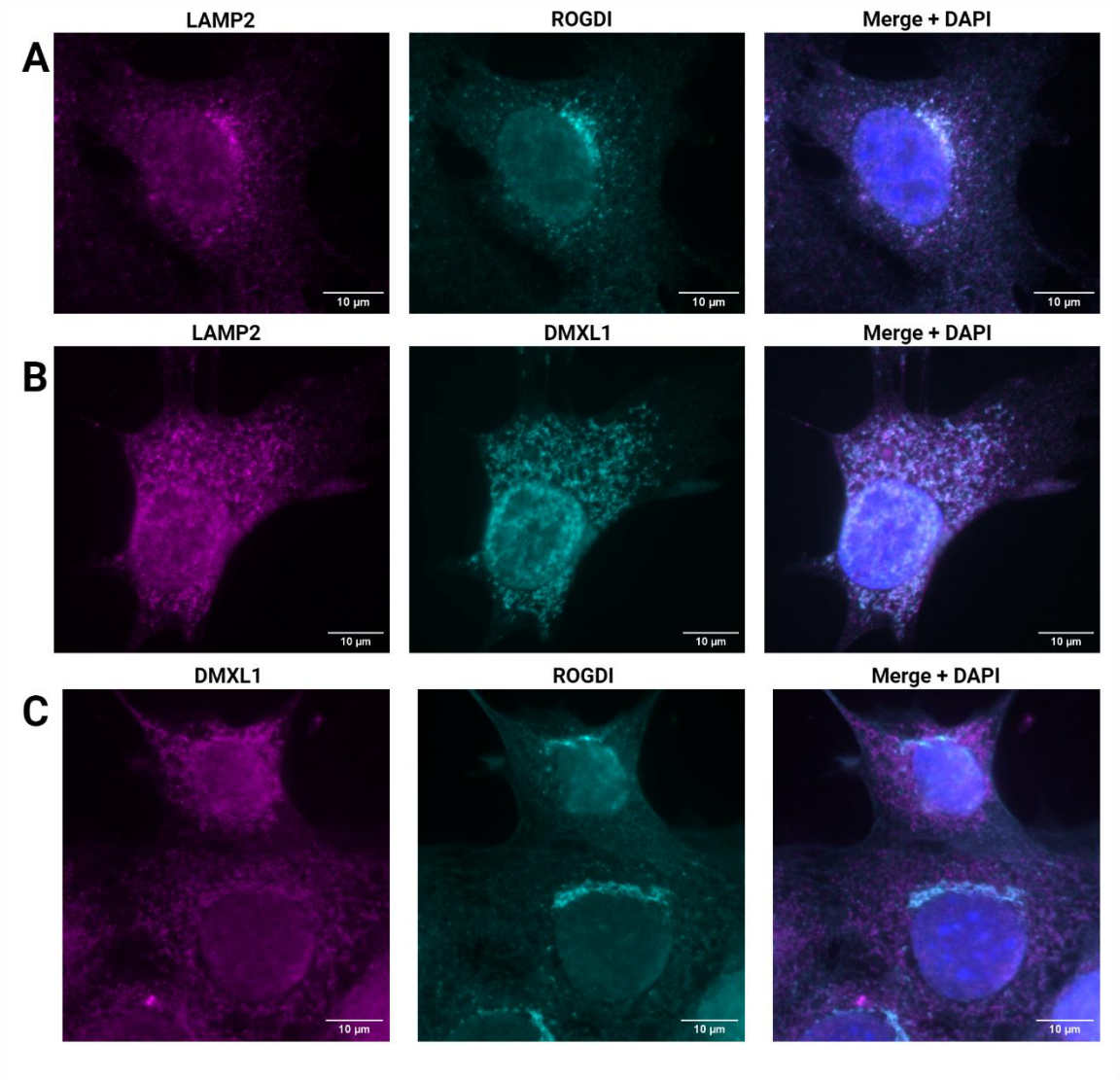

Figure 2-6- DMXL1 and ROGDI partially colocalize on perinuclear lysosomes

A, immunoflourescence micrograph of a 4T1 cell co-stained with indirectly labeled anti-LAMP2 (magenta) and anti-ROGDI (cyan) antibodies. LAMP2 serves as a lysosomal marker. The composite image with DAPI (blue) shown to the right illustrates partial overlap between the anti-LAMP2 and anti-ROGDI channels on perinuclear lysosomes. **B,** immunofluorescence micrograph of a 4T1 cell co-stained with indirectly

labeled anti-LAMP2 (magenta) and anti-DMXL1 (cyan) antibodies. The composite image to the right shows extensive overlap between the anti-LAMP2 and anti-DMXL1 channels on both perinuclear and peripheral lysosomes. **C,** micrograph of several 4T1 cells co-stained with directly labeled anti-DMXL1 (magenta) and anti-ROGDI (cyan) antibodies. Composite image shown to the right shows a partial overlap between the anti-ROGDI and anti-DMXL1 channels adjacent to the cell nucleus. Images shown are representative of images from three separate biological replicates.

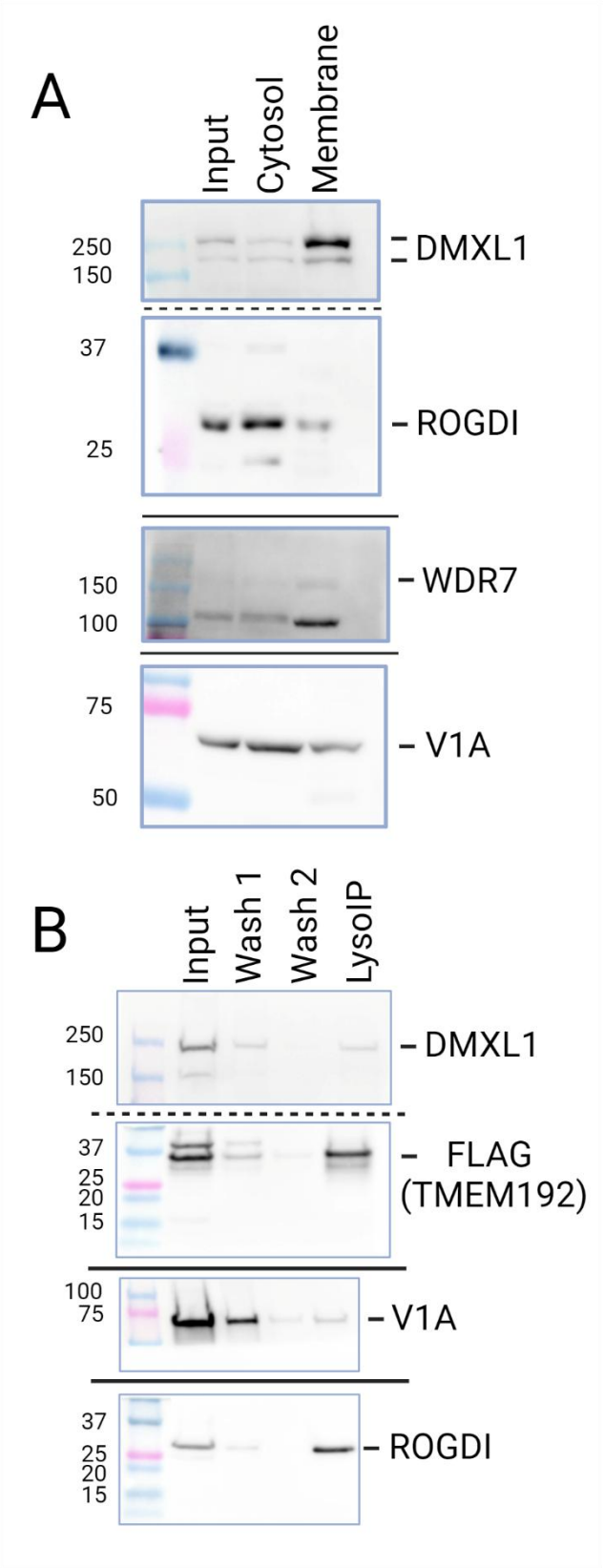
A
Input
Cytosol
Membrane
250
150
DMXL1
37
25
ROGDI
150
100
WDR7
75
50
V1A
B
Input
Wash 1
Wash 2
LysoIP
250
150
DMXL1
37
25
20
15
FLAG
(TMEM192)
100
75
V1A
37
25
20
15
ROGDI

Figure 2-7- Subcellular distribution of ROGDI and Rabconnectin-3

A, subcellular fractionation of 4T1 cell lysate. Cells were lysed mechanically by passing through a 27-gauge needle and centrifuged at 10,000 x g to pellet nuclei and mitochondria. A portion of the resulting post-mitochondrial supernatant was reserved as input as described in Experimental Procedures. The post-mitochondrial supernatant was then centrifuged to pellet membranes and supernatant (cytosol). Both the membrane pellet and cytosolic samples were denatured and analyzed by SDS-PAGE and western blotting with antibodies against the indicated proteins. Molecular mass markers are shown on left. All samples were run on a single SDS-PAGE gel, and immunoblots probed anti-ROGDI and anti-DMXL1 blots were cut at the 50 kDa molecular mass marker. The experiment was repeated twice and the blots shown are representative. **B,** a lysosomal fraction was isolated by affinity purification from mechanically lysed 4T1 cells as described in Experimental Procedure. Cells were transiently transfected with pCDNA3-TMEM192-FLAG-HA and a a post-mitochondrial supernatant was generated as in figure 7a. A portion of this sample was set aside as input. Lysosomes were isolated by binding to anti-HA nanobody magnetic beads. Input (0.75% of total), sequential washes of the beads (washes 1 and 2), and the final eluted sample (lysoIP) were separated by SDS-PAGE and analyzed by immunoblotting. All blots were from a single gel that was blotted and cut vertically after transfer. The V_1A/ROGDI blot and DMXL1/TMEM-192 blots were then cut horizontally and probed with the indicated antibodies. Blots shown are representative of three biological replicates.

2.4 DISCUSSION

The work described here shows that the structural similarity between mammalian ROGDI and yeast Rav2 (Wang, Tarsio et al. 2024) extends to function, as indicated by the ability of human ROGDI to complement a *rav2*Δ mutant in yeast. In parallel with the interaction of Rav2 with the N-terminal b-propeller of Rav1, ROGDI exhibits two-hybrid interactions with the b-propeller domains of both Rav1 and Rabconnectin-3α subunit DMXL2, which share sequence homology. Previous work indicated that amino acids 1-240 of Rav1 were required for Rav2 binding (Smardon, Nasab et al. 2015) and the recent cryo-EM structure of RAVE places Rav2 on the third and fourth blades of the first propeller in Rav1. The AlphaFold3 model (Abramson, Adler et al. 2024) of Rabconnectin-3 (Figure 3) independently indicates an interaction with Rogdi with a similar region in first N-terminal propeller in DMXL1, suggesting that this interface is similar between RAVE and Rabconnectin-3. There is no homolog of either Rabconnectin-3b isoform in the yeast genome, and although Rabconnectin-3α and β isoforms are isolated together, the details of their molecular interaction are not known. As noted previously (Jaskolka, Winkley et al. 2021), Rabconnectin-3α and β have similar secondary structures, characterized by predicted b-propellers in the N-terminal half and an α-solenoid region in the C-terminal half, but no direct sequence homology. The two-hybrid assay in Figure 2 indicates that the first N-terminal b-propeller of WDR7 interacts with ROGDI, and this interaction is also seen in the AlphaFold3 model, along with interactions of a second N-terminal "half-propeller". The model in Figure 3 contains only the N-terminal domains of DMXL1 and WDR7, but Supporting Information Figure S2 shows a model of the complete DMXL1, WDR7, and ROGDI complex. Importantly,

both models suggest that ROGDI bridges the N-terminal regions of Rabconnectin-3α and 3b subunits. Removal of ROGDI from the model in Figure S2 reveals relatively few direct interactions between the two Rabconnectin-3 subunits. Further validation of this model is required, but as described below, the phenotypes accompanying loss of ROGDI in vivo would be compatible with functionally significant interactions with both Rabconnectin-3 subunits.

Through immunofluorescence microscopy and subcellular fractionation of mouse 4T1 cells, we found that DMXL1 appears to be primarily membrane-bound and enriched in lysosomes. WDR7 also appears to be membrane-bound. ROGDI coimmunoprecipitates with DMXL1 and is present in lysosomal membrane fractions, but a substantial proportion of ROGDI is soluble and cytosolic. Significantly, none of these proteins has apparent transmembrane domains. Rabconnectin-3 complexes containing DMXL2 and WDR7 are highly expressed in brain and enriched at the pre-synaptic region of neurons (Gandini, Souza et al. 2019, Dittrich, Ramesh et al. 2023) and in the dense core vesicles of neuroendocrine cells (Crummy, Mani et al. 2019). In the latter, both DMXL2 and WDR7 appear to be membrane-bound but WDR7 is implicated in recruitment of DMXL2 to the membrane (Crummy, Mani et al. 2019). Subcellular localization of DMXL1 has not been explored previously, but the data presented here indicate strong lysosomal association in 4T1 cells. We cannot compare the cellular levels of DMXL1 and ROGDI from these data, so it is possible that ROGDI is stoichiometric with DMXL1 at the membrane and "excess" ROGDI is soluble and cytosolic. However, it is also possible that ROGDI is not always associated with the other Rabconnectin-3 subunits. This would be a significant difference from the yeast RAVE complex, where

Rav2 and Rav1 form a stable complex that associates with cytosolic V_1 and both subunits are required for glucose-dependent recruitment to the vacuolar membrane and V-ATPase assembly (Jaskolka and Kane 2020, Jaskolka, Tarsio et al. 2021). A substantial proportion the V_1 subunit A (likely present as part of V_1 subcomplexes) is cytosolic in the 4T1 cells, as in many mammalian cell lines (McGuire and Forgac 2018, Collins, Stransky et al. 2020). Further experiments will be needed to determine whether ROGDI reversibly associates with Rabconnectin-3α and b at lysosomal membranes, possibly in combination with V_1, and the effect of these associations on V-ATPase function.

We were unable to generate a ROGDI knockout in 4T1 cells. However, other existing evidence associates ROGDI, as well as Rabconnectin-3α and β, with the V-ATPase function in acidification. DMXL1 and WDR7 coimmunoprecipitated with the V_1B1 subunit from kidney and RNAi of DMXL1 affected organelle acidification (Merkulova, Păunescu et al. 2015). ROGDI was also coimmunoprecipitated with V_1B1 at lower levels. Similarly, ROGDI, along with DMXL2 and WDR7, was isolated with the V-ATPase from a synaptic vesicle fraction (Coupland, Karimi et al. 2024), where assembly of V-ATPases drives vesicle acidification and neurotransmitter loading (Bodzęta, Kahms et al. 2017). The localization of ROGDI and DMXL1 to perinuclear lysosomes in 4T1 cells shown here is consistent with enrichment of ROGDI and Rabconnectin-3 in areas of V-ATPase assembly. Perinuclear lysosomes are highly acidic in the 4T1 cells, as indicated by Lysotracker staining. This population of lysosomes has been demonstrated to be a site of V-ATPase reassembly in other cells (Ebner, Puchkov et al. 2023, Sava, Davis et al. 2024). We propose that complexes containing ROGDI, DMXL1, and WDR7 promote association of V_1 subcomplexes (represented by the V_1A subunit here) with V_o

subcomplexes at sites of ongoing acidification, including perinuclear lysosomes as well as synaptic vesicles.

Human disease phenotypes and mouse models also indicate that ROGDI could affect V-ATPase-driven acidification in combination with Rabconnectin-3α and β isoforms. Complete loss of function mutations in human ROGDI cause Kohlschutter-Tonz syndrome, characterized by severe epilepsy, developmental delay, amelogenesis imperfecta (defects in tooth enamel formation), and in some cases, kidney disease (Schossig, Wolf et al. 2012, Liepina, Kalnina et al. 2021). Many of these phenotypes are recapitulated in a recent ROGDI knockout mouse model, which exhibited susceptibility to seizures, defective enamel formation, digestive problems, and in most cases, death before 12 weeks of age (Jimenez-Armijo, Morkmued et al. 2024). Importantly, these authors associate these phenotypes with defects in pH homeostasis likely to involve V-ATPase activity. DMXL2 knockout mice develop normally, but die shortly after birth of neurological defects that prevent feeding (Tata, Huijbregts et al. 2014). A DMXL1 knockout appears to be lethal in mice (Eaton, Danielson et al. 2024). Taken together, these data suggest that complete loss of ROGDI may be somewhat better tolerated than complete loss of either Rabconnectin-3α isoform. A mouse kidney-specific DMXL1 knockdown exhibited an incomplete distal renal tubule acidosis (DRTA) (Eaton, Danielson et al. 2024). Mutations in several kidney-enriched V-ATPase subunit isoforms also result in DRTA (Stover, Borthwick et al. 2002), while mutations in Rabconnectin-3b isoform WDR72 are associated with both DRTA and amelogenesis imperfecta (El-Sayed, Parry et al. 2009, Katsura, Horst et al. 2014, Rungroj, Nettuwakul et al. 2018). It is intriguing that Kohlschutter-Tonz patients exhibit neurological symptoms associated with

defects in Rabconnectin-3α (DMXL2) and kidney and tooth phenotypes characteristic of Rabconnectin-3b (WDR72). This combination of phenotypes could be consistent with ROGDI structurally bridging Rabconnectin-3α and b. Loss of ROGDI may destabilize the Rabconnectin-3 complex and compromise its assembly function. The compromised Rabconnectin-3 complex may still catalyze V-ATPase reassembly but less efficiently than the fully functional complex. This could explain why complete loss of Rabconnectin-3α is more severe than the loss of ROGDI in mice.

2.5 EXPERIMENTAL PROCEDURES

2.5.1 Materials and Media

Oligonucleotides were purchased from Eurofins Genomics. Anti-ROGDI (ab184954, rabbit) antibody and anti-ATP6V$_1$A antibody (ab199326, rabbit) were purchased from Abcam. DMXL1 polyclonal antibody (24413-1-AP, rabbit) and WDR7 polyclonal antibody (24413-1-AP, rabbit) were purchased from Proteintech. Anti-LAMP2 (ABL-93) was purchased from the Developmental Studies Hybridoma Bank. Anti-HA nanobody M-270 magnetic beads were purchased from Proteintech (atd). Q5 Hot Start polymerase was purchased from New England Biolabs (NEB, M0493S). Phire Plant Direct PCR master mix was purchased from ThermoFisher Scientific (F130WH). Human ROGDI cDNA (clone ID: 3861570), DMXL2 (clone ID: 9053066), and WDR72 (clone ID: 8069120) were purchased from Horizon Discovery. WDR7 cDNA was purchased from Genscript (clone ID: OHu06923). Yeast codon optimized ROGDI was synthesized by Genscript.

Yeast and cell culture media were purchased from Fisher Scientific. Other reagents were purchased from Millipore-Sigma.

2.5.2 Yeast strains

Yeast strains that were used in this work are listed in Table 1. All yeast strains (other than those used for two-hybrid assay) were constructed in a SF-838-5A WT background. Yeast genomic integrations were done using PCR constructs with at least 50 bp of flanking homologous sequence used to target into the genome. Oligonucleotides used in this study are listed in Table 2. Q5 Hot Start polymerase from NEB was used to amplify constructs used for yeast transformation. Yeast cells were transformed using a lithium acetate protocol (Gietz, St Jean et al. 1992). Genotyping was done using Phire Plant Direct PCR Master Mix (as described in by manufacturer in 'Direct PCR from Yeast Cells').

The PCR product used generate *rav2*Δ was amplified with oligonucleotides RAV2URA3F and RAV2URA3R using pRS316 as a template; the PCR product was designed to give a clean deletion of the *RAV2* ORF. Cells were transformed and colonies were selected on SD-URA media. The oligonucleotides YDR1-1 and URA-int were used to confirm rav2 deletion.

Rogdi was integrated at the *RAV2* locus by transformation of the *rav2*Δ*::URA3* strain with a PCR product amplified from pCMV-SPORT6-ROGDI (Horizon Discovery) using oligonucleotides Rav2-RogdiFnew, and Rav2-Rogdi Rev. Colonies were selected on supplemented minimal medium containing 5-fluoro-orotic acid to select against the colonies retaining the *URA3* gene (Boeke, La Croute et al. 1984). Yeast codon optimized ROGDI (RecHu ROGDI) was PCR amplified from pUC57-containing codon-optimized ROGDI (Genscript) using oligonucleotides Rav2RogdirecodeF and RogdirecodeR. The

product was then transformed into *rav2Δ::URA3 cells* and transformants were selected on medium containing 5-fluoro-orotic acid as described above. Integration was confirmed by PCR with oligonucleotides YDR1-1 and rav2c4.

The strong yeast TEF promoter placed upstream of ROGDI in *TEF-rav2Δ*::RecHuROGDI strain was constructed by amplification of a rav2-Rogdi-TEF construct using Rav2-S1, S4-Rogdi-V3 and pYM-N19 as a template (Janke, Magiera et al. 2004). The TEF construct was transformed into *rav2Δ*::yeROGDI and transformants selected on YEPD medium containing 100µg/mL clonNat. Genotype was confirmed using and RogdirecodeintR and YDR1-1. The *rav1Δ::KanMX* allele was amplified from genomic DNA of the BY4741 *rav1Δ::KanMX* strain (Winzeler, Shoemaker et al. 1999) using oligonucleotides YJR1-7 and YJR6-12. The product was then transformed into the strain created above, and colonies were selected on YEPD medium containing 200µg/mL G418. Genotype was confirmed by PCR as described above.

2.5.3 Rav- phenotyping

Cells were grown until log phase and a volume equivalent to 1 OD_{600}/ml was pelleted. Cells were washed and resuspended in 1 mL of YEPD. Serial 1/5 dilutions of the cell suspensions were made in a 96 well plate and cells were pinned, using a 48 spoke inoculating manifold, to YEPD buffered to pH5 and YEPD containing 4 mM $ZnCl_2$. Plates were placed in a 37°C incubator and imaged daily following two days of growth.

2.5.4 Yeast two-hybrid assay

Two-hybrid assays were performed as described by James et al (James, Halladay et al. 1996). In this system the Gal4 DNA binding domain is encoded in pAS2 and activating domain is encoded in pACT2(Bai and Elledge 1996). The genes *HIS3* and *ADE2* in yeast strains PJ69-4a and PJ69-4α are under the control of the *GAL1* and *GAL2* promoters, respectively. Genes for proteins of interest are subcloned into the plasmid so that they result in a fusion protein with the corresponding GAL4 component. ROGDI was cloned into pAS2 with RogdipAS2F and RogdipAS2R and into pACT2 with RogdipAS2 and RogdipACT2R using a megaprimer cloning method (Barik 2002). WDR7 (1-596) was cloned into pACT2 with WDR7 1F and WDR7pAS2 596R. DMXL2 1-625 was cloned into pAS2 with Rbcn3a 1-625F and Rbcn3a 1-625R. Both primers were constructed using megaprimer based cloning. WDR72 was cloned into pACT2 using WDR721-589pACT2rev and WDR721-589pACT2R using In-Fusion Snap Assembly cloning (Takara). pACT2 plasmids were transformed into PJ69-4α and selected on supplemented minimal medium (SD) lacking tryptophan. pAS2 plasmids were transformed into PJ69-4a and selected on SD medium lacking leucine. Empty pACT2 vector was used as a negative control for pACT2 plasmids and pAS1-Lamin was used for pAS2 plasmids. Transformed cells were mated in YEPD, then transferred to supplemented minimal medium (SD) lacking tryptophan and leucine media to select for diploids with both plasmids. Cells were resuspended in SD-Trp,Leu at 1 OD/mL and 1/5 serial dilutions were performed. Cells were inoculated onto SD-Trp, Leu, Ade, His and SD-Trp, Leu, Ade plates as described above using an inoculation manifold. They were placed in a 30°C incubator and imaged when growth was observed at 6 days post inoculation.

2.5.5 Cross-linking and immunoprecipitation

Mouse 4T1 breast cancer cells (ATCC, CRL-2539) were grown in T75 flasks using DMEM (Dulbecco's Modified Eagle medium) containing 10% fetal bovine serum (FBS). For each immunoprecipitation (including the specific antibody and negative control of isotype-specific antibody) two T75 flasks grown to greater than 80% confluency were lysed in PBS lysis buffer (PBS, 0.5% NP-40, and protease inhibitors (PMSF, Leupeptin, Aprotinin, Pepstatin, Chymostatin)) and lysates were pooled. Lysate was rocked at 4°C for 20 minutes to complete lysis, then insoluble material was pelleted by centrifugation at 6,000x g for 10 minutes. The supernatant was brought to 1.2 ml total volume using PBS lysis buffer. Crosslinking was done by adding dithiobis (succinimidyl propionate) (DSP) to a final concentration of 0.5 mM and rocking the mixture at 4°C for 30 minutes. After 30 minutes, the remaining DSP was quenched by the addition of 1M Tris-HCl pH 7.4 to a final concentration of 50 mM and incubation at 4°C for 15 minutes. Following quenching, 10% of the total lysate was set aside as an input sample. Prior to incubation with lysate, antibody was bound to protein-A Dynabeads (ThermoFisher Scientific, 10001D) according to manufacturer instructions. For the anti-DMXL1 antibody, 4 mg of total antibody was added. An equivalent amount of non-specific rabbit IgG was used as a control. Lysate and antibody-bound beads were incubated on a rocker at 4°C for 4 hours. Beads were then removed from lysate using a magnet stand and washed with PBS lysis buffer with protease inhibitors according to manufacturer instructions. Protein was eluted from beads by denaturing at 98°C with cracking buffer (8M Urea, 5% SDS, 50 mM Tris HCl pH 6.8, 5% b-mercaptoethanol). Samples were run on a 4-15% gradient SDS-PAGE

gel (Biorad) and transferred onto a PVDF membrane using a Bio-Rad Transblot Turbo. Blots were blocked in 5% milk in TBS containing 0.1% Tween-20 (TBST). Primary antibody was diluted in blocking buffer for 1.5 hours at room temperature or overnight on a rocker. Blots were washed 3 times for 5 minutes each with TBST. Clean-blot IP Detection Reagent (HRP conjugate, 21230, ThermoFisher Scientific) was used (in place of an IgG secondary antibody) at a concentration of 1:500 in blocking buffer and incubated at room temperature for 1 hour. BioRad Clarity Max ECL (1705062) substrate and an Azure Sapphire Biomolecular Imager were used to visualize the blots. The data shown are representative of three biological replicates.

2.5.6 Immunofluorescence Microscopy

Coverslips were washed with ethanol and water and coated with human collagen 4 at a concentration of 50 ug/mL for 30 minutes and then UV sterilized. Coverslips were placed in a 24 well plate and 30,000 4T1 cells were seeded and allowed to grow overnight. The following day cells were washed with PBS and fixed with 4% formaldehyde in PBS for 10 minutes followed by permeabilization with 0.1% Triton X-100 for 10 minutes. Cells were labeled with LysoTracker Red DND-99 by incubating cells in fresh media containing 50 μM LysoTracker for 30 minutes immediately prior to fixation. Coverslips were incubated in blocking buffer (1% BSA, 22.5 mg/mL, 0.1% Tween-20 in PBS) for 1 hour. Blocked coverslips were then incubated in primary antibody (diluted in blocking buffer) for 1 hour. Anti-ROGDI (Abcam, ab184954) was diluted to 1:100. Anti-DMXL1 (Proteintech, 24413-1-AP) was diluted to 1:100. Anti-LAMP2 (DSHB, ABL-93) was diluted to 1:100. Secondary antibodies, anti-Rat-AlexaFluor568 (A11077, ThermoFisher Scientific) and anti-Rabbit-AlexaFluor488

(A32731, ThermoFisher Scientific) were diluted 1:1000. Antibodies for ROGDI/DMXL1 and ROGDI/V_1A co-staining were labeled with FlexAble IgG labeling kits from Proteintech. the anti-ROGDI antibody was labeled with CoraLite Plus 488 (KFA001) and the anti-V_1A and anti-DMXL1 antibodies were labeled with CoraLite Plus 647 (KFA003). Coverslips were washed 3 times for 5 minutes each after primary antibody incubation. Coverslips requiring secondary antibodies were incubated in the appropriate secondary antibody for 1 hour. Coverslips were washed 3 times for 5 minutes following secondary antibody incubation. Slides were mounted onto the glass coverslips using ProLong Glass with NucBlue mountant (Invitrogen, P36983) then cured for 24 hours before imaging. Imaging was done on a Zeiss AxioImager Z1 widefield microscope equipped with a Hammamatsu ORCA-ER CCD camera using a 100x 1.4NA objective. Images were analyzed using FIJI (Schindelin, Arganda-Carreras et al. 2012). The images shown are representative of images from three separate biological replicates.

2.5.7 LysoIP

In order to collect a lysosomal fraction from cells, we employed an adapted LysoIP protocol (Abu-Remaileh, Wyant et al. 2017). Mouse lysosomal protein TMEM192 (Horizon Discovery, 3708193) was subcloned into pcDNA3 FLAG-HA (Addgene, #10792) using muTMEMF, muTEMEMR, pCDNAF, and pcDNAR to create a TMEM192-FLAG-HA fusion protein. This plasmid was transfected into 4T1 cells using Lipofectamine 3000 (L3000150, ThermoFisher Scientific) at a cell density of 70%. Cells were grown for 24 hours and then scraped in lysis buffer (150mM NaCl, 50mM Tris HCl pH 7.4, 5 mM EDTA, 250 mM Sucrose) with protease inhibitors (PMSF, Leupeptin, Aprotinin, Pepstatin, Chymostatin). Cells were lysed by passing through a 26-gauge

needle 10 times. Cell debris and nuclei were pelleted by spinning at 700xg for 5 minutes at 4°C. 25 mL of HA-Trap magnetic particles (atd, Chromotek) for each immunoprecipitation were equilibrated in lysis buffer by washing twice using a magnet stand collect beads and allow removal of supernatant. The post-nuclear supernatant was added to the HA-Trap magnetic particles and incubated on a rocker at 4°C for 30 minutes. Magnetic particles were then separated using a magnet stand, supernatant was removed and set aside, and the magnetic particles were washed 2x with 200uL lysis buffer. Protein bound to the magnetic particles was denatured in cracking buffer (8M urea, 5% SDS, 50mM Tris HCl pH 6, 1mM EDTA, 5% b-mercaptoethanol, 0.3% Bromophenol blue) and analyzed by SDS-PAGE and western blotting. The experiment was repeated twice and the blots shown are representative.

2.5.8 Subcellular Fractionation

4T1 cells were grown in T75 flasks until they were at 70-80% confluency. Cells were washed in PBS and then scraped from dish in TBSE+ protease inhibitors (150mM NaCl, 50mM Tris-HCl pH 7.4, 5mM EDTA with PMSF, Leupeptin, Aprotinin, Pepstatin, Chymostatin). Cells were homogenized by passing thorough a 26-gauge needle 10 times. Cell debris and nuclei were pelleted by centrifugation at 700xg for 5 minutes at 4°C. Supernatant was moved to a new 1.5 mL tube and centrifuged at 10,000xg for 5 minutes to pellet mitochondria. Supernatant was then spun at 100,000xg for 1 hour in a Beckman-Coulter Optima XP ultracentrifuge to pellet the membrane fraction. Supernatant containing the cytosolic fraction was removed and protein was precipitated with 10% trichloroacetic acid (TCA). The precipitated protein was solubilized in cracking buffer. The membrane pellet was also solubilized in cracking buffer. Samples were analyzed by

SDS-PAGE followed by western blotting as described above. Blots shown are representative of three biological replicates.

2.5.9 Computational modeling

Predictive protein models were generated by AlphaFold 2 and AlphaFold3 (Cramer 2021, Abramson, Adler et al. 2024). Analysis of the protein structures was done with USCF ChimeraX (Meng, Goddard et al. 2023). AlphaFold3 models of individual proteins are assigned a pTM (predicted template modeling) score and multi-protein complexes are assigned an ipTM (interface predicted template modeling) score (Abramson, Adler et al. 2024). A pTM score >0.5 reflects a confident model that is likely similar to the true structure of the protein. An iPTM score between 0.6-.8 represents low confidence in the relative position of proteins within a complex while a score >0.8 reflect high confidence in the modeling of a complex. Both pTM and iPTM reflect more confident models as scores approach 1.

Strain	Genotype
SF838-5Aα	*MATα leu2-3, 112; ura3-52; ade6*
rav2Δ	SF838-5Aα *rav2Δ::URA3*
rav2Δ::huRogdi	SF838-5Aα *rav2Δ*::huRogdi
rav2Δ::RecHu Rogdi	SF838-5Aα *rav2Δ*::RecHu Rogdi
TEF-*rav2Δ*::RecHu Rogdi	SF838-5Aα *natNT2-TEF-rav2Δ*::RecHu Rogdi
rav1Δ TEF-*rav2Δ*::RecHu Rogdi	SF838-5Aα *rav1Δ*::*kanMX4 natNT2-TEF-rav2Δ*::RecHu Rogdi
PJ69-4a	*MATa trp1-901 leu2-3,112 ura3-52 his3-200 gal4 gal80 LYS2::GAL1-HIS3 GAL2-ADE2 met2::GAL7-lacZ*
PJ69-4α	*MATα trp1-901 leu2-3,112 ura3-52 his3-200 gal4 gal80 LYS2::GAL1-HIS3 GAL2-ADE2 met2::GAL7-lacZ*

Table 2-1- Yeast strains used

Name	Sequence (5'-3')
RAV2URA3F	GTG AAT TAC AAA ATT ATA GTA TCT GAT CAA GCA CAC AGT GGA AGT GCT CGA AAA GCA ATC TGA GAG TGC ACC ACG CTT TTC
RAV2URA3R	CTC TTT ATC CAG TTT GTA TTA TAA ATT ATT GTT AAT GTT ATC GCT AGT AGA TTA TTA GTT TTG CTG GCC GCA TCT TCT
URA-int	CCTTAGCATCCCTTCCCTTTG
RAV2-RogdiFnew	GTG AAT TAC AAA ATT ATA GTA TCT GAT CAA GCA CAC AGT GGA AGT GCT CGA AAA GCA ATA TGG CCA CCG TGA TGG CAG CGA C
Rav2-Rogdi Rev	CTC TTT ATC CAG TTT GTA TTA TAA ATT ATT GTT AAT GTT ATC GCT AGT AGA TCA GAA GGG TCT GTA GCT CCA
HuRogdi IntR	GCA TGC AGC TGG TAC ACC GT
Rav2RogdirecodeF	GTG AAT TAC AAA ATT ATA GTA TCT GAT CAA GCA CAC AGT GGA AGT GCT CGA AAA GCA ATA TGG CCA CCG TTA TGG CTG CT
Rav2RogdirecodeR	CTC TTT ATC CAG TTT GTA TTA TAA ATT ATT GTT AAT GTT ATC GCT AGT AGA TCA GAA TGG TCT GTA AGA CCA
Rogdirecode intR	ACC ACC TGC TGG TCT AAA GTT CTT
YDR1-1(rav2)	GTTGTACCGAGGTTCCATTG
rav2-c4	GGGTCAAGAATACGAAGGCAG
Rogdirecode intR	ACC ACC TGC TGG TCT AAA GTT CTT
YJR1-7	CCATCTCCTCCCTCGGATCAAACTTTC
YJR6-12	CGTTCCTAACAGAGATCAAGC
NatR forward	ACATGGAGGCCCAGAATACCC
NatR reverse	CAGTATAGCGACCAGCATTCAC
RogdipAS2F	GGT CAT ATG GAG GCC CCG GGA ATG GCC ACC GTG ATG GCA GCG AC
RogdipAS2R	GCT TGG CTG CAG GTC GAC GGA TCC GAT CAG AAG GGT CTG TAG CTC CA
RogdipACT2R	GAT CTC TCG AGC TCG AAT TCG GAT GAT CAG AAG GGT CTG TAG CTC CA
WDR721-589pACT2rev	GCT TGG CTG CAG GTC GAC GGA TCC GCC TGT TTC AAT TTC CCA GAT
WDR721-589pACT2R	GAT CTC TCG AGC TCG AAT TCG GAT GCC TGT TTC AAT TTC CCA
WDR7 1F	CATATGGCCATGGAGGCCCCGGGAATGGCAGGAAACAGCCTTGTTCTACC

WDR7 pAS2 596R	GCTTGGCTGCAGGTCGACGGATCCACGATCCAATGCACCAGTATCCAT
Rbcn3a 1-625F	CATATGGCCATGGAGGCCCCGGGAACAGAGGGAAACGGCTCTCGCAGC
Rbcn3a 1-625R	GCTTGGCTGCAGGTCGACGGATCCTGTGGCTGTGATCCGTGAGGACTG
muTMEMF	ACTATAGGGAGACCCATGGCGGCGGCCGGCCGG
MuTMEMR	GTCCATGGTAAGCTTAGTCCTGGCTGGCTGAGTTGC
pcDNAF	AAGCTTACCATGGACTACAAGGACG
pcDNAR	GGGTCTCCCTATAGTGAGTCG

Table 2-2 Oligonucleotides used

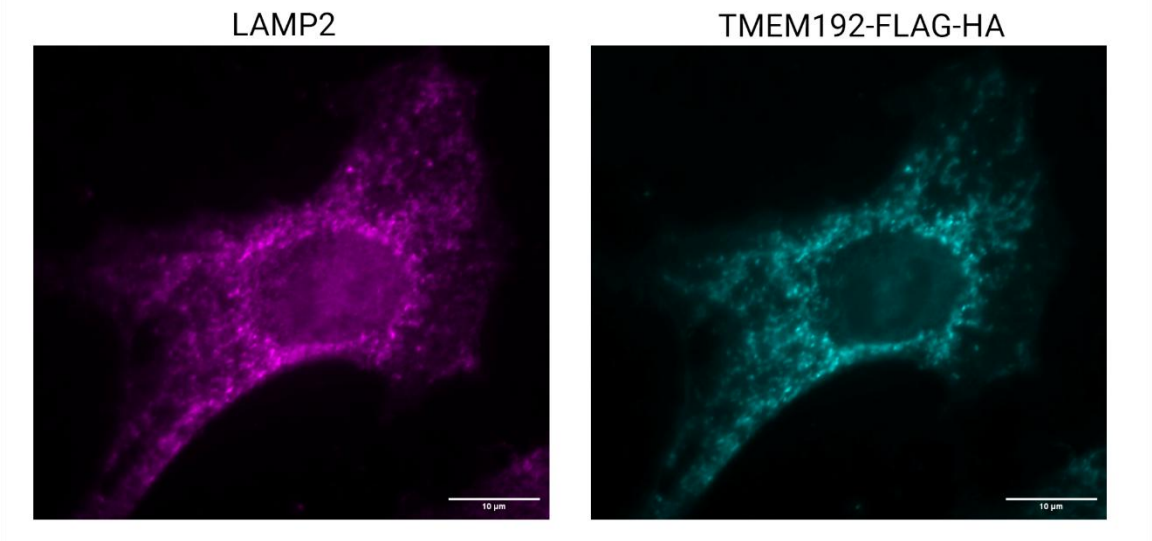

Figure 2-6- S1 TMEM192-FLAG-HA localizes to lysosomes

Immunoflourescent micrograph of a 4T1 cell co-stained with indirectly labeled anti-LAMP2 (magenta) and directly labeled anti-FLAG antibodies (cyan) as described in Experimental Procedures.

2.6 Supplemental Figures

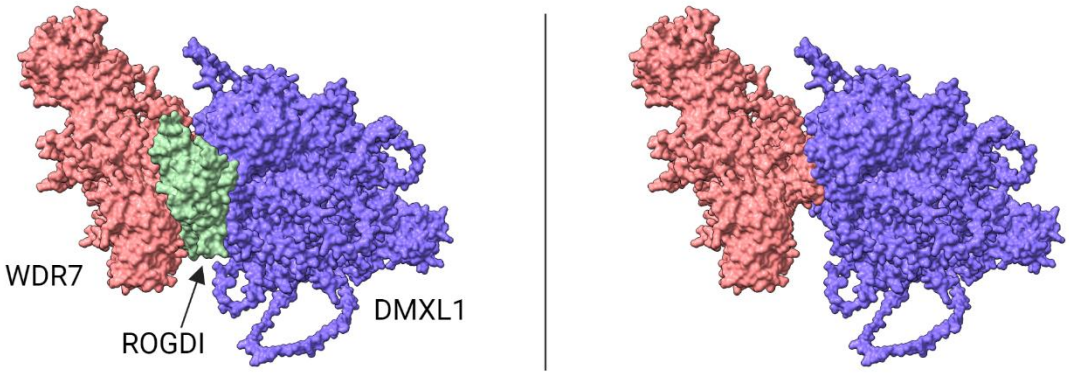

Figure 2-7- S2 AlphaFold3 model of Rabconnectin-3

(Left) AlphaFold3 model of Rabconnectin-3 containing DMXL1 (purple) and WDR7 (pink) bound to ROGDI (green). The model has an ipTM: 0.74 and pTM:0.7. **(Right)** Rabconnectin-3 model where ROGDI is removed.

2.7 References

Abramson, J., et al. (2024). "Accurate structure prediction of biomolecular interactions with AlphaFold 3." Nature: 1-3.

Abu-Remaileh, M., et al. (2017). "Lysosomal metabolomics reveals V-ATPase-and mTOR-dependent regulation of amino acid efflux from lysosomes." Science **358**(6364): 807-813.

Bai, C. and S. J. Elledge (1996). "[27] Gene identification using the yeast two-hybrid system." Methods in enzymology **273**: 331-347.

Banerjee, S., et al. (2019). "Interaction of the late endo-lysosomal lipid PI (3, 5) P2 with the Vph1 isoform of yeast V-ATPase increases its activity and cellular stress tolerance." Journal of Biological Chemistry **294**(23): 9161-9171.

Barik, S. (2002). "Megaprimer PCR." PCR Cloning Protocols: 189-196.

Bodzęta, A., et al. (2017). "The presynaptic v-ATPase reversibly disassembles and thereby modulates exocytosis but is not part of the fusion machinery." Cell reports **20**(6): 1348-1359.

Boeke, J. D., et al. (1984). "A positive selection for mutants lacking orotidine-5'-phosphate decarboxylase activity in yeast: 5-fluoro-orotic acid resistance." Molecular and General Genetics MGG **197**(2): 345-346.

Collins, M. P. and M. Forgac (2020). "Regulation and function of V-ATPases in physiology and disease." Biochimica et Biophysica Acta (BBA)-Biomembranes **1862**(12): 183341.

Collins, M. P., et al. (2020). "AKT Ser/Thr kinase increases V-ATPase–dependent lysosomal acidification in response to amino acid starvation in mammalian cells." Journal of Biological Chemistry: jbc. RA120. 013223.

Coupland, C. E., et al. (2024). "High-resolution electron cryomicroscopy of V-ATPase in native synaptic vesicles." Science: eadp5577.

Cramer, P. (2021). "AlphaFold2 and the future of structural biology." Nature structural & molecular biology **28**(9): 704-705.

Crummy, E., et al. (2019). "The priming factor CAPS1 regulates dense-core vesicle acidification by interacting with rabconnectin3β/WDR7 in neuroendocrine cells." Journal of Biological Chemistry **294**(24): 9402-9415.

Dittrich, A., et al. (2023). "Rabconnectin-3α/DMXL2 Is Locally Enriched at the Synaptic Ribbon of Rod Photoreceptor Synapses." Cells **12**(12): 1665.

Eaton, A. F., et al. (2024). "Dmxl1 is an Essential Mammalian Gene that is Required for V-ATPase Assembly and Function In Vivo." Function: zqae025.

Ebner, M., et al. (2023). "Nutrient-regulated control of lysosome function by signaling lipid conversion." Cell **186**(24): 5328-5346. e5326.

Einhorn, Z., et al. (2012). "Rabconnectin3α promotes stable activity of the H+ pump on synaptic vesicles in hair cells." Journal of Neuroscience **32**(32): 11144-11156.

El-Sayed, W., et al. (2009). "Mutations in the beta propeller WDR72 cause autosomal-recessive hypomaturation amelogenesis imperfecta." The American Journal of Human Genetics **85**(5): 699-705.

Evans, R., et al. (2022). "Protein complex prediction with AlphaFold-Multimer." bioRxiv: 2021.2010. 2004.463034.

Gandini, M. A., et al. (2019). "Interactions of Rabconnectin-3 with Cav2 calcium channels." Molecular brain **12**(1): 62.

Gietz, D., et al. (1992). "Improved method for high efficiency transformation of intact yeast cells." Nucleic acids research **20**(6): 1425.

Inoue, H., et al. (1999). "Targeted disruption of the gene encoding the proteolipid subunit of mouse vacuolar H+-ATPase leads to early embryonic lethality." Biochimica et Biophysica Acta (BBA)-Bioenergetics **1413**(3): 130-138.

James, P., et al. (1996). "Genomic libraries and a host strain designed for highly efficient two-hybrid selection in yeast." Genetics **144**(4): 1425-1436.

Janke, C., et al. (2004). "A versatile toolbox for PCR-based tagging of yeast genes: new fluorescent proteins, more markers and promoter substitution cassettes." Yeast **21**(11): 947-962.

Jaskolka, M. C. and P. M. Kane (2020). "Interaction between the yeast RAVE complex and Vph1-containing Vo sectors is a central glucose-sensitive interaction required for V-ATPase reassembly." Journal of Biological Chemistry **295**(8): 2259-2269.

Jaskolka, M. C., et al. (2021). "Defining steps in RAVE-catalyzed V-ATPase assembly using purified RAVE and V-ATPase subcomplexes." Journal of Biological Chemistry **296**.

Jaskolka, M. C., et al. (2021). "RAVE and rabconnectin-3 complexes as signal dependent regulators of organelle acidification." Frontiers in cell and developmental biology **9**: 698190.

Jimenez-Armijo, A., et al. (2024). "The Rogdi knockout mouse is a model for Kohlschütter–Tönz syndrome." Scientific reports **14**(1): 445.

Johnson, D. E., et al. (2016). "The position of lysosomes within the cell determines their luminal pH." Journal of Cell Biology **212**(6): 677-692.

Jumper, J., et al. (2021). "Highly accurate protein structure prediction with AlphaFold." Nature **596**(7873): 583-589.

Kane, P. M. (1995). "Disassembly and reassembly of the yeast vacuolar H+-ATPase in vivo." Journal of Biological Chemistry **270**(28): 17025-17032.

Katsura, K., et al. (2014). "WDR72 models of structure and function: A stage-specific regulator of enamel mineralization." Matrix Biology **38**: 48-58.

Kawabe, H., et al. (2003). "A novel rabconnectin-3-binding protein that directly binds a GDP/GTP exchange protein for Rab3A small G protein implicated in Ca2+-dependent exocytosis of neurotransmitter." Genes to Cells **8**(6): 537-546.

Kawasaki-Nishi, S., et al. (2001). "Yeast V-ATPase Complexes Containing Different Isoforms of the 100-kDa a-subunit Differ in Coupling Efficiency and in VivoDissociation." Journal of Biological Chemistry **276**(21): 17941-17948.

Kelley, L. A., et al. (2015). "The Phyre2 web portal for protein modeling, prediction and analysis." Nature Protocols **10**(6): 845-858.

Phyre2 is a web-based tool for predicting and analyzing protein structure and function. Phyre2 uses advanced remote homology detection methods to build 3D models, predict ligand binding sites, and analyze amino acid variants in a protein sequence.

Lee, H., et al. (2017). "The crystal structure of human Rogdi provides insight into the causes of Kohlschutter-Tönz Syndrome." Scientific reports **7**(1): 3972.

Lemieux, B., et al. (2004). "Quantitation of the lysosomotropic character of cationic amphiphilic drugs using the fluorescent basic amine Red DND-99." Analytical biochemistry **327**(2): 247-251.

Liepina, L., et al. (2021). "Kohlschütter–Tönz syndrome: Case report with novel feature and detailed review of features associated with ROGDI variants." American Journal of Medical Genetics Part A.

McGuire, C. M., et al. (2019). "Isoform-specific gene disruptions reveal a role for the V-ATPase subunit a4 isoform in the invasiveness of 4T1-12B breast cancer cells." Journal of Biological Chemistry **294**(29): 11248-11258.

McGuire, C. M. and M. Forgac (2018). "Glucose starvation increases V-ATPase assembly and activity in mammalian cells through AMP kinase and phosphatidylinositide 3-kinase/Akt signaling." Journal of Biological Chemistry **293**(23): 9113-9123.

Meng, E. C., et al. (2023). "UCSF ChimeraX: Tools for structure building and analysis." Protein Science **32**(11): e4792.

Merkulova, M., et al. (2015). "Mapping the H+(V)-ATPase interactome: identification of proteins involved in trafficking, folding, assembly and phosphorylation." Scientific reports **5**: 14827.

Nagano, F., et al. (2002). "Rabconnectin-3, a novel protein that binds both GDP/GTP exchange protein and GTPase-activating protein for Rab3 small G protein family." Journal of Biological Chemistry **277**(12): 9629-9632.

Nakamura, S. (2004). "Glucose activates H+-ATPase in kidney epithelial cells." American Journal of Physiology-Cell Physiology **287**(1): C97-C105.

Nelson, H. and N. Nelson (1990). "Disruption of genes encoding subunits of yeast vacuolar H (+)-ATPase causes conditional lethality." Proceedings of the National Academy of Sciences **87**(9): 3503-3507.

Parra, K. J. and P. M. Kane (1998). "Reversible association between the V1and V0 domains of yeast vacuolar H+-ATPase is an unconventional glucose-induced effect." Molecular and cellular biology.

Parra, K. J., et al. (2000). "The H subunit (Vma13p) of the yeast V-ATPase inhibits the ATPase activity of cytosolic V1 complexes." Journal of Biological Chemistry **275**(28): 21761-21767.

Ratto, E., et al. (2022). "Direct control of lysosomal catabolic activity by mTORC1 through regulation of V-ATPase assembly." Nature communications **13**(1): 4848.

Rice, P., et al. (2000). "EMBOSS: the European molecular biology open software suite." Trends in genetics **16**(6): 276-277.

Rungroj, N., et al. (2018). "Distal renal tubular acidosis caused by tryptophan-aspartate repeat domain 72 (WDR72) mutations." Clinical genetics **94**(5): 409-418.

Santos-Pereira, C., et al. (2021). "Emerging insights on the role of V-ATPase in human diseases: Therapeutic challenges and opportunities." Medicinal Research Reviews **41**(4): 1927-1964.

Sautin, Y. Y., et al. (2005). "Phosphatidylinositol 3-kinase-mediated effects of glucose on vacuolar H+-ATPase assembly, translocation, and acidification of intracellular compartments in renal epithelial cells." Molecular and cellular biology **25**(2): 575-589.

Sava, I., et al. (2024). "Reversible assembly and disassembly of V-ATPase during the lysosome regeneration cycle." Molecular biology of the cell **35**(5): ar63.

Schindelin, J., et al. (2012). "Fiji: an open-source platform for biological-image analysis." Nature methods **9**(7): 676-682.

Schossig, A., et al. (2012). "Mutations in ROGDI cause Kohlschütter-Tönz syndrome." The American Journal of Human Genetics **90**(4): 701-707.

Schossig, A., et al. (2012). "Epileptic encephalopathy and amelogenesis imperfecta: Kohlschütter–Tönz syndrome." European journal of medical genetics **55**(5): 319-322.

Seol, J. H., et al. (2001). "Skp1 forms multiple protein complexes, including RAVE, a regulator of V-ATPase assembly." Nature cell biology **3**(4): 384-391.

Sethi, N., et al. (2010). "Rabconnectin-3 is a functional regulator of mammalian Notch signaling." Journal of Biological Chemistry **285**(45): 34757-34764.

Smardon, A. M., et al. (2014). "The RAVE complex is an isoform-specific V-ATPase assembly factor in yeast." Molecular biology of the cell **25**(3): 356-367.

Smardon, A. M., et al. (2015). "Molecular interactions and cellular itinerary of the yeast RAVE (regulator of the H+-ATPase of vacuolar and endosomal membranes) complex." Journal of Biological Chemistry **290**(46): 27511-27523.

Smardon, A. M., et al. (2002). "The RAVE complex is essential for stable assembly of the yeast V-ATPase." Journal of Biological Chemistry **277**(16): 13831-13839.

Stover, E., et al. (2002). "Novel ATP6V1B1 and ATP6V0A4 mutations in autosomal recessive distal renal tubular acidosis with new evidence for hearing loss." Journal of medical genetics **39**(11): 796-803.

Tata, B., et al. (2014). "Haploinsufficiency of Dmxl2, encoding a synaptic protein, causes infertility associated with a loss of GnRH neurons in mouse." PLoS biology **12**(9): e1001952.

Tuttle, A. M., et al. (2014). "Rabconnectin-3a regulates vesicle endocytosis and canonical Wnt signaling in zebrafish neural crest migration." PLoS biology **12**(5).

Uhlén, M., et al. (2015). "Tissue-based map of the human proteome." Science **347**(6220): 1260419.

Wang, H., et al. (2024). "Structure of yeast RAVE bound to a partial V1 complex." bioRxiv: 2024.2007. 2018.604153.

Winzeler, E. A., et al. (1999). "Functional characterization of the S. cerevisiae genome by gene deletion and parallel analysis." Science **285**(5429): 901-906.

Zoncu, R., et al. (2011). "mTORC1 senses lysosomal amino acids through an inside-out mechanism that requires the vacuolar H+-ATPase." Science **334**(6056): 678-683.

Chapter 3

Computational modeling of Rabconnectin-3 and RAVE

We intend to submit this work alongside planned cross-linking mass spectroscopy experiments with RAVE-V_1-V_1C.

3.1 Rabconnectin-3 and RAVE structural modeling

AlphaFold3 and other predictive modeling programs have enabled the investigation of protein complexes that do not have published experimentally determined structures. Large protein complexes like Rabconnectin-3 have proven challenging in solving structures. Methods like Cryo-EM and X-ray crystallography require high concentrations of pure protein, which is a time-consuming and, at times, challenging task. Using predictive modeling allows for the rapid generation of complete structures. Recent advances have permitted the modeling of several polypeptides together, allowing for the modeling of entire complexes. These models should not be treated the same way as an experimentally determined structure and should be evaluated against what is already known about a protein. We have found that the models of RAVE and Rabconnetin-3 structures are consistent with previously published homology modeling-based findings for both complexes. An experimentally determined structure for RAVE bound to a partial V_1 subcomplex has only recently been published, (Wang, Tarsio et al. 2024) and no structural information is available for Rabconnectin-3. We have used AlphaFold multimer and AlphaFold3 to investigate RAVE and Rabconnectin-3 subunit structure and function.

AlphaFold3 models include two measures of confidence for the resulting models. pTM (predicted template modeling) and ipTM (interface predicted template modeling) enable easy model quality evaluation. The pTM score reflects the confidence in the accuracy of polypeptide folding. When multiple polypeptides are included in a model, a single collective pTM (predicted template modeling) is calculated for all polypeptides submitted. A pTM value higher than 0.5 indicates that the structure is likely to be similar to the 'true' structure of the protein. As the value approaches 1, the confidence increases,

reflecting that the predicted structure is increasingly similar to the true structure. The ipTM (interface predictive template modeling) score reflects the confidence in modeling the relative positions of multiple polypeptides within a complex. A score below 0.6 reflects a failed modeling of a complex. An ipTM value between 0.6 and 0.8 is described as a grey area where the model may be inaccurate. A score higher than .8 reflects a high confidence model that is similar to the 'true' complex.

3.2 RAVE

3.2.1 Rav1-Rav2

AlphaFold3 modeling of Rav1 and Rav2 results in a model with an ipTM score of 0.78 and a pTM score of 0.68 (Figure 3-1). This indicates reasonably high confidence in the modeling between Rav1 and Rav2. The pTM score falls on the edge of low confidence and confidence but may result from the disordered tail of Rav1. However, removing this region only resulted in a slight improvement in pTM to 0.69. Modeling of Rav1 and Skp1 results in a model with a pTM of 0.74 and an ipTM of 0.73. When Rav1, Rav2, and Skp1 are modeled together as one complex, it results in a lower confidence model with a pTM of 0.68 and ipTM of 0.65. Modeling all three proteins together introduces more uncertainty into the model than modeling the subunits in separate pairs. However, there are no substantial differences in the folding or placement of individual subunits within the larger complex. AlphaFold3 returns five models for each set of submitted polypeptides, which are ranked by pTM and ipTM scores. All five RAVE models converge, with only minor differences between them. This indicates that AlphaFold3 is confident in the overall structure of the complex. If there is substantial

uncertainty in the positioning of subunits of a complex, the individual models are often substantially different.

Yeast two-hybrid analysis found that Rav1 residues 2-240 are required for binding with Rav2 (Smardon, Nasab et al. 2015). Rav1 residues 2-240 comprise 5 of 7 blades of the first beta-propeller. The AlphaFold3 models the N-terminal tail of Rav2 (Ser2-Asn19) inserts into Rav1 β-propeller 1. Hydrophobic amino acids within the Rav2 tail come close with hydrophobic amino acids within the center of Rav1 β-propeller 1 (Figure 3-2). A portion of the Rav2 α-domain (F20-L39, A332-K351) contacts the portion of β-propeller 1 encompassed by Rav1 amino acids 2-240. Rav1 and Rav2 have complementary surface charges; Rav2 has a more negative surface charge, while Rav1 has a more positive charge. The Rav2 N-terminal tail contains hydrophobic residues that interact with corresponding hydrophobic residues lining the center of Rav1 propeller 1. The following pairs of residues make hydrophobic contacts: Rav2 Y17, Rav1 Y165; Rav2 F11, Rav1 Y148; Rav2 F6, Rav1 L352 and Y329. Interacting residues between Rav1 and Rav2 are highlighted in red in Figure 3-1. Rav2 binding Rav1 with its N-terminus means that Rav2 extends away from Rav1, resembling an arm. The Rav2 tail connecting to Rav1 is relatively disordered, potentially serving as a flexible linker between Rav1 and Rav2. This would enable Rav2 to move around Rav1 with β-propeller 1 serving as a pivot point. This binding model for Rav1 and Rav2 is consistent with the cryo-EM structure of RAVE-V_1 (Figure 3-5). This structure shows Rav2 binding to Rav1 using β-propeller 1. AlphaFold3 models the tail of Rav2 to bind with the center of Rav1 β-propeller 1, which is unresolved in the Cryo-EM structure. This region may be too flexible for Cryo-EM to resolve because of class averaging. Additionally, the part of

Rav2 that is most peripheral from β-propeller one is poorly resolved in the cryo-EM structure (Wang, Tarsio et al. 2024), indicating that this region is flexible. The only known V-ATPase binding partner for Rav2 is V_1C (*VMA5*); however, no AlphaFold3 models between these proteins result in an acceptable ipTM. It is possible that the flexibility of Rav2 would enable an interaction with V_1C. Additionally, the cryo-EM structure indicates if Rav2 were bound rigidly to Rav1, then it would clash with the vacuolar membrane (Wang, Tarsio et al. 2024). Data suggests that the RAVE-V_1 complex is only an intermediate partly because it does not contain the V_1C subunit that must be recruited during reassembly (Jaskolka, Tarsio et al. 2021). Additionally, the position of Rav1 in the cryo-EM structure is too far from Vph1 for the two proteins to bind. Rav1 would need to move substantially for the Vph1-binding sequence in Rav1 to interact with Vph1 NT. Additionally, if Rav2 is flexibly bound to Rav1, it could move out of the way of the membrane, preventing a clash with the membrane.

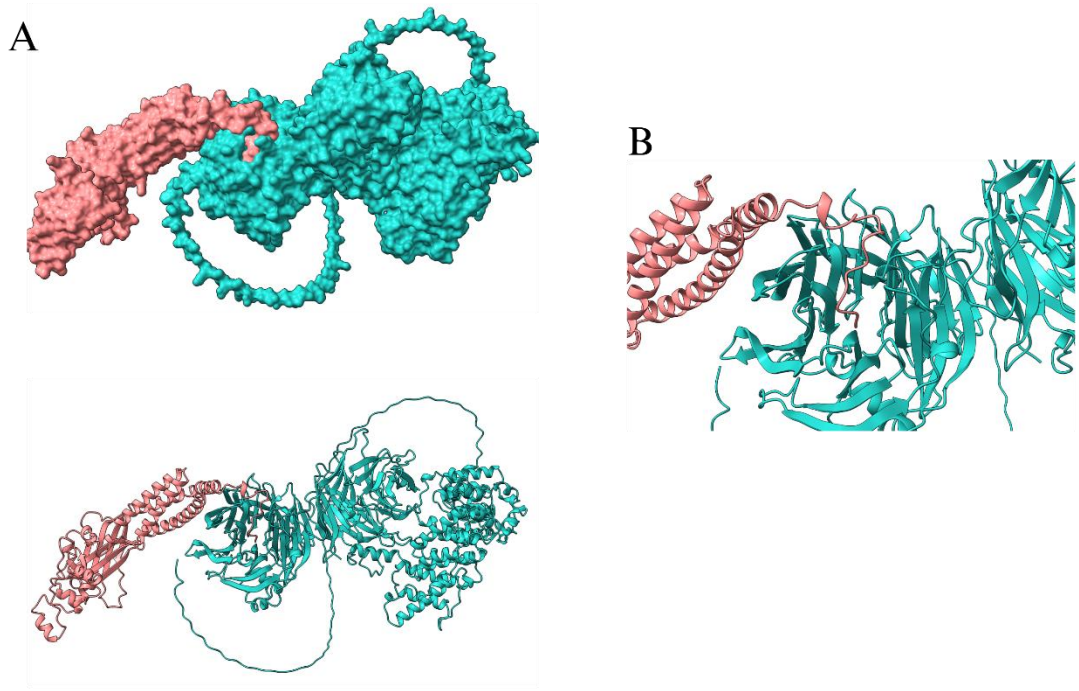

Figure 3-1- AlphaFold3 model of Rav1 and Rav2 binding

(**A**) AlphaFold3 model of Rav1-Rav2 binding (ipTM: 0.78, pTM: 0.68). Rav2 (pink) uses an extended N-terminal tail to bind to Rav1 (blue) β propeller 1. (**B**) Zoomed image of an AlphaFold3 model of Rav2 binding to Rav1 β propeller 1.

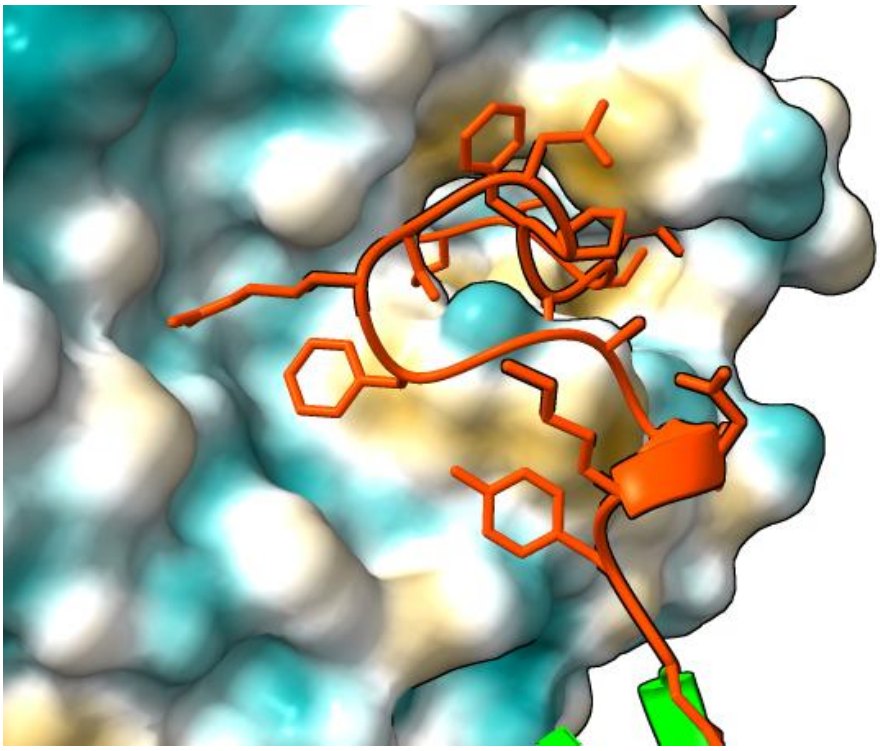

Figure 3-2 Hydrophobic binding of Rav2 to Rav1.

Rav2 N-terminal tail binds to the center of beta-propeller 1. The Rav2 tail (2-19, red) contains hydrophobic residues that are placed near hydrophobic residues lining the center of Rav1 propeller 1. Yellow is hydrophobic, blue is hydrophilic.

Rav1-Skp1

Skp1 is modeled to interact with a region of the Rav1 α-solenoid encompassed within A1165-I1203. Previous yeast two-hybrid analysis found that Skp1 interacts with a Rav1 fragment from amino acids Asp1126-V1271. This region was originally thought to be primarily the start of the C-terminal disordered region, but based on this model, the Skp1 binding site is within the α-solenoid domain (Figure 3-3). The positioning of Skp1 in the AlphaFold3 models is consistent with the RAVE-V1 cryo-EM structure (Figure 3-5). Skp1 also has an extended C-terminal tail. P163-R194 of Skp1 is modeled to extend towards β-propeller 1 and 2. In this model, Skp1 contacts propeller one through residues Rav1 K319-T322 and A377-L378. Skp1 contacts propeller 2 though Q416-H420, R425, R466, E468, E652-Y653. This interaction has not previously been observed and needs further experimental validation. In addition, it is unknown what the functional consequences are of the Skp1-Rav1 β-propeller two interaction. There are additional contacts between Skp1 and the α-solenoid between Rav1 K723-Y851. All contacts between Rav1 and Skp1 are red and shown in Figure 3-3. The Skp1 amino acid that disrupts the Rav1-Skp1 interaction (Asn139Tyr) (Brace, Parkinson et al. 2006) is located at the interface between Skp1 and Rav1 in the AlphaFold3 model. This partially reinforces the positioning of Skp1 in the Rav1-Skp1 AlphaFold3 model. The position of Skp1 Asn139 in the cryo-EM structures is consistent with the AlphaFold3 model.

As mentioned earlier, RAVE is an isoform-specific complex. RAVE catalyzes the reassembly of Vph1 but not Stv1 containing V-ATPases (Smardon, Diab et al. 2014). An amino acid sequence within Rav1 (L^{757}PVYHP) is required for interacting with Vph1 and is conserved in both DMXL1 and DMXL2 (Jaskolka, Tarsio et al. 2021). As a result, this

amino acid sequence must be exposed to the surface at the time of reassembly to facilitate RAVE-Vph1 binding. Both AlphaFold3 models and cryo-EM structures of Rav1 show a conformation where the Vph1 binding sequence is within the α-solenoid at the junction between β-propeller two and the α-solenoid. Adjacent loops and α-helixes partially occlude the Vph1 binding loop. This suggests a substantial conformational change in Rav1 is required before binding to Vph1. As mentioned, a model exists for RAVE-V_1 binding in the cytosol where RAVE first binds to free V_1 subcomplexes and then binds to V_1C (Jaskolka, Tarsio et al. 2021). Under this model of RAVE-catalyzed assembly, only after generating the RAVE-V_1-C complex is the V-ATPase competent for rejoining V_o. The sequential binding of V-ATPase subunits suggests there are matching sequential conformational changes that enable the next binding step. The binding of V_1C to RAVE-V_1 may result in a conformation competent for Vph1 binding.

Skp1 binding to RAVE may influence the ability of Rav1 to bind to Vph1. The C-terminal tail of Skp1 partially obscures the Vph1 binding site in Rav1. Conformational changes in Skp1 that move the C-terminus away from the Vph1 binding site may enable Rav1 binding to Vph1. The Skp1 Asn139Tyr mutation allows the canonical F-Box binding functions of Skp1 while preventing binding to Rav1. Loss of Skp1 from RAVE does not result in a Rav- or Vma- phenotype, indicating that Skp1 is not required to catalyze V-ATPase reassembly. However, *skp1* (Asn139Tyr) mutants have much more Rav1 localized to intracellular membranes compared to WT strain (Brace, Parkinson et al. 2006). Skp1 may function in the releasing of RAVE from the membrane post-reassembly rather than localizing RAVE before reassembly. If the function of Skp1 is to

release RAVE after assembly, then cells would not have a Rav- phenotype because assembly is occurring, and the defect follows V-ATPase assembly.

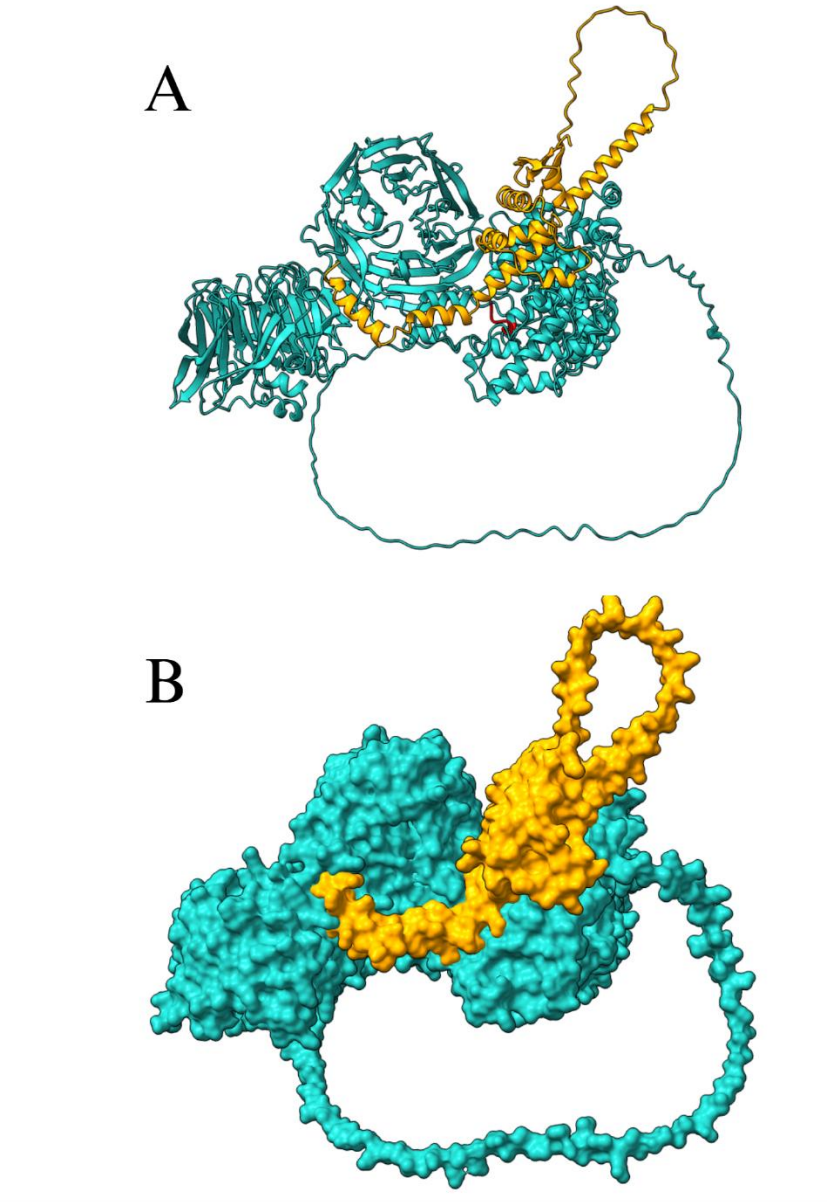

Figure 3-3- AlphaFold3 model of Rav1-Skp1 binding.

AlphaFold3 model (ipTM:0.73, pTM:0.74) of Rav1 (blue) and Skp1 (orange). Skp1 makes minor contacts with Rav1 β-propeller 1 and β-propeller 2 and significant contacts with the α-solenoid domain. The Vph1 binding sequence in Rav1 is highlighted in red.

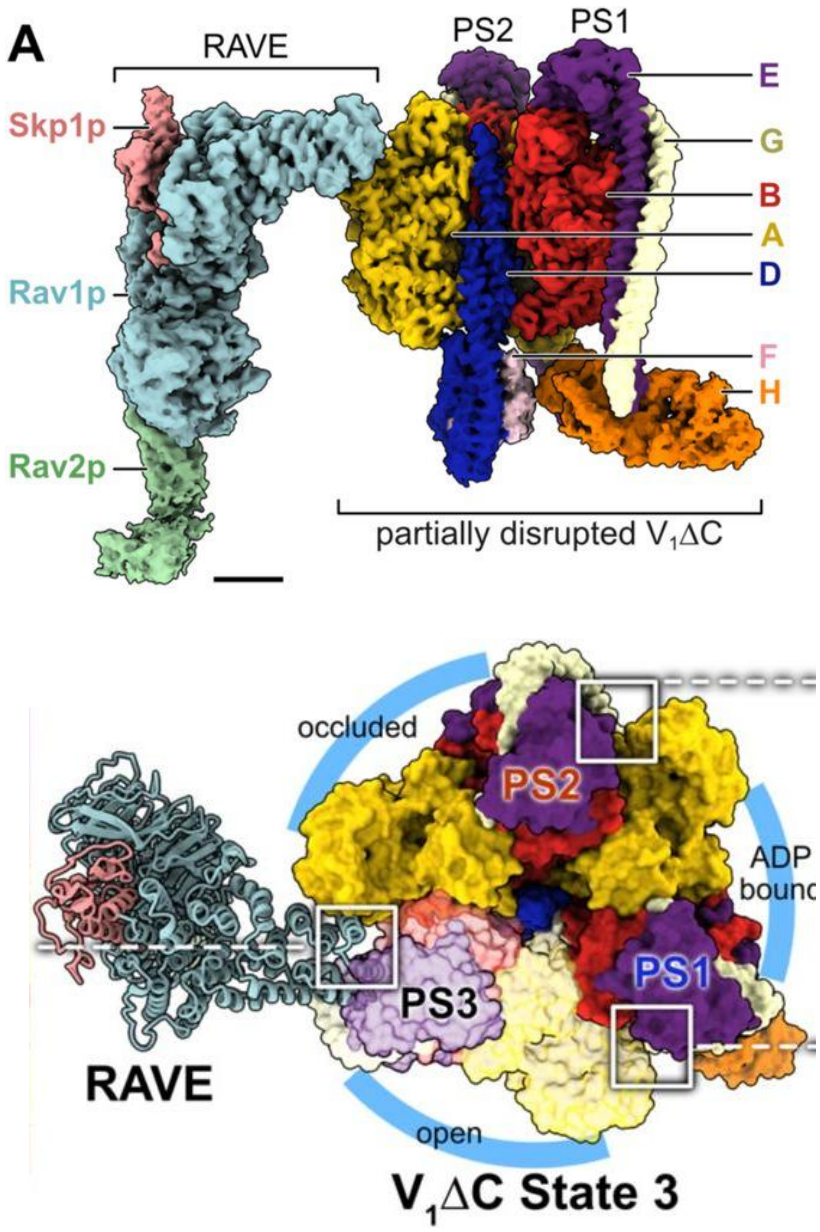

Figure 3-4 CryoEM structure of RAVE-V1 (partial)

Cryo-EM structure of RAVE-V1, adapted from Wang et al (2024). RAVE binds preferentially to V1 in rotation state 3. Rav2 and Skp1 binding to Rav1 is consistent with the AlphaFold3 models. Binding of Rav2 and Skp1 to Rav1 is consistent with predictive AlphaFold3 models.

3.3 Rabconnectin-3

3.3.1 DMXL1 and DMXL2

DMXL1 and DMXL2 are very similar in size and overall structure. The overall structure of DMXL1 and DMXL2 resemble Rav1 but are substantially larger. DMXL1 contains three full β-propellers; like Rav1, there are two propellers on the N-terminus, but there is an additional C-terminal propeller (Figure 3-4). This replaces the C-terminal disordered tail present in Rav1. Unlike Rav1, which contains almost exclusively β-sheets in the β-propeller containing domain, DMXL1 and DMXL2 contain additional helices. Propeller 1 is encompassed within N2-Y633; additional bundled α-helices intervene in this region from amino acids S302-R319 and N397-K488. The purpose of these helices is not known. H639-G1240 includes the second β-propeller and a smaller set of α-helices (776-812, 893-941). Compared to Rav1, the loops between the blades of propellers of DMXl1 and DMXL2 are much larger, adding molecular mass to the protein and creating a 'fuzzier' protein. The α-solenoid spans residues 1282-2613, and the broad structure resembles the Rav1 α-solenoid domain. This region contains the highest degree of sequence homology between Rav1 and DMXL1/DMXL2. This region of Rav1 is primarily responsible for binding to V-ATPase subunits (Smardon, Nasab et al. 2015). Based on the strong homology in this region, we speculate this region of DMXL1 and DMXL2 is also responsible for V-ATPase binding. Like in the N-terminal domain (1-1240), the loops between the α-helices comprising the α-solenoid in DMXL1 and DMXL2 are longer than the comparable loops in Rav1. A substantial difference between DMXL1/DMXL2 and Rav1 is the inclusion of another full β-propeller at the C-terminus

of DMXL1/DMXL2 instead of the disordered tail found in Rav1. The C-terminal β-propeller is positioned adjacent to the two N-terminal propellers, with all three on one side of the protein.

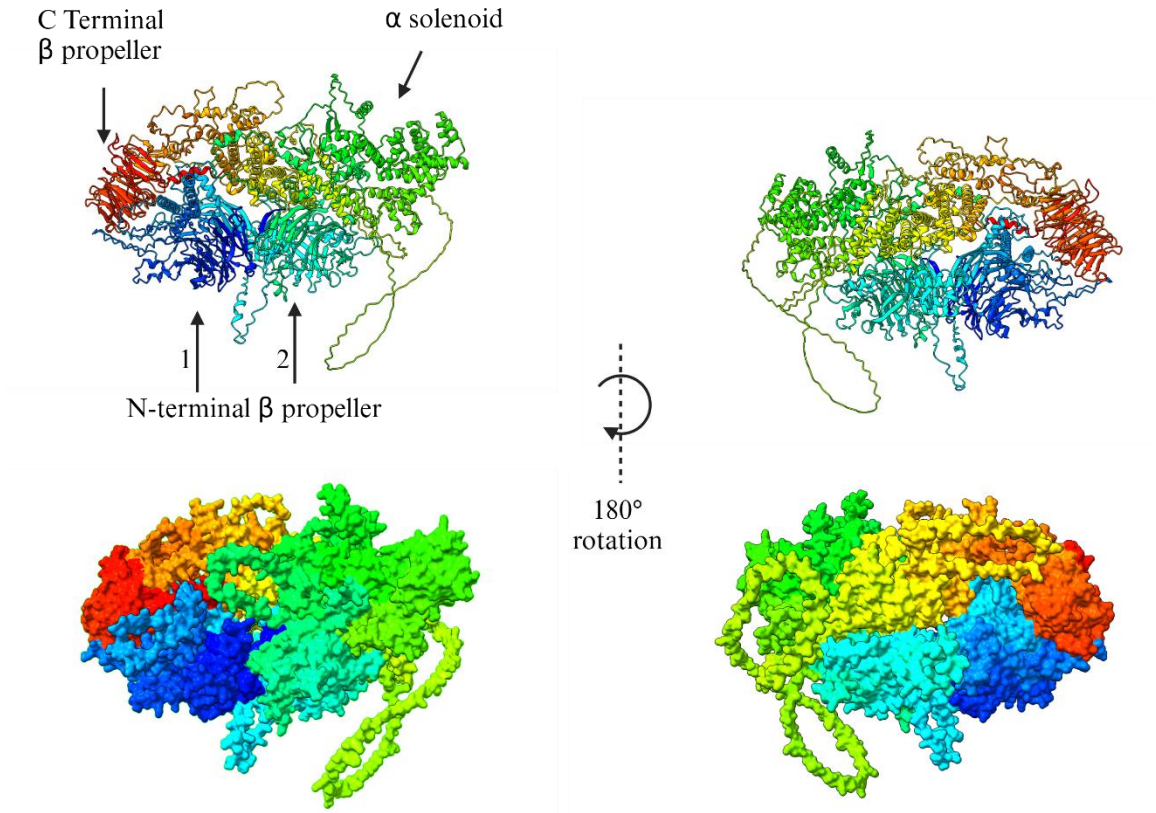

Figure 3-5 AlphaFold3 model of DMXL1.

AlphaFold3 model of human DMXL1 (pTM .69). DMXL1 contains two N-terminal β propellers that are labeled 1(light blue) and 2 (dark blue). The α-solenoid domain is colored yellow/green, and the C-terminal β propeller is colored red.

3.3.2 WDR7

WDR7 is a much smaller protein (1490 amino acid, 163.8 kDa) compared to DMXL1 (3027 amino acid, 337.8 kDa) or DMXL2 (3036 amino acid, 339.6 kDa). It is more comparable to the size of yeast Rav1 (1,357 amino acids, 154.9 kDa). Unlike Rav1 and DMXL1/DMXL2, which have two full N-terminal propellers, WDR7 has one and a half N-terminal β-propellers (Figure 3-5). The WDR7 N-terminal β-propellers are encompassed within amino acids 1-694. Like DMXL1, DMXL2, and Rav1 following the β-propellers is an α-solenoid domain is encompassed within amino acids 695-1358. While the α-solenoid of Rav1 and WDR7 are structurally homologous, they share relatively little sequence homology when compared to homology shared between Rav1 and DMXL1/DMXL2. This suggests that DMXL1 and DMXL2 are likely more functionally related to Rav1 than WDR7. The lack of homology between WDR7 and Rav1 suggests that WDR7 may not bind directly to V-ATPase subunits like DMXL1 and DMXL2. Like DMXL1 and DMXL2, WDR7 has long disordered loops between α-helices in the solenoid domain. These loops appear to be a feature present in both Rabconnectin-3 complexes but are not present in RAVE. Like DMXL1 and DMXL2, WDR7 has a β-sheet rich region at the c-terminus instead of the Rav1 disordered tail. However, WDR7 only has a partial β-propeller (3/7 blades) instead of the full propeller found in DMXL1 and DMXL2. The C-terminal β-propeller fragment is on the opposing side of the protein compared to the N-terminal β-propeller domain.

3.3.3 WDR72

WDR72 is most homologous to WDR7 but is even smaller (1,102 amino acid, 123.4 kDa). An AlphaFold3 structure of WDR72 is shown in Figure 3-5. Like WDR7, WDR72 includes one and a half β-propellers at the N-terminus encompassed within amino acids 1-685. The size of this domain is comparable to the corresponding region of WDR7 (1-694). Like WDR7, there are disordered loops between the individual blades of the β-propeller. The α-solenoid domain of WDR72 is about half the size of the solenoid domain of WDR7 and accounts for much of the difference in size between the two proteins. The WDR72 α-solenoid domain is encompassed by amino acids 685-1008. Like WDR7, WDR72 shares relatively little sequence homology with Rav1. Following the α-solenoid domain is a C-terminal tail that resembles the disordered tail found in Rav1 and is unlike the structured C-terminal domain of all other Rabconnectin-3 proteins. The other Rabconnectin-3 proteins include either an additional β-propeller or a fractional β-propeller. It is not currently known what the functional consequences are of the different C-terminal domains of WDR7 and WDR72.

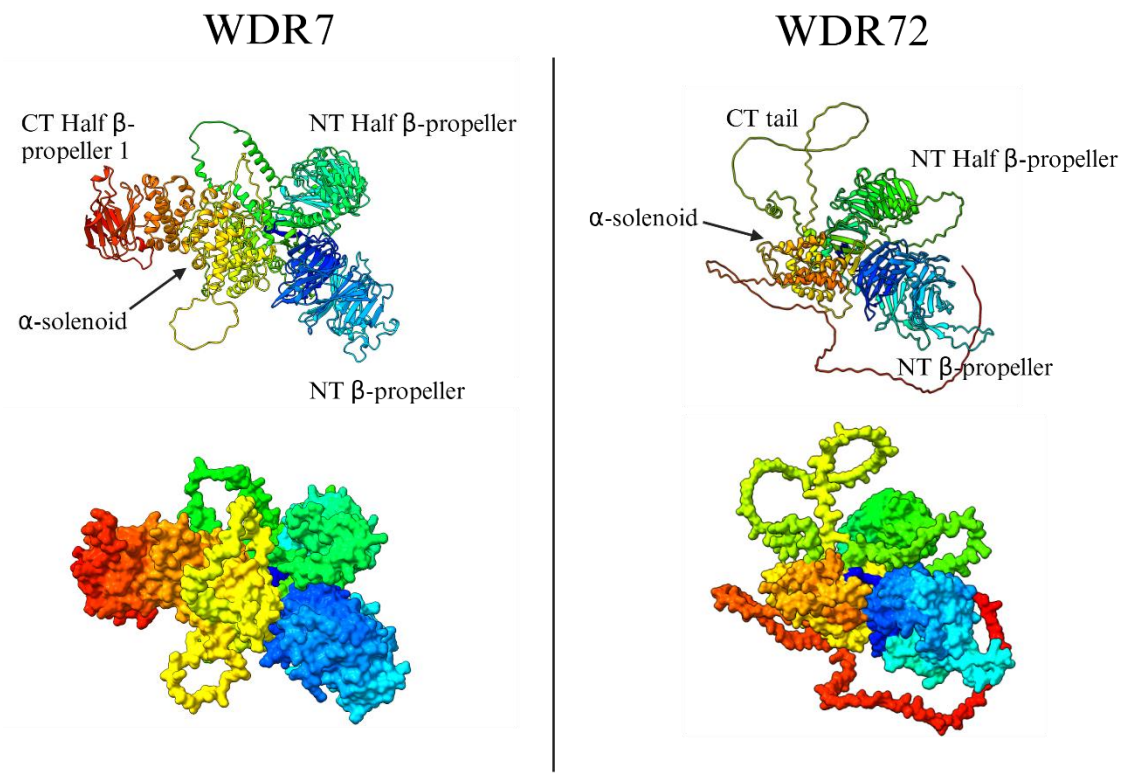

Figure 3-6 AlphaFold3 model of human WDR7 and WDR72.

AlpaFold3 models of WDR7 (left, pTM:0.78) and WDR72 (right, pTM:0.72). WDR7 contains one and a half N-terminal β-propellers, an α-solenoid, and a half C-terminal β-propeller. WDR72 also contains one and a half N-terminal β-propellers, an α-solenoid with a disordered tail on the C-terminus**.**

3.4 Rabconnectin-3/ROGDI complex

As mentioned earlier, Rabconnectin-3 was originally identified as a 1:1 stoichiometric complex of DMXL2 and WDR7 (Kawabe, Sakisaka et al. 2003). Later biochemical characterization of the DMXL2-WDR7 Rabconnectin-3 complex showed that an experimentally determined molecular mass of approximately 570 kDa is larger than the calculated molecular mass of 480 kDa (Sakisaka and Takai 2005). This additional mass was attributed to potential subunits that had not yet been identified but are major Rabconnectin-3 binding partners or the conformation of the complex. Including ROGDI (32 kDa) helps bring the calculated mass closer to the observed 570 kDa. The substantial disparity in size between the Rabconnectin-3 subunits and ROGDI may have contributed to the delayed identification of ROGDI.

AlphaFold3 modeling of ROGDI and Rabconnectin-3α and Rabconnectin-3β results in a model where ROGDI binds to the N-terminal domains of both Rabconnectin-3 (Chapter 2- Figure 2 S2). Permutations of modeling DMXL1 or DMXL2 and WDR7 or WDR72 result in similar overall models. These models are consistent with the earlier yeast two-hybrid findings that show interactions between ROGDI and fragments encompassing the N-terminal β-propellers from each subunit (Chapter 2). ROGDI binds to DMXL1 and DMXL2 through both its α and β domains. The ROGDI α-domain contacts the side of DMXL1 β-propeller 1 through the partially ordered loops connecting individual β-strands within propeller 1. A partially structured loop encompassed by DMXL1 A319-F357 contacts the ROGDI β-domain. ROGDI does not contact either DMXL1 N-terminal β-propeller 2 or the C-terminal β-propeller, like how Rav2 is modeled to interact exclusively with Rav1 propeller 1.

ROGDI is modeled to bind with WDR7 through both the full and half N-terminal β-propellers. The faces of both the full β-propeller and the half β-propeller contact ROGDI through the α domain, creating a ROGDI binding pocket between the two propellers. WDR7 makes few contacts with the ROGDI β-domain through a long loop from within the α-solenoid encompassed by WDR7 1053-1117.

As mentioned earlier, we speculate that ROGDI may serve a bridging function between the Rabconnectin-3 subunits. ROGDI facilitates many indirect interactions between Rabconnectin-3α and 3β. When ROGDI is removed from the complex, there are relatively few direct contacts between Rabconnectin-3α and 3β. The most substantial intraRabconnectin-3 contacts are between the N-terminal half propeller of WDR7 and the first N-terminal β-propeller and the C-terminal β-propeller of DMXL1 (Figure 3-6). When ROGDI is absent, like in individuals with Kohlschutter-Tonz syndrome, the direct contact between the Rabconnectin-3 subunits may not be enough to hold the complex together. Weakened binding between Rabconnectin-3 may impair the function of the complex, resulting in the symptoms associated with KTS.

The generation of AlphaFold3 models of Rabconnectin-3 and RAVE allows us to propose new testable hypotheses about RAVE and Rabconnectin-3 structure and function. The proposed Rav1-Rav2 binding model can be evaluated by deleting the N-terminal tail of Rav2. If the Rav2-tail contributes to binding with Rav1, then a strain with this mutation would have a Rav- phenotype. Since ROGDI can partially replace Rav2 function in yeast (Chapter 2) even without the extended tail that Rav2 contains, there may only be a partial Rav- phenotype. Cross-linking mass spectroscopy can validate the

proposed interactions between the Skp1 C-terminal tail and Rav1 β propeller two. We could try to make mutations to the C-terminal tail of Skp1, but it is very possible that these mutations could impact the other functions of Skp1 and make cells non-viable. As mentioned at the start of this chapter, the size of Rabconnectin-3 proteins makes the expression and purification of the whole protein complex challenging. Interactions proposed in this chapter could be validated by expressing and testing individual domains. These domains could also be expressed and tested using yeast two-hybrid.

DMXL1 + ROGDI

A

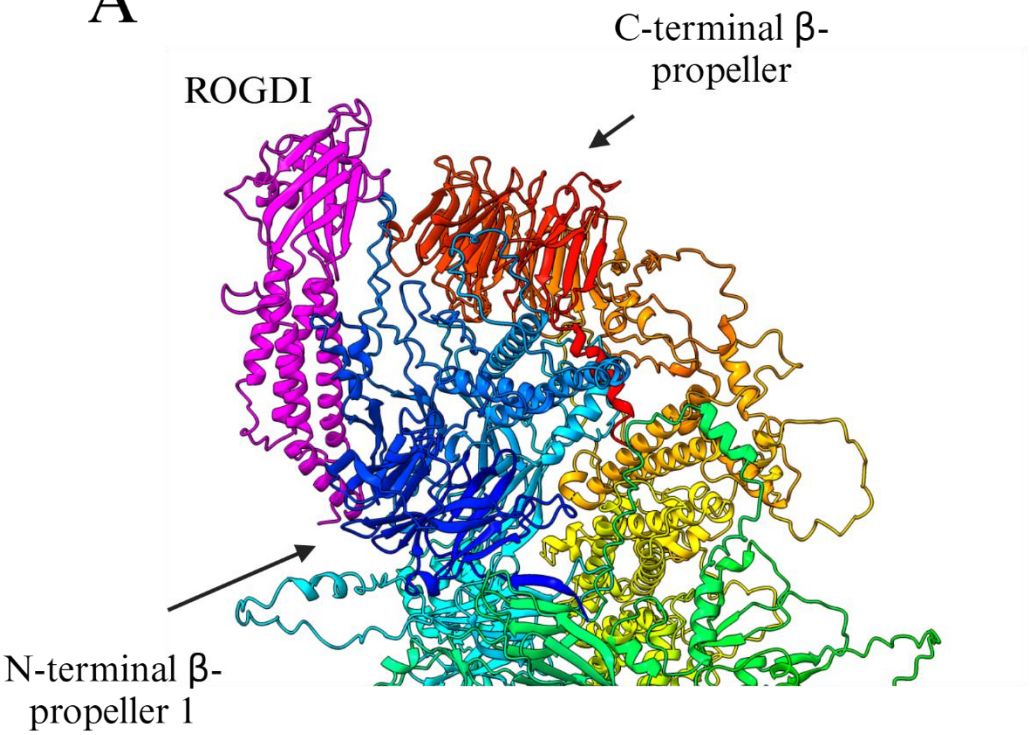

B

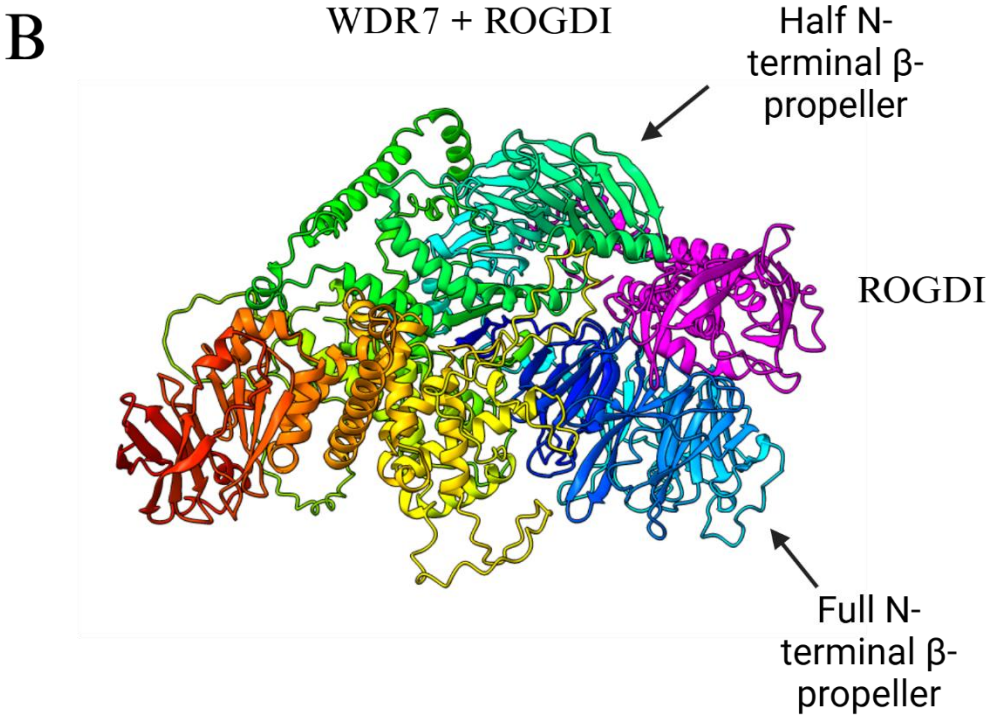

Figure 3-7 ROGDI binding to DMXL1 and WDR7

(A) AlphaFold3 model of ROGDI (pTM:0.86) bound to DMXL1 (pTM:0.79, ipTM:.74). (B) AlphaFold3 model of ROGDI (pTM:0.86) bound to WDR7 (pTM:0.78, ipTM:.74). The full and half β-propellers and ROGDI are labeled.

3.5 References

Brace, E., et al. (2006). "Skp1p regulates Soi3p/Rav1p association with endosomal membranes but is not required for vacuolar ATPase assembly." Eukaryotic cell **5**(12): 2104-2113.

Jaskolka, M. C., et al. (2021). "Defining steps in RAVE-catalyzed V-ATPase assembly using purified RAVE and V-ATPase subcomplexes." Journal of Biological Chemistry **296**.

Kawabe, H., et al. (2003). "A novel rabconnectin-3-binding protein that directly binds a GDP/GTP exchange protein for Rab3A small G protein implicated in Ca2+-dependent exocytosis of neurotransmitter." Genes to Cells **8**(6): 537-546.

Sakisaka, T. and Y. Takai (2005). "Purification and Properties of Rabconnectin-3." Methods in enzymology **403**: 401-407.

Smardon, A. M., et al. (2014). "The RAVE complex is an isoform-specific V-ATPase assembly factor in yeast." Molecular biology of the cell **25**(3): 356-367.

Smardon, A. M., et al. (2015). "Molecular interactions and cellular itinerary of the yeast RAVE (regulator of the H+-ATPase of vacuolar and endosomal membranes) complex." Journal of Biological Chemistry **290**(46): 27511-27523.

Wang, H., et al. (2024). "Structure of yeast RAVE bound to a partial V1 complex." bioRxiv: 2024.2007. 2018.604153.

Chapter 4

Discussion and Future Directions

4.1 ROGDI as a Rav2 homolog and Rabconnectin-3 subunit

ROGDI shares structural and functional homology with the yeast RAVE subunit, Rav2. Expression of human ROGDI in a rav2Δ yeast strain partially alleviates the Rav- phenotype associated with loss of function RAVE mutations, indicating an improvement in V-ATPase activity. ROGDI interacts with the N-terminal domains of both Rabconnectin-3 subunits. AlphaFold3 modeling of the Rabconnectin-3 and ROGDI results in a model where ROGDI is positioned between both Rabconnectin-3 subunits. The binding of ROGDI between the Rabconnectin-3 subunits indicates that ROGDI serves a bridging function between the Rabconnectin-3 subunit.

Loss of function mutations in ROGDI cause Kohlschutter-Tonz syndrome, an epileptic encephalopathy accompanied by amelogenesis imperfecta and occasionally nephrocalcinosis. Mutations in Rabconnectin-3 subunits lead to similar phenotypes. DMXL2 mutations lead to Ohtahara syndrome (an epileptic encephalopathy) (Esposito, Falace et al. 2019) and sensorineural deafness (Chen, Liu et al. 2017). Mutations in WDR7 cause amelogenesis imperfecta and distal renal tubule acidosis accompanied by nephrocalcinosis (El-Sayed, Parry et al. 2009, Jobst-Schwan, Klämbt et al. 2020, Khandelwal, Mahesh et al. 2021). V-ATPase subunit mutations have been associated with the development of sensorineural deafness, distal renal tubule acidosis, and epileptic encephalopathy (Karet, Finberg et al. 1999, Fassio, Esposito et al. 2018, Jobst-Schwan, Klämbt et al. 2020, Bott, Forouhan et al. 2021). As a result, we hypothesize that Kohlschutter-Tonz syndrome is a disease resulting from decreased V-ATPase activity due to decreased Rabconnectin-3 activity. We speculate that ROGDI functions to stabilize the Rabconnectin-3 complex (Figure 4-1).

Immunoprecipitation of DMXL1 from 4T1 cells results in the coimmunoprecipitation of ROGDI, V_1A, and WDR7, demonstrating that ROGDI associates with Rabconnectin-3 and V-ATPase subunits. In 4T1 cells, ROGDI has both cytosolic and membrane-associated populations. ROGDI is associated more strongly with central lysosomes adjacent to the cell nucleus. Lysosomes exist as less catabolically active peripheral lysosomes and central lysosomes that are more catabolically active. ROGDI localizes primarily to central lysosomes but is present on peripheral lysosomes to a lesser extent. The increased catabolic activity on central lysosomes may require increased V-ATPase activity, which in turn requires increased Rabconnectin-3 activity. Further investigation is needed to better understand the function of ROGDI as part of the Rabconnectin-3 complex and the consequences of loss of ROGDI expression.

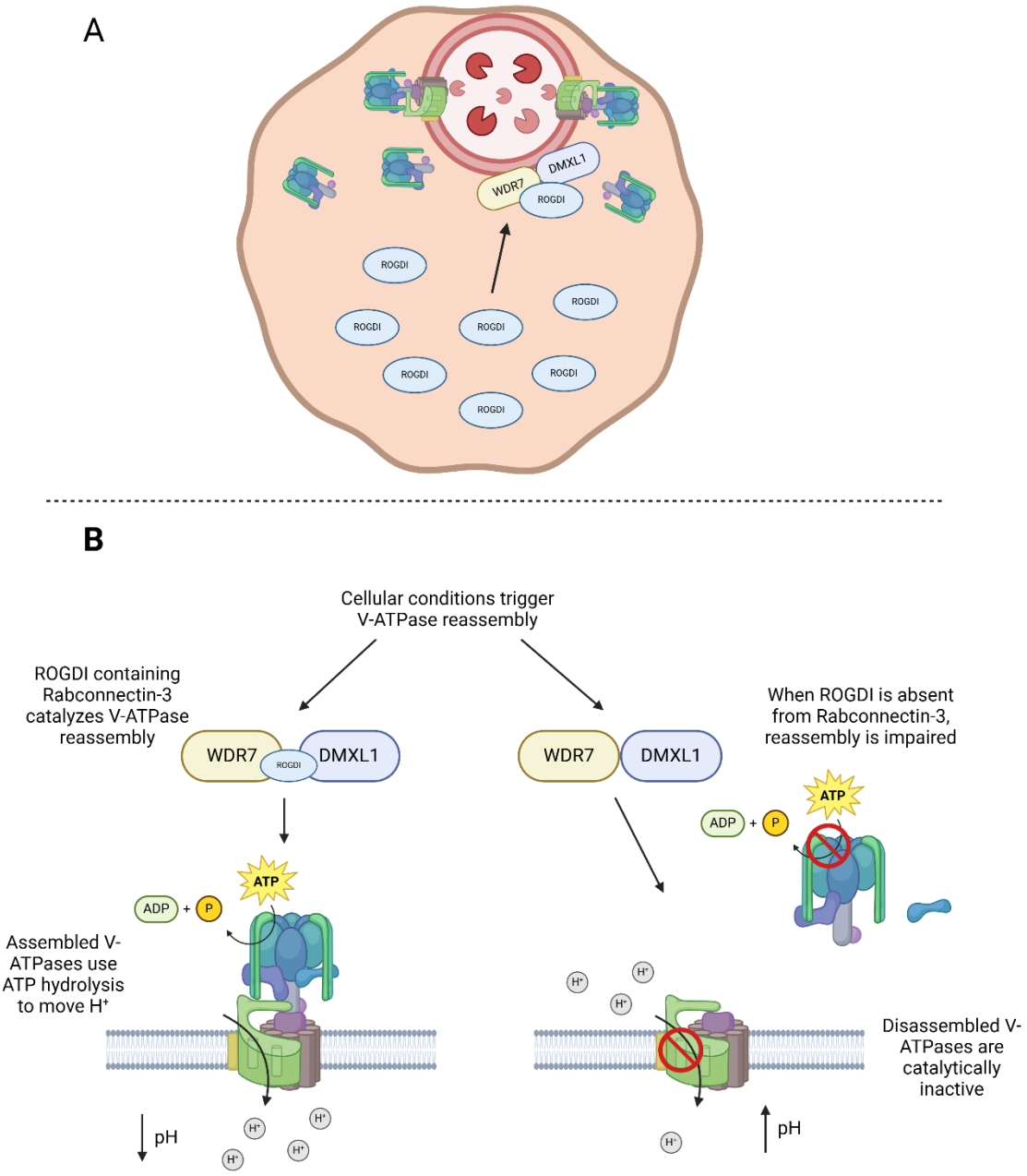

Figure 4-1 ROGDI as part of reversible disassembly

(A) ROGDI is localized both diffusely in the cytosol and on lysosomal membranes. Cytosolic ROGDI may serve as a pool for ROGDI that is recruited to lysosomes.

(B) Under our model, Rabconnectin-3 complexes require ROGDI to properly catalyze V-ATPase reassembly. When ROGDI is absent from the Rabconnectin-3 complex, V-ATPase reassembly is impaired. As a result, V-ATPase activity is reduced.

4.2 DMXL1 lysosomal localization

We found through immunofluorescence microscopy that DMXL1 localizes almost exclusively to LAMP2 positive puncta that we interpret as lysosomes. Additionally, subcellular fractionation experiments show that DMXL1 segregates primarily with cellular membranes and not with cytosol. Based on AlphaFold3 models, it does not appear DMXL1 or DMXL2 have any characteristic transmembrane domains. This suggests that DMXL1 is not an integral membrane protein but instead is more peripherally associated. As a result, it is not known what part of DMXL1 is responsible for its lysosomal localization. Expression of DMXL1 fragments is a possible experimental strategy for determining which domain is required for proper localization. For example, both N-terminal β-propellers, the α-solenoid, and C-terminal propeller can be expressed individually.

A couple of different mechanisms can recruit DMXL1 to lysosomal membranes. One is an interaction between DMXL1 and lysosomal membrane lipids. A wide variety of proteins use the various compositions of phosphoinositide phosphate lipids of different intracellular compartments for targeting and activation. Both human and yeast V-ATPase V_oa subunits interact with PIP lipids (Banerjee and Kane 2017, Banerjee, Clapp et al. 2019, Mitra, Winkley et al. 2023). PROPPINs are β-propellers that function to interact with PIP lipids, specifically PI(3)P and PI(3,5)P2 (Busse, Scacioc et al. 2015); PI(3)P is a PIP lipid present on lysosomal membranes while PI35P2 are localized to endosomes and lysosomes (Banerjee and Kane 2020). If one of the DMXL1 β-propellers functioned as a PROPPIN, DMXL1 would be localized to areas rich in PI(3)P or PI(3,5)P2. Reduction of PI(3,5)P2 or PI(3)P would result in DMXL1 mislocalization if PIP lipid binding is

responsible for lysosomal localization. Treatment of cells with apilimod (a PIKFYVE kinase inhibitor) would reduce PI(3,5)P2 levels (Cai, Xu et al. 2013). Reducing PIK3C2 expression would inhibit the formation of PI(3). RAVE localization in *S. cerevisiae* depends entirely on the binding of RAVE to Vph1. If Rav1 is mutated (Rav1-6Δ)(Jaskolka and Kane 2020) or the RAVE binding region of Vph1 is lost (Tuli and Kane 2023) then RAVE does not localize to the vacuolar membrane. DMXL1 localization could be driven by the binding of DMXL1 to V_0a present in disassembled V-ATPases on lysosomal membranes. Silencing of individual V_0a isoforms would result in redistribution of DMXL1 if DMXL1-V_0a binding is the primary mechanism for DMXL1 localization.

4.3 Rav2 function investigation

The function of Rav2 in the RAVE complex is not currently known. The only known binding partners for Rav2 are Rav1 and V_1C. However, it is not known what part of Rav2 is responsible for binding to Rav2. Considering that the only available RAVE structure is bound to a partial V_1 without V_1C, there is no information about Rav2 function. Additionally, it is unknown if ROGDI binds to V1C in mammals, so a homology comparison between ROGDI and Rav2 to find a conserved region that might function in V_1C binding is not ideal. However, given the small size of Rav2 and Vma5 and the relative ease of recombinant expression, in-vitro experiments can be performed to investigate the details of Rav2-V_1C binding. Structural determination X-ray crystallography of the Rav2-V_1C complex would provide atomic-level information on how the two proteins bind. Other techniques like cross-linking mass spectroscopy or NMR spectroscopy would provide similar information.

The cryo-EM structure of RAVE bound to partial V_1 shows that when RAVE is bound to Rav1, Rav2 would be in close proximity to the membrane. As discussed in the previous chapter, one explanation for this is that Rav2 is flexible about Rav1 and would be able to move out of the way of the membrane. A second option is that Rav2 interacts with the membrane directly and may play a part in the RAVE localization to the vacuolar membrane. The part of Rav2 that would contact the membrane contains an additional domain (Arg238-G297) that is not conserved in ROGDI. The ability of this domain to bind to the vacuolar membrane could be evaluated by the expression of Rav2-GFP in a *rav1Δ* strain and assess the ability to localize to the vacuolar membrane. Additionally, any association could be further investigated using a liposome pelleting assay.

4.4 Generation of a ROGDI knockout cell line

Generating a stable ROGDI knockdown or knockout cell line would be useful in investigating how ROGDI affects V-ATPase activity. Measure of lysosomal pH and concanamycin-sensitive ATPase activity would highlight any global changes in V-ATPase activity between the ROGDI knockout and wild type. We are also interested in evaluating changes in V-ATPase assembly and distribution of Rabconnectin-3 subunits. Based on our model for how ROGDI binds to and influences Rabconnectin-3, we speculate there may be changes in Rabconnectin-3 localization and function.

As mentioned in Chapter 2, we have been unable to generate a ROGDI knockout 4T1 cell line. We have used a transiently transfected Cas9 plasmid with a puromycin drug-resistance cassette and two guide RNAs. The drug-resistant clones had varying

degrees of partial knockdown but no complete loss of ROGDI. Evaluation of the ROGDI gene showed at least one ROGDI allele was edited. However, attempts to repeat the process to eliminate ROGDI failed because cells developed resistance to puromycin during the first round of CRISPR editing. We have also generated GFP-expressing Cas9 plasmids and are planning on using FACS to isolate a group of GFP-positive Cas9-expressing cells instead of using drug resistance.

Recently, a group published a study documenting the generation of a ROGDI knockout mouse. The mouse was viable and lived past the neonatal stage, indicating that ROGDI is not essential for cellular function. We speculate that the cell line we use for this experiment may be an issue. The 4T1 cell line is an aggressive, metastatic mouse mammary cancer. These cells might be particularly sensitive to the loss of ROGDI expression. As a result, cells that would be a complete ROGDI knockout might not be viable and do not survive clonal isolation and drug selection. Using the earlier mentioned GFP plasmids may partially alleviate this issue. We also want to try a shRNA-expressing plasmid as an alternative to CRISPR-based gene editing. A final option is trying a different cell line that might respond better to a CRISPR knockdown of ROGDI than the 4T1 cell line we have been using.

4.5 Investigation of Skp1 mutant

The aforementioned Skp1 Asn139Tyr mutation could be a valuable tool for investigating the function of Skp1 as part of the RAVE complex. Investigators found that preventing the binding of Skp1 to the RAVE complex did not impair RAVE-catalyzed V-ATPase assembly but instead impaired the release of RAVE from the vacuolar membrane

after V-ATPase assembly (Brace, Parkinson et al. 2006). This was evaluated through immunofluorescence microscopy. If the Skp1 Asn139Tyr results in RAVE being 'trapped' at the membrane after V-ATPases are assembled, we could detect this using immunoprecipitation followed by western blot. Tagging and immunoprecipitation of Vph1 ($V_{o}a$) in a *Skp1 Asn139Tyr* mutant would result in an increased amount of Rav1 in the immunoprecipitation compared to wild type if Skp1 catalyzes the release of RAVE from the membrane. Using subcellular fractionation to generate a membrane and cytosolic fractions would show if there is a shift in Rav1 localization. An increased Rav1 signal in the membrane fraction from *Skp1 Asn139Tyr* and a decrease in the cytosol compared to the wild type would reinforce the RAVE-releasing function of Skp1. Fluorescent microscopy could also be used to evaluate the changes to RAVE function in real-time. Our lab has experience using microfluidic chambers in conjunction with confocal microscopy. A strain with a fluorescently-tagged vacuolar protein (Vph1 for example) and Rav1 tagged with a different fluorescent tag would be used. Using microfluidics, we would remove glucose (triggering V-ATPase disassembly), re-add glucose (triggering rapid reassembly), and examine RAVE localization in real time. We could directly observe if the fluorescent tag associated with Rav1 remains at the vacuole longer in the *skp1* mutant strain compared to the wild-type strain.

4.6 Generation of a Rabconnectin-3 structure

While we have AlphaFold3 models of both the Rabconnectin-3 and Rabconnectin-3/ROGDI complex, it would be useful to generate an experimentally determined structure. An experimentally determined structure would allow us to confirm the

AlphaFold3 models and investigate the interaction between subunits on an atomic level. This would allow us to better model in pathogen mutations and try to predict how they will impact the overall complex. Additionally, a high-quality structure would enable us to begin evaluating how Rbaconnectin-3 interacts with the V-ATPase.

Given the size of the complex, cryo-EM would likely be the best experimental method. However, this requires high concentrations of relatively pure protein. We have found that ROGDI expresses robustly in a bacterial system, so there will be enough ROGDI. WDR72 expresses well in *S. cerevisiae*; we have not tried the larger WDR7 isoform. The most substantial issue would be the expression and purification of either DMXL1 or DMXL2. DMXL1 and DMXL2 are too large to be expressed in either yeast or bacteria. As a result, we would need a mammalian expression system or baculovirus with insect cells. Expressing in mammalian cells would involve generating a mammalian cell line stably expressing an affinity tagged DMXL1 or DMXL2 and growing enough cells to purify the protein needed. Using a baculovirus and insect cell-based system would involve cloning and creating the DMXL1 or DMXL2 containing baculovirus and infecting insect cells with the recombinant virus. Our lab is unfamiliar with insect cells or viruses, so this would be a new venture.

4.7 References

Banerjee, S., et al. (2019). "Interaction of the late endo-lysosomal lipid PI (3, 5) P2 with the Vph1 isoform of yeast V-ATPase increases its activity and cellular stress tolerance." Journal of Biological Chemistry **294**(23): 9161-9171.

Banerjee, S. and P. M. Kane (2017). "Direct interaction of the Golgi V-ATPase a-subunit isoform with PI (4) P drives localization of Golgi V-ATPases in yeast." Molecular biology of the cell **28**(19): 2518-2530.

Banerjee, S. and P. M. Kane (2020). "Regulation of V-ATPase activity and organelle pH by phosphatidylinositol phosphate lipids." Frontiers in cell and developmental biology **8**: 510.

Bott, L. C., et al. (2021). "Variants in ATP6V0A1 cause progressive myoclonus epilepsy and developmental and epileptic encephalopathy." Brain communications **3**(4): fcab245.

Brace, E., et al. (2006). "Skp1p regulates Soi3p/Rav1p association with endosomal membranes but is not required for vacuolar ATPase assembly." Eukaryotic cell **5**(12): 2104-2113.

Busse, R. A., et al. (2015). "Characterization of PROPPIN-phosphoinositide binding and role of loop 6CD in PROPPIN-membrane binding." Biophysical journal **108**(9): 2223-2234.

Cai, X., et al. (2013). "PIKfyve, a class III PI kinase, is the target of the small molecular IL-12/IL-23 inhibitor apilimod and a player in Toll-like receptor signaling." Chemistry & biology **20**(7): 912-921.

Chen, D.-Y., et al. (2017). "A dominant variant in DMXL2 is linked to nonsyndromic hearing loss." Genetics in Medicine **19**(5): 553-558.

El-Sayed, W., et al. (2009). "Mutations in the beta propeller WDR72 cause autosomal-recessive hypomaturation amelogenesis imperfecta." The American Journal of Human Genetics **85**(5): 699-705.

Esposito, A., et al. (2019). "Biallelic DMXL2 mutations impair autophagy and cause Ohtahara syndrome with progressive course." Brain **142**(12): 3876-3891.

Fassio, A., et al. (2018). "De novo mutations of the ATP6V1A gene cause developmental encephalopathy with epilepsy." Brain **141**(6): 1703-1718.

Jaskolka, M. C. and P. M. Kane (2020). "Interaction between the yeast RAVE complex and Vph1-containing Vo sectors is a central glucose-sensitive interaction required for V-ATPase reassembly." Journal of Biological Chemistry **295**(8): 2259-2269.

Jobst-Schwan, T., et al. (2020). "Whole exome sequencing identified ATP6V1C2 as a novel candidate gene for recessive distal renal tubular acidosis." Kidney international **97**(3): 567-579.

Karet, F. E., et al. (1999). "Mutations in the gene encoding B1 subunit of H+-ATPase cause renal tubular acidosis with sensorineural deafness." Nature genetics **21**(1): 84-90.

Khandelwal, P., et al. (2021). "Phenotypic variability in distal acidification defects associated with WDR72 mutations." Pediatric Nephrology **36**: 881-887.

Mitra, C., et al. (2023). "Human V-ATPase a-subunit isoforms bind specifically to distinct phosphoinositide phospholipids." Journal of Biological Chemistry **299**(12).

Tuli, F. and P. M. Kane (2023). "Chimeric a-subunit isoforms generate functional yeast V-ATPases with altered regulatory properties in vitro and in vivo." Molecular biology of the cell **34**(3): ar14.

Chapter 5- Appendix

5.1 ROGDI and Rav2 are structurally homologous

Through homology modeling with the Phyre2 homology server, we identified a protein with unknown function as a potential homolog of yeast Rav2. ROGDI has a partial crystal structure available, which was solved by X-ray crystallography by Lee et al. (2017, Scientific Reports) to shed light on the pathology of a disease called Kohschutter-Tonz syndrome, which is caused by mutations in ROGDI (Schossig, Wolf et al. 2012).

ROGDI has two structurally distinct domains, an α-domain and a ß-domain, named after the secondary structure they adopt when folded (see Chapter 2). The arrangement of the α-domain and β-domain are not distinct halves of the polypeptide chain but alternates throughout. ROGDI secondary structure includes 6 α-helices (α1-α6) and 8 ß-sheets (ß1-ß8) (Lee, Jeong et al. 2017). The α-domain is formed by α1, α2, α3, and α6. The α-helices interact to form an anti-parallel coiled-coil structure where hydrophobic side chains of the helices hold the coiled-coil together. The α-domain resembles the leucine zipper motif found commonly in DNA binding proteins. However, little evidence suggests that ROGDI binds DNA or is even localized to the nucleus. ROGDI lacks the basic amino acid motifs necessary to facilitate DNA binding by many leucine zipper-containing proteins. The ß-domain is composed of all eight ß-strands α4 and α5. Within the ß-domain, there are two distinct ß-sheets, namely, ß1-ß4 and ß5-ß8. The two ß-sheets along with α4 andα 5, form a ß sandwich where one ß-sheet is stacked flat on top of another. Within the ß-domain, there are many disordered loops between

neighboring ß-strands, which could provide opportunities for binding other proteins or ligands.

As mentioned earlier, there is no experimentally determined structure for either Rav1 or Rav2. However, AlphaFold enabled us to generate a modeled Rav2 structure (Chapter 2). Similarly, we can also model full-length ROGDI, allowing for the comparison of regions omitted from the crystal structure for experimental reasons. When comparing the AlphaFold2 structures of ROGDI and Rav2, there is substantial similarity between the two proteins. The α-domain is essentially the same between the two proteins; α1,α2,α3, and α6 are conserved between the two proteins. Rav2 α1 and α6 are modeled to adopt a bent conformation compared to ROGDI. Additionally, Rav2 contains an 18 amino acid N-terminal tail compared to ROGDI, which includes a nine amino acid tail. The core of the ß-domain i conserved between ROGDI and Rav2. The ß-strands that make up the ß-sandwich are structurally almost identical between Rav2 and ROGDI. Differences in loops connecting α1 to α4 and α5 result in some difference in the position of α4 and α5 in ROGDI compared to Rav2. The most substantial difference between Rav2 and ROGDI is in an additional domain in Rav2 that is not conserved in ROGDI. The domain is between ß6 and ß7 in ROGDI (Ala223-Gln237), corresponding to Rav2 Arg250-Asn302. The additional Rav2 domain includes four α-helices and one ß-strand. ROGDI contains a long loop of non-structured 14 amino acids in this region. It's not currently known what the function of this additional domain is, but it is noteworthy as the main structural difference between two largely homologous proteins.

5.2 References

Lee, H., et al. (2017). "The crystal structure of human Rogdi provides insight into the causes of Kohlschutter-Tönz Syndrome." Scientific reports **7**(1): 3972.

Schossig, A., et al. (2012). "Mutations in ROGDI cause Kohlschütter-Tönz syndrome." The American Journal of Human Genetics **90**(4): 701-707.